ELECTRICAL PROPERTIES OF CELLS USING NONUNIFORM FIELD EFFECTS

By

JAY KENT POLLOCK

Bachelor of Science

Oklahoma State University

Stillwater, Oklahoma

1972

Submitted to the Faculty of the
Graduate College of the
Oklahoma State University
in partial fulfillment of
the requirements for
the Degree of
DOCTOR OF PHILOSOPHY
December, 1986

Thesis
1986D
P776e
cop. 2.

OKLAHOMA STATE UNIVERSITY LIBRARY

ELECTRICAL PROPERTIES OF CELLS USING

NONUNIFORM FIELD EFFECTS

Thesis Approved:

Paul Worthaus

Thesis Adviser

Wm. L. Hughes

Norman N. Durham

Dean of the Graduate College

1291701

PREFACE

Electrical Properties of cells are investigated in this study using various aspects of biological dielectrophoresis. An automated cell sorter/analyzer, which is capable of measuring the dielectrophoretic spectra of cells and using that information to separate cells, was developed. A different aspect of cellular electrical properties was investigated using rotating electric fields. Variations of yeast spectra with stage in the life cycle were studied. Differences in the spin spectra of normal and cancer human lung cells were found. Dielectrophoresis (DEP) was also used to detect the presence of AC fields produced by cells.

A number of people were instrumental in aiding me in the course of this work. I am grateful for the invaluable assistance and friendship of co-workers, Dr. Karan Kaler, Tim Braden, Hiram Rivera, and Dr. Bill Phillips.

I am also thankful to the members of my committee, Dr. Paul A. Westhaus, Dr. Bruce J. Ackerson, and Dr. William L. Hughes for their helpful suggestions on this work.

I am especially indebted to my major adviser, Dr. Herbert A. Pohl, whose enthusiasm, knowledge, and inventiveness was an inspiration. He will be greatly missed by his friends and colleagues

TABLE OF CONTENTS

LIST OF TABLES

LIST OF FIGURES

Figure Page

CHAPTER I

INTRODUCTION

Nonuniform electric fields can produce unique, often unexpected effects on matter, even electrically neutral matter. These effects have long been observed, but only appreciated rather recently. Nonuniform field effects are among the earliest recorded observations of electrical phenomena. In 600 B. C., Thales of Miletus observed that amber attracted small bits of lint when rubbed with a cloth. This was a nonuniform field effect. The electric charge on the amber first polarized the lint. The lint then experienced a net attractive force toward the amber. This force is now called the dielectrophoretic force.

It wasn't until the last half of this century that dielectrophoresis (DEP) was defined by Pohl (1951). From the Greek word *phoresis* meaning motion, dielectrophoresis was defined as the motion of neutral matter in a nonuniform electric field. It is important to differentiate DEP from the response of charged particles in an external electric field, electrophoresis.

DEP

DEP can easily be illustrated with figure 1. Part A shows a neutral particle and a charged particle in a uniform electric field. The neutral particle polarizes, with one side becoming slightly more positive and the other slightly more negative. All charges experience a force equal to the charge times the local field, F=q x E. Since the field is uniform, the neutral particle will experience no net force. The charged particle will experience a translational force, electrophoresis, whose direction depends on the field direction.

Part B shows the same particles in a nonuniform electric field. The charged particle will again exhibit electrophoresis. The neutral particle will again be polarized. However, in the nonuniform field, the neutral particle will experience a net force (DEP) toward the strong field region. The DEP force arises because the local field varies over the dimension of the particle, so that the force on one side of the particle is greater than the force on the other.

Another aspect of DEP can be seen in part B. If the field is reversed, the neutral particle will still be attracted to the strong field region. The charged particle will reverse its motion. By applying an ac field, only DEP can be observed as the neutral particle moves steadily toward the strong field region and the charged particle

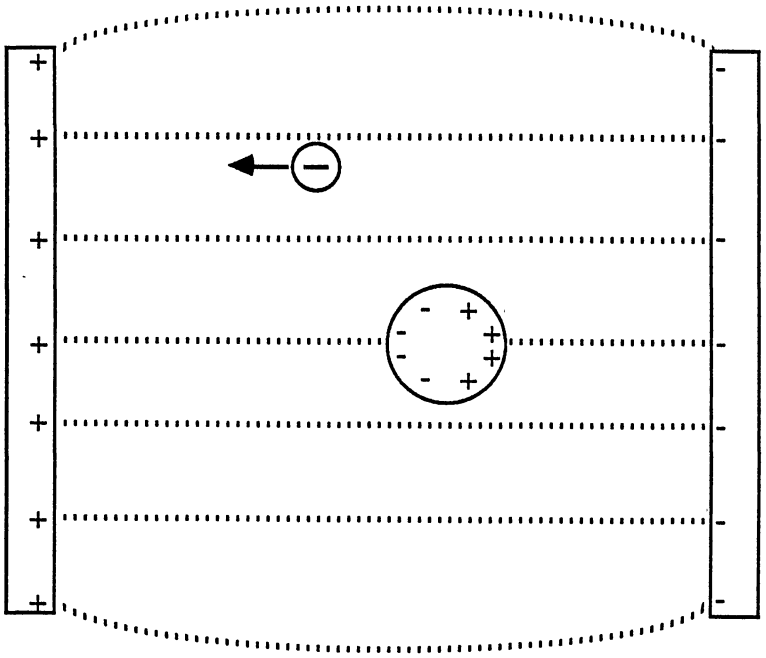

A

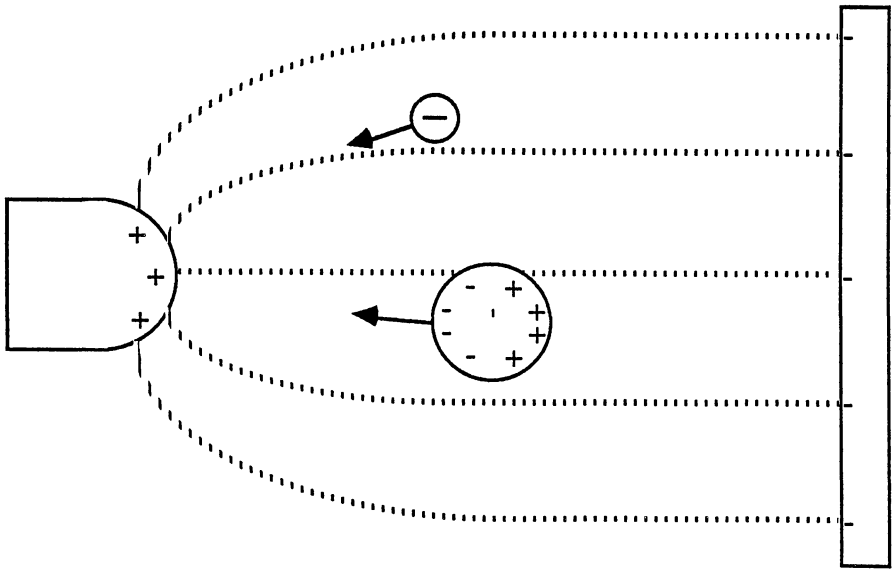

B

Figure 1. Illustration of Dielectrophoresis

merely "shudders" about its original position.

Another distinction concerning DEP must be kept in mind. Previously the term electrostriction encompassed both the translational movement of neutral matter and the distortional response of neutral matter in a nonuniform electric field. In modern usage, the term electrostriction is confined to the distortional response of neutral matter to a nonuniform electric field, while DEP refers to translational motion of neutral matter.

Particles not only move toward the strong field region but can also move away from it. This negative DEP arises from the interaction of the particle and its supporting medium. In actual practice, particles are suspended in air or liquid and the field affects both the particle and the suspending medium. In such a case, the DEP force experienced by the particle depends on the difference between the polarizability of the particle and the polarizability of the medium. If the particle is in a liquid medium more polarizable than itself, the DEP force will be away from the strong field region and the particle will experience negative DEP.

Another effect, observable even in a uniform field, is mutual DEP. Mutual DEP is the interaction of polarized particles in an electric field with each other. As particles in the field are polarized, they distort the field and produce small local nonuniformities. These nonuniformities cause particles to be attracted to each other. Mutual DEP

was first studied by Muth (1927) who observed the formation of long strands of emulsified fat particles when subjected to high frequency ac fields. However, mutual DEP was not recognized at the time as the mechanism that caused the formation of these "pearl chains".

Early Studies

Early studies of DEP were conducted with inanimate (polymer and mineral) particles in insulating liquids. In a series of papers Pohl and his co-workers investigated the dependence of DEP collection on particle size, electrode dimensions, applied voltage, and dielectric constants of particle and the supporting medium (Pohl,1951,1958,1960; Pohl and Schwar,1959,1960; Pohl and Plymale,1960).

Pohl and Schwar (1959,1960) developed semi-batch and continuous separation techniques using a cylindrical electrode chamber and poly(vinyl chloride) particles suspended in a 1:1 v/v mixture of carbon tetrachloride and benzene. Pohl and Plymale (1960) conducted separation experiments with a cylindrical electrode chamber and with an isomotive electrode chamber (Pohl,1968). Verschure and Ijlst (1966) used a grid and plate electrode chamber to obtain separations of various minerals. Terry and Pohl (Pohl,1978) later used isomotive electrodes to successfully separate different colors of glass.

DEP characterization techniques were further developed with methods for dielectric constant measurement (Pohl and Pethig,1977; Kallio and Jones,1980; Morgan and Pethig,1979) and for levitation (Kallio and Jones,1980; Jones and Bliss,1977; Jones and Kallio,1979). Jones and his co-workers developed stable DEP levitation of bubbles and spheres and used it to determine dielectric constants. Pohl and Pethig (1977) and later Morgan and Pethig (1979) developed an isomotive electrode chamber for dielectric constant measurements. This isomotive chamber was later used in a determination of the DEP force expression (Pohl, Pollock, and Crane,1978).

DEP studies were extended to lossy materials in aqueous media by Feeley (1969), Chen (1969), and Scrimager (1974). Feeley studied the DEP force on particles of varying dielectric constant. The particles were suspended in water-dioxane mixtures of varying dielectric constant. The DEP force was investigated at several different frequencies.

Chen investigated the DEP force at various frequencies. The force on different particles was investigated as cations and anions of different valence were added to the aqueous supporting medium.

Scrimager studied the DEP collection of SiO_2 particles over a large number of frequencies. The collection was studied as the pH and the valence of various added cations was varied.

Biological DEP

As was mentioned previously, Muth (1927) was probably the first to study the response of biological particles to uniform electric fields. He observed pearl chains formed by the action of mutual DEP. Liebesney (1939) observed pearl chain formation in red blood cell suspensions and Manegold (1950) reported pearl chains in emulsions of fatty ester particles similar to Muth.

Heller and his co-workers (Heller,1959; Teixera-Pinto et. al.,1960) subjected several organisms to high frequency fields. They observed pearl chain formation, spinning, and frequency regions of preferential orientation. Griffin and his co-workers (Griffin and Stowell,1966; Griffin and Ferris,1970) studied orientation and bunching effects in suspensions of *Euglena*. Saito, Schwan, and Schwarz (1966) were able to propose a good explanation for these orientation effects. Pohl (1972) used this phenomenon along with DEP to devise a method to construct model tissue samples.

The first application of DEP to biological particles was reported by Pohl and Hawk (1966). They successfully separated a mixture of live and dead yeast cells using a batch pin-plate chamber. This was the first separation of live and dead cells using purely physical means. Crane and Pohl (1968) and later Mason and Townsley (1971) confirmed the separation. Mason and Townsley performed an even more

delicate separation by separating yeast that had been cultured on different media.

DEP has since been used to characterize a wide assortment of cells and cell organelles. Crane (1970) and Pohl and Crane (1971) made a detailed study of the yeast, *S. cerevisiae*. Chen (1972) studied yeast, rat liver mitochondria, and a number of different bacteria. Ting and his co-workers (1971) reported on the DEP collection of spinach chloroplasts. Red blood cells were studied by Wiley (1970) while Rhoads, Buckner, and Pohl (1976) compared canine platelets from normal, hemophilic, and transmitter animals.

A very powerful and sensitive technique for cell characterization, single cell levitation, was first reported by Chen and Pohl (1974). This method was further developed by Crane and Pohl (1977,1978) and by Kaler and Pohl (1980).

A continuous DEP chamber for biological applications was first developed by Pohl, Kaler, and Pollock (1981). This chamber was also used by Pohl and Kaler (1979) to separate mixtures of algae and yeast.

Another phenomenon of nonuniform fields is that under certain conditions, particles can be observed to spin. As was mentioned above, Heller and his co-workers (1959; Teixera-Pinto et. al.,1960) observed cells spinning when subjected to RF electric fields. Crane (1970) and Pohl and Crane (1971) made the first systematic study of the spinning of yeast cells, and established that the spinning was

responsive to narrow frequency ranges. This Cellular Spin Resonance, or CSR, was further developed by Pohl and his co-workers (Pohl and Braden,1982; Mischel, Voss, and Pohl,1982; Mischel and Pohl,1983; Rivera,1984).

DEP has also been used to detect the RF fields generated by cells. Pohl developed the technique of micro-DEP to detect the fields from cells that had been postulated by Fröhlich. If the cell is indeed generating a nonuniform electric field, then small, highly polarizable particles placed near the cell should be attracted; while weakly polarizable particles should be unaffected or repelled from the cell. In a series of experiments, Pohl and his co-workers (Pohl et. al.,1981; Pohl,1981) showed that highly polarizable particles such as $BaTiO_3$ are attracted to cells in twice the numbers that weakly polarizable particles, such as $BaSO_4$, are.

It is clear from the preceding discussion that DEP can be applied to the study of biological systems in several ways. It can determine the electrical polarization characteristics of cells and cell organelles. It can use the differing electrical characteristics of cells to separate them. It can also reveal the presence of RF electric fields produced by cells themselves.

Scope of the Current Study

This study will be concerned with examining the

electrical properties of cells using nonuniform field effects, DEP. An automated, continuous DEP analyzer/sorter will be developed, extending the work of Pohl, Kaler, and Pollock (1981, or Appendix A) and Pohl and Kaler (1979). The technique of CSR will be used to study the polarizabilities of cells and how the CSR information differs from that obtained from DEP translational motion studies. Finally, a hanging drop technique similar to μ-DEP will be used to investigate the production of ac electric fields by several different cells.

CHAPTER II

THEORY

This chapter will examine theoretical aspects involved in the study of biological DEP. First, the polarization responses of cells to applied electric fields will be discussed, along with several polarization mechanisms that have been proposed to explain such cellular responses. The nature of the DEP force expression will be examined. Finally, an overview of Fröhlich's theory of coherent oscillations in cells will be given.

Polarization Mechanisms

The DEP response of matter depends on its degree of polarization in a nonuniform electric field. Consequently, we wish to examine the currently recognized mechanisms for understanding polarization. Polarization occurs on both a molecular level and on a more macroscopic level involving regions of matter. The four modes of polarization that occur on a molecular scale are: (1) electronic, (2) atomic, (3) dipolar orientation, and (4) nomadic (giant, long range, usually involving delocalized electronic orbitals). There are also several modes involving interfacial and inter-regional polarization operating on a more macroscopic

scale. These supramolecular modes are (1) interfacial (bulk-bulk) polarization, (2) surface-associated interfacial polarization, (3) plasmoidal polarization, and (4) polymeric electrolytes.

Molecular Modes

Matter can respond to a small electric field in two principal ways. A continuous or semi-continuous motion of charges through a body of matter appears as a conductive response to the experimenter. A restricted or constrained movement of charges would appear as a polarization response. These two quantities are related over the frequency range. An applied field of low frequency would allow many charges to reach their limits of movement and their response would appear as a polarization. In a field of higher frequency, these charges would not reach their limit of travel and would move freely. Their response would then appear as a conductivity. The Kramers-Kronig relations linking these two processes is well discussed by Fröhlich (1949).

Electronic Polarization. Electronic Polarization is the universal and common polarization response of all matter. It occurs when the elemental charges, electrons and nuclei, are distorted from their positions by the application of an external electric field. This distortion of the electrons about the nucleus is usually very small (von Hippel, 1954; Dekker, 1962). In most organic solids, the electronic polarization produces only a modest increment

to the relative dielectric constant, K, of 2 to 4. In inorganic solids, such as elemental silicon, an increment of 12 occurs. This small effect is not unexpected considering the field within the atom (about 10^{11} V/m) is much larger than the external fields that are usually applied (0 to 10^{8} V/m).

Atomic Polarization. Atomic Polarization arises from the shifts of oppositely charged atoms relative to one another. KCl, for example, is an ionic solid in which the potassium ions shift their positions slightly relative to the chlorine ions when placed in an external electric field. In organic solids, this increment of the dielectric constant is low, about 1/7 that due to the electronic polarization.

Orientational Polarization. Orientational Poloarization arises from the orientation of dipolar molecules or parts of molecules. The atoms making up a molecule carry differing net charges so that regions of relative positive and negative charge may exist, thus creating a dipole. These dipoles will minimize their potential energy in an external field by reorienting themselves. Some common dipolar molecules with biological significance are: RNA, DNA, amino acids, proteins, and H_2O.

The contribution of dipolar orientation to the total dielectric constant can be quite large. Water, for example, has a relative dielectric constant of 78, the greater portion being due to dipolar orientation and proton

migration. As might be expected, such large objects as molecules have only a limited ability to follow a high frequency applied field. The relative dielectric constant of water at low frequencies is 78, but it drops to 1.8 above 20 GHz. There are excellent reviews (Kittel, 1973; von Hippel, 1954; Dekker, 1962) which discuss electronic, atomic, and orientational polarization of solids, liquids, and gases in greater depth.

Nomadic Polarization. Nomadic Polarization is a rather recently recognized phenomenon (Pollak and Pohl, 1975; Pohl and Pollak, 1977; Pohl, 1978; Pohl et. al., 1983) which can give rise to huge dielectric constants. These giant polarizations are due to the great distances that the charges are able to travel.

This can be more easily understood by considering the following simple equation for the polarization:

$$P = Nqx \qquad (1)$$

where N is the number of dipoles per unit volume, q is the magnitude of charge at the ends of the dipole, and x is the distance separating the charge centers of the dipole.

There may be many charges responding to the field in the cases of electronic and atomic polarization, but the distances they move are usually very short. The resulting effective dielectric constant is therefore also small. Charges move longer distances in the case of orientational

polarization, as the dipoles reorient. The effective dielectric constant is consequently larger. In nomadic polarization, charges may easily move very long distances, as much as several molecular segments away (thus the term "nomadic"). The effective dielectric constants are correspondingly huge. Nomadic polarization in organic solids can give dielectric constants of from 1000 to 100,000, when the usual range of dielectric constants in organic solids is from 2 to 38.

Nomadic polarization can add substantially to the dielectric constant in biological materials (Pollak and Pohl, 1975; Pohl and Pollak, 1977). The charge carriers can be mobile holes, mobile electrons, or mobile ions such as H^+, K^+, or Na^+. For example, the cytochrome-c complexes and the chlorophyll complexes exhibit polarizations due to electronic charge carriers (Pethig, 1979). Polarization due to ionic charge carriers is exhibited by various membrane ionophores and DNA (Takashima, 1967).

We can use Table I to compare the estimates of the incremental change in the relative dielectric constant, ΔK, contributed by each of the above types of polarization.

Supramolecular Modes

It has been recognized since the middle of the 19th century that the existence of physical interfaces in matter provides the discontinuities to the movement of charges, and

therefore provides opportunities for restrictions in their travel in response to an applied field. An experimenter would view these restrictions as an electrical polarization. An effective dielectric constant could then be assigned to the system containing contributions of both these macroscopic polarizations and the polarizations due to the molecular modes discussed previously.

TABLE I

TYPICAL CONTRIBUTIONS OF VARIOUS TYPES OF MOLECULAR POLARIZATION TO THE RELATIVE DIELECTRIC CONSTANT, ΔK

Polarization Type	ΔK
Electronic	1 to 10
Atomic (most organic compounds)	1/7 of electronic value
Atomic (inorganic solids)	1 to 6,000
Dipole orientation	0 to 160
Nomadic (hyperelectronic, organic polymers)	0 to 300,000
Nomadic (hyperprotonic salts)	0 to 1,000,000

These supramolecular modes of polarization can be divided into those modes associated with the bulk properties of the different phases, and those modes more closely associated with the surfaces.

Interfacial Polarization. Interfacial Polarization

is also known as Maxwell-Wagner polarization. It occurs when two media, having different electrical properties, are in contact. A strong field and a disparity of charges arises at the interface, giving rise to the possibility of high effective polarizations. The myriad interfaces present in biological systems make this type of polarization universal in biology.

Surface-Associated Interfacial Polarization. This type of polarization arises from the region of contact between two different materials. The two materials will usually have different work functions or chemical potentials which will result in a potential difference across the interface and hence, a dipolar surface layer. If one or both of the materials is easily dissociated or has a high dielectric constant, then the creation of ions at this surface dipole layer can occur. These ionic double layers can be greatly affected by the presence of easily dissociated or easily adsorbed impurities. The presence of ionic double layers in aqueous suspensions of cells or colloidal particles is very common.

The ionic double layer, often referred to as the Helmholz double layer, can be thought of as having two types of mobile ions. An inner layer, known as the Stern layer, contains closely bound ions of low mobility, and an outer layer, known as the Gouy layer, contains loosely bound ions of high mobility.

Grimley and Mott (1947) showed that another electrical

double layer can exist within solids near their surfaces. AgBr particles in aqueous suspension, for example, have an ionic double layer on the solid side of the solid-liquid interface consisting of Ag^+ and Br^- ions, and an ionic double layer on the aqueous side consisting of aqueous ions. Such "double-double" layers also occur in biological systems.

Aqueous suspensions, such as suspensions of cells, are extremely difficult to characterize electrically. A seemingly simple system of water (dielectric constant 78) and suspended polymer particles (dielectric constant 2) can yield an effective dielectric constant of 10,000, due to the surface active ionic double layer associated with the particles. It is therefore clear that both bulk-bulk properties as well as ionic double layers play a part in such large dielectric constants. Similar results to the above example have been found with glass spheres or living cells suspended in aqueous media (Schwan, 1957; Cole et. al., 1935, 1936, 1938; Fricke and Curtis, 1937).

A large advance in understanding these extremely high effective dielectric constants was made by Schwan et. al. (1962) and Schwarz (1962) by using a model considering the bound or inner ion layer of the Helmholz double layer. The theory fit well with experiments on aqueous suspensions of polystyrene spheres. Schwarz's model assumed spheres of radius a with mobile but closely bound ions of charge e, mobility μ_b, and surface density p_o. The model further

assumes a double layer of negligible thickness compared with the particle radius. A volume fraction of spheres in suspension, p, will contribute a static dielectric increment of:

$$\Delta K_s = \frac{9}{4} \frac{pe^2 a p_o}{[1+(p/2)]^2 \varepsilon_o kT} \qquad (2)$$

An electrical dispersion of simple Debye-type was predicted, having a critical frequency, ν_{crit}, of

$$\nu_{crit} = \frac{1}{2\pi\tau} = (\mu_b kT/\pi a^2), \qquad (3)$$

or

$$\tau_{bound\ layer} = a^2/(2\mu_b kT) \qquad (4)$$

The critical relaxation time is predicted to be proportional to the square of particle radius, which agrees with experimental observations. The Schwarz theory was limited in that it did not consider the possibility of the bound ions exchanging with ions in the surrounding medium. It also ignored any contributions to the particle polarizability arising from the diffuse or loosely bound ions of the double layer.

Dukhin and Shilov (1970a, 1970b, 1970c, 1974; Dukhin,1973) considered the contributions of the diffuse ion layer and allowed ion exchanges with the medium. They concluded that neglecting these effects leads to an error in

determining the major source of the polarization. Dukhin and Shilov state that the major source of the polarization is the diffuse, outer, ionic layer and not the bound inner layer as proposed by Schwarz. Dukin's expression for the dielectric increment for the diffuse ion layer model is:

$$\Delta K = (9/2)pK_1[3m \exp(e\zeta/kT) + \exp(e\Psi^\delta/kT)]^2 \qquad (5)$$

where

$$m = \frac{e^2 K_1}{(kT)^2 6\pi n D},$$

ζ = zeta potential,

Ψ^δ = potential at the outer Helmholtz plane,

n = the viscosity of the medium and

D = the diffusion coefficient of the counterions.

The details of these two models were reviewed by Pohl (1978).

Plasmoidal Polarization. Plasmoidal Polarization occurs in wet porous solids such as ion exchange resins, or in the cell walls of bacteria. Some of the ions can be bound in such porous structures and be fixed, while the counterions are relatively free and mobile. Carstensen and Marquis (1974) report that the polarizabilities of such structures can be very large at low frequencies, about 10^2 to 10^5 Hz.

Polymeric Electrolytes. Polymeric Electrolytes exhibit both polar and ionic characteristics that are complex and difficult to describe simply. These biopolymers

can show features of both polymeric solutes and of colloidal particles. Huge polarizations can occur at low frequencies. Minakata et. al. (1972a, 1972b) have studied solutions of tetra-N-butyl-ammonium polyacrylate (Bu_4NPA), a polyelectrolyte. They observed two low-frequency dielectric dispersion peaks at 100,000 and 1,000 Hz. They assign the higher frequency peak of the two to bulk-bulk Maxwell-Wagner polarization. The lower frequency peak they associate with the displacement of counterions along the convoluted polymer chains. Similar studies on such poly-ions as DNA and RNA were made by a number of authors (Takashima, 1967). A theory for these systems has been proposed (Meyer and Vaughan, 1980).

An overview of both molecular and supramolecular dielectric response mechanisms can be found in Table II and in figure 2. Table II is a list of the major types of electrical polarization mechanisms. The table gives the magnitude of the dielectric response, in terms of the increment of the relative dielectric constant, that might be anticipated for each mechanism. Typical frequencies at which these mechanisms operate are given. Figure 2 plots the relative magnitudes of these mechanisms against frequency.

DEP Force

For the case of a perfectly insulating sphere of radius a, having a dielectric constant of ε_2, and immersed in a perfectly insulating medium of dielectric constant ε_1,

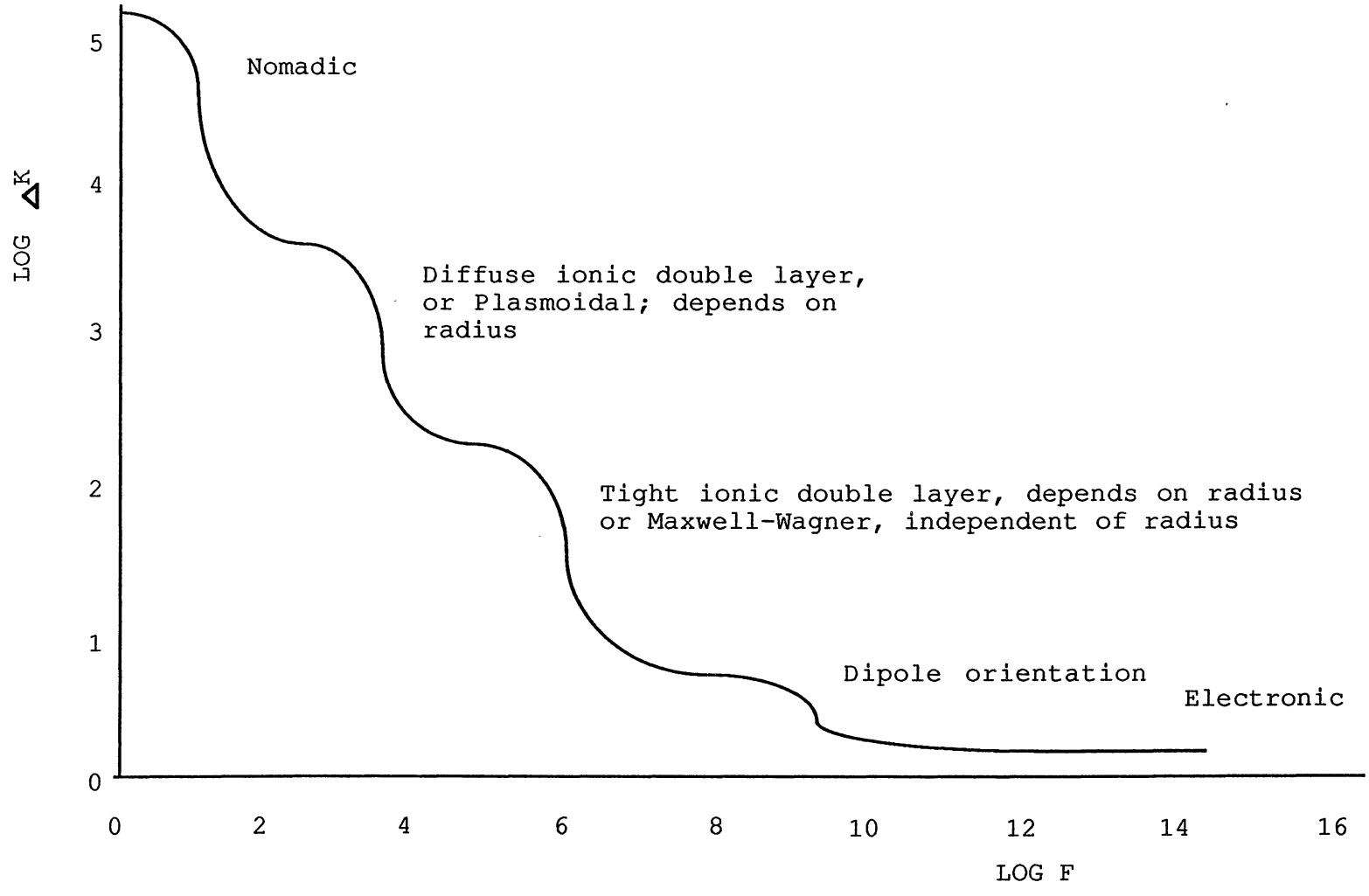

Figure 2. Contributions to the Dielectric Constant from the Various Polarization Mechanisms

TABLE II

TYPES OF ELECTRICAL POLARIZATION IN BIOMATTER

Type	Mechanism	Typical Frequency Response Maxima	Typical Dielectric Constant Increment $\Delta\varepsilon_r$ or ΔK
Electronic	Shift of electron orbitals relative to nucleus	10^{16} Hz	1 - 15
Atomic	Shifts of atoms of one charge relative to others of differing charge	10^{12} - 10^{14} Hz	0.1 - 1
Dipole Orientation	Twisting of pre-existing group of molecular dipoles	10^{6} - 10^{11} Hz	1 - 38
Nomadic	Long range drift of electrons, holes, or protons	10^{2} - 10^{4} Hz	100 - 10^{6}
Maxwell-Wagner	Interfacial charge accumulations of charge drifting in bulk-to-bulk contents	10^{5} - 10^{7} Hz	1 - 10^{5}
Surface-Associated	Distortion of ionic double layers, at a liquid-solid juncture		
a) Schwarz	Response of ions of inner (tightly bound) Stern layer of Helmholtz double layer	10^{5} - 10^{7} Hz	1 - 1000
b) Dukhin	Response of diffuse ions of outer (Gouy) layer of Helmholtz double layer	10^{2} - 10^{5} Hz	1 - 100,000
c) Grimley-Mott	Electron-hole or ion population shifts near interface within solids	10^{4} - 10^{9} Hz	1 - 100
Plasmoidal	Ion drift in porous networks of relatively fixed counterions	10^{2} - 10^{5} Hz	1 - 1000

the DEP force has been given by Pohl (1958,1978) as:

$$F = 2\pi a^3 \varepsilon_o \left[\frac{\varepsilon_1(\varepsilon_2-\varepsilon_1)}{\varepsilon_2+2\varepsilon_1} \right] (\vec{\nabla}|E_o|^2) \qquad (6)$$

where ε_o is the permittivity of free space and $|E_o|$ is the magnitude of the electric field (dc or rms ac) in the medium. This expression was verified experimentally by Pohl, Pollock, and Crane (1978, or Appendix B)

The calculation of the force expression for real materials, (a lossy dielectric particle in a lossy dielectric medium), is more difficult, indeed it is the subject of some debate (Sher, 1968; Pohl and Crane, 1972; Jones and Kallio, 1979; Jones, 1979, 1984; Denner and Pohl, 1982; Sauer, 1983; Mognaschi and Savini, 1984). Pohl and Crane (1972) have derived a general force equation for the time average force on a body of complex permittivity $\varepsilon_2=\varepsilon_2'-i\sigma_2/w$ in a medium of complex permittivity $\varepsilon_1=\varepsilon_1'-i\sigma_1/w$, placed in a nonuniform electric field originally of strength E_o, as

$$F = -\tfrac{1}{4}\varepsilon_o \int_{body} \mathrm{Re}\ \vec{\nabla}(\varepsilon_1^*(1-\varepsilon_2/\varepsilon_1)E_o\ E)\ dv \qquad (7)$$

Where ε_1^* indicates the complex conjugate of ε_1, and E is the resultant field inside the body. For a spherical body, this expression reduces to the expression given by Sher (1968) and Pohl (1978)

$$F = 2\pi a^3 \varepsilon_o \, \mathrm{Re}\left[\frac{\varepsilon_1^*(\varepsilon_2-\varepsilon_1)}{\varepsilon_2+2\varepsilon_1}\right] \nabla(E_o)^2 \qquad (8)$$

Where a is the particle radius. Equation 8 can be seen to be the same as equation 6 with the static dielectric constants being replaced by their complex counterparts.

Sauer (1983) and Jones (1979) and Jones and Kallio (1979) have arrived at a slightly different expression for the DEP force using differing approaches.

Jones defines an effective dipole moment and derives the force expression as:

$$F = 2\pi a^3 \varepsilon_o \varepsilon_1' \, \mathrm{Re}\left[\frac{(\varepsilon_2-\varepsilon_1)}{\varepsilon_2+2\varepsilon_1}\right] (\nabla|E_o|^2) \qquad (9)$$

Equation 9 differs from equation 8 only in that the complex conjugate of ε_1, (ε_1^*) in equation 8 is replaced by the real part of ε_1 (ε_1') in equation 9.

Sauer (1983) takes a more fundamentally correct approach by noting that in a system with frictional losses, (i.e. lossy dielectrics), energy is not conserved and the energy method (Schwarz,1963; Pohl and Crane,1972), which uses the energy of the body in the field to calculate the force, is invalid. Sauer uses the principle of the conservation of momentum of the field to derive a DEP force on the body in the field. Sauer's expression is identical to the expression derived by Jones, shown in equation 9.

To determine how much equations 8 and 9 differ, calculations were made using the values for $BaTiO_3$, a high dielectric constant material, as the test sphere. Figures 3 and 4 show the calculated effective dielectric constant as a function of the frequency of the applied field. Figure 3 shows the results assuming a solution conductivity of 1 μS/cm, a commonly used conductivity in DEP experiments. As can be seen, the curves for the two equations start diverging greatly in the range of 1 to 10 kHz. Figure 4 assumes a solution conductivity of 1000 μS/cm, quite high for DEP. Here, the two equations diverge at a much higher frequency, 1MHz. These figures show that the two equations do give different results at conditions of frequency and solution conductivity that are likely to occur in biological DEP experiments. Care must be taken, then, to use the correct equation, equation 9.

CSR Torque Expression

The behavior of cells in a rotating electric field is quite different than might normally be expected. Cells exhibit a positive DEP force, i.e. towards the strong field region, over the frequency range 100 Hz to 10^6 Hz, and a similar response might be expected for a rotating field. However, instead of following the rotation of the field, cells exhibit negative rotation, in the opposite direction from the field. The rotation rate of the cells is low, from 10^{-1} Hz to 1 Hz.

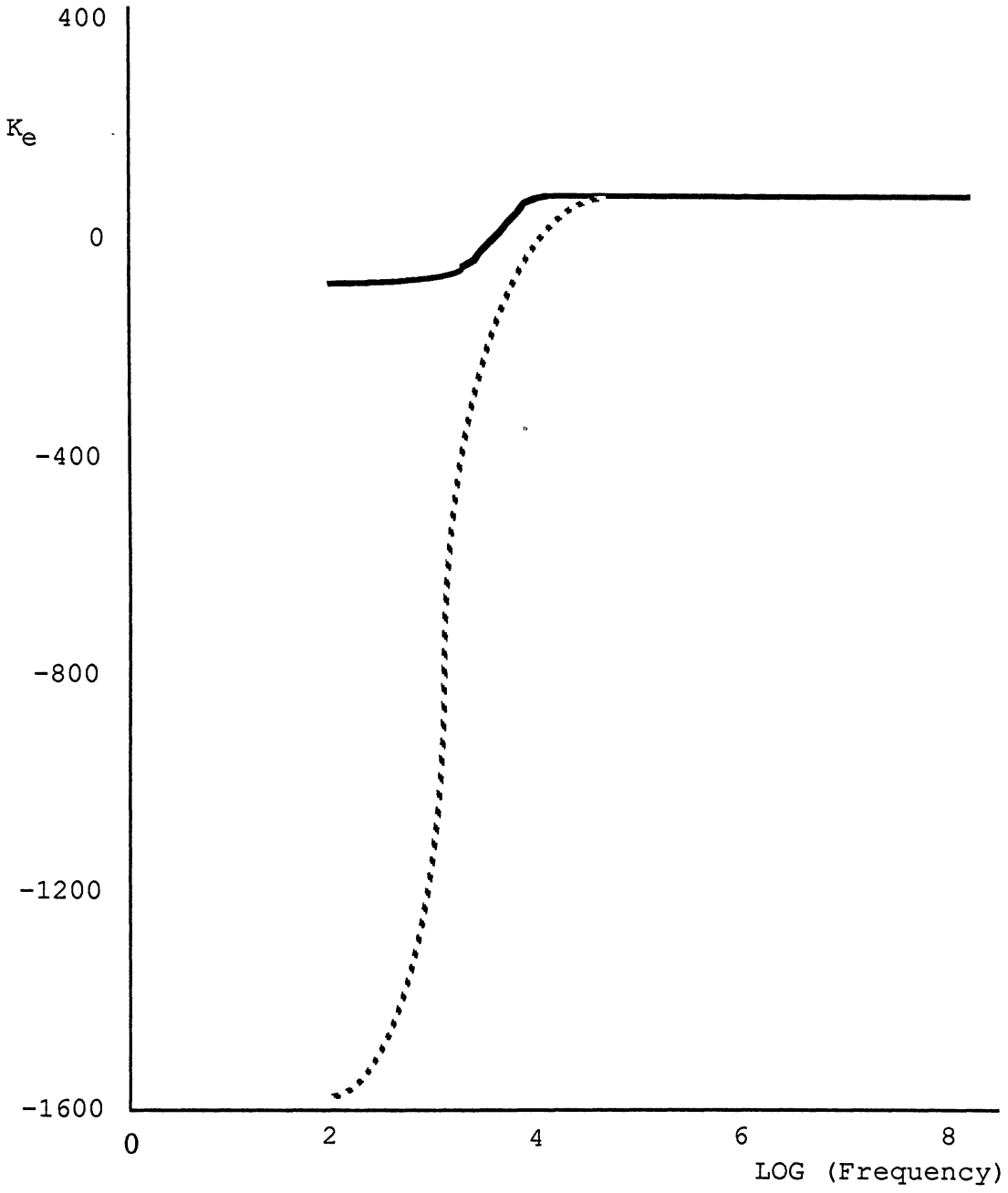

Figure 3. Two DEP Force Equations at Low Solution Conductivity. ····· Equation 8; —— Equation 9

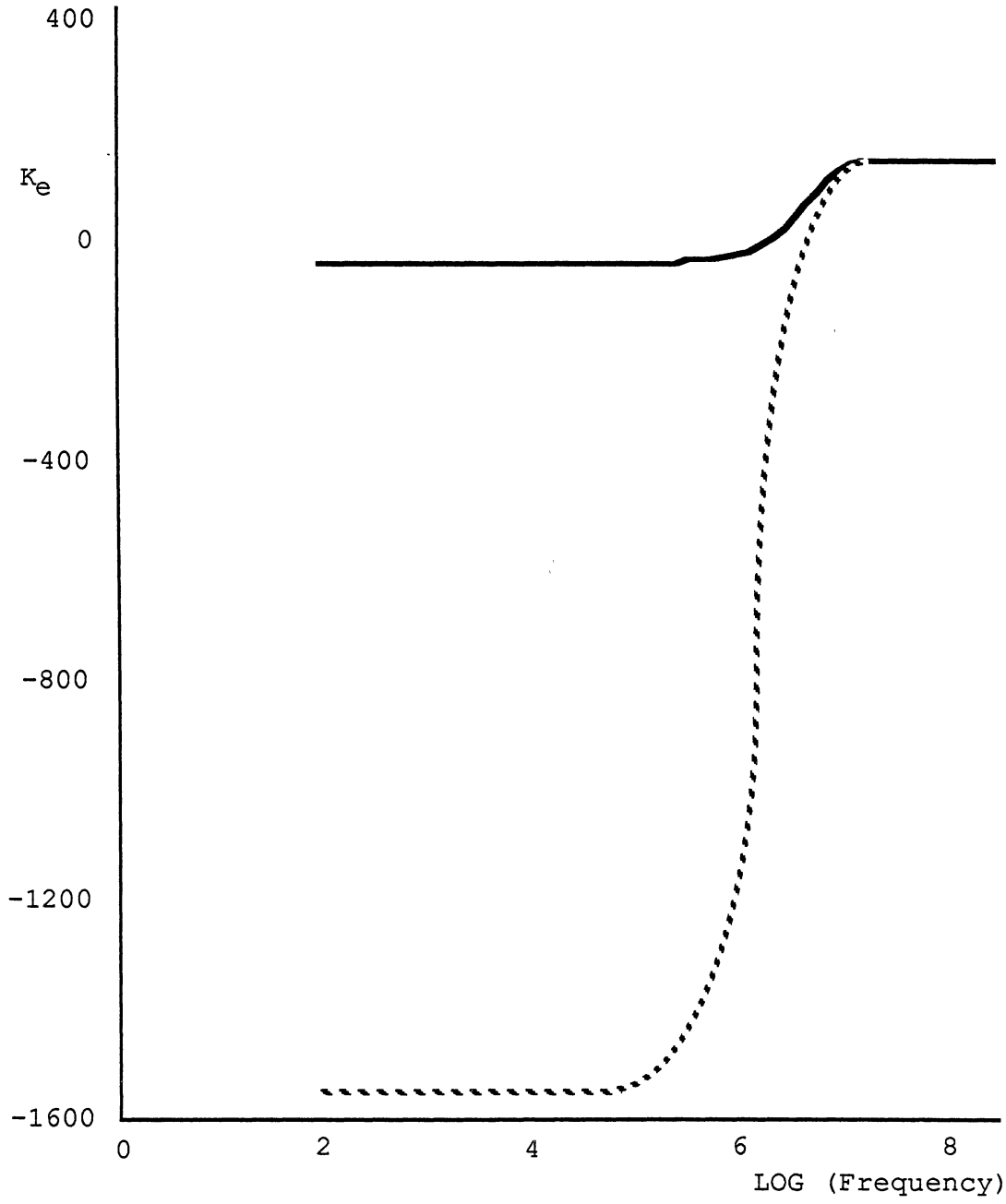

Figure 4. Two DEP Force Equations at High Solution Conductivities.·····Equation 8; ——— Equation 9.

A model for cellular CSR has been proposed (Polk, 1985). Assuming a cell of conductivity σ_2 and dielectric permittivity ε_2, suspended in a fluid medium of conductivity σ_1 and dielectric permittivity ε_1, the cellular rotation rate is given by:

$$\Omega = \frac{3wE_0^2\varepsilon_1 \quad (\sigma_2\varepsilon_1 - \sigma_1\varepsilon_2)}{2n(2\varepsilon_1 + \varepsilon_2)^2 \quad \left[\frac{2\sigma_1 + \sigma_2}{2\varepsilon_1 + \varepsilon_2} + w^2\right]} \qquad (10)$$

where w is the frequency of the applied field, E_0 is the magnitude of the applied field, and n is the viscosity of the fluid medium.

The model correctly predicts the dependence of rotation rate on the square of the applied voltage (Mischel and Pohl,1983).

The ac Fields from Cells

Fröhlich (1980) observed that the electric field across a cell membrane is on the order of 10^8 volts/meter, which causes the membrane molecules to be highly polarized. These highly polarized molecules interact and, under certain conditions, behave in a cooperative fashion. Fröhlich's theory predicts that if the membrane is supplied with energy above a minimum level, then one phonon mode will predominate and the molecules will interact in a coherent vibrational mode that is calculated to be on the order of 10^{11} Hz.

Rowlands and his co-workers (Rowlands et. al.,1981;

Rowlands, Sewchand, and Ennis,1982a,1982b; Sewchand, Roberts, and Rowlands,1982) have discovered an attraction between red blood cells that causes the formation of rouleaux at a greater rate than expected from Brownian motion. This force has been attributed to a Fröhlich interaction; it disappears in metabolically depleted cells or when the membrane potential is not present. The force seems to be mediated by long chain macromolecules in the suspending medium.

The attraction of high dielectric constant particles in the micro-DEP experiments of Pohl et. al. (1981) has been attributed to cellular ac fields produced by coherent electromagnetic vibrations postulated by Fröhlich. The frequency of these fields is lower than predicted by Fröhlich, 10^5 to 10^6 Hz.

CHAPTER III

A CONTINUOUS DEP SORTER/ANALYZER

This chapter will describe the development and operation of an automated, continuous DEP Sorter/Analyzer. Pohl, Kaler, and Pollock (1981 and Appendix B) were the first to demonstrate a continuous DEP chamber capable of measuring both positive and negative DEP deflections. This chamber was also used to separate cells (Pohl and Kaler,1978). The automated system described in this chapter is an extension of this work.

An automated system has the advantage of ease of operation and speed in obtaining a spectrum. Traditional batch methods require about two hours to obtain a DEP spectrum of ten to fifteen points. A manually operated continuous system has about the same performance. An automated continuous system is much faster, being able to complete a spectrum of thirty points in about an hour. Some cells are delicate and deteriorate rapidly after being prepared. An automated system can produce a spectrum from these cells that would be very difficult or impossible to do manually.

Principle of Operation

The chosen system, seen schematically in figure 5, is a stream-centered continuous flow system. This system was selected because it has many desirable qualities not possessed by other DEP methods. In this system, a stream of particles is established in the center of the flow chamber. The stream then moves past the electrodes and is deflected one way or the other (positive or negative DEP). Since the stream is in the center of the flow chamber and can move in any direction, it is the only method that can easily quantify both a positive and negative DEP response. Both batch and semi-batch methods rely on the collection of cells on the electrodes so only positive DEP is measurable. Single cell DEP can measure either positive or negative response but not both in the same experiment.

The fact that the stream is free to move in any direction is also an important factor in achieving sharp separations. With the proper choice of solution conductivity and applied field frequency, one type of particle can experience negative DEP while another type of particle experiences positive DEP. The particles will move in opposite directions providing a sharp separation.

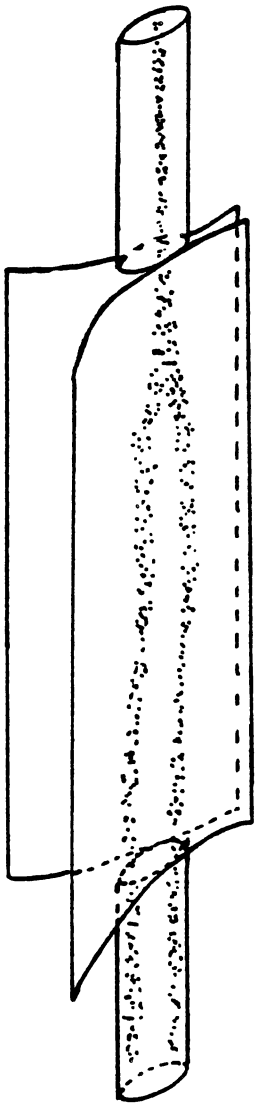

Figure 5. Schematic Representation of Continuous DEP

Chamber Design Considerations

Electrode Dimensions

Biological DEP places a second restriction on the electrode configuration in that the size of the electrodes must be smaller than those used in mineral separations. The following calculation will determine the practical size limit for a biological DEP separator/analyzer. Mason and Townsley (1971), in their attempt to demonstrate a continuous DEP separator, used a cylindrical electrode design that had been used successfully as a mineral separator by Pohl and Schwar (1959, 1960). The velocity of cells in this chamber will be calculated to show that DEP chambers used for biological particles in aqueous solutions must be smaller than those used with insulating liquids. The DEP force on a cell can be written as

$$F_{DEP} = 2\pi a^3 \varepsilon_o K_\bullet \nabla(E_o)^2 \qquad (11)$$

where a is the cell radius and $K_\bullet$ is the effective net polarizability. For frequencies in the range of interest, $K_\bullet$ has been observed to range from 0 to 100 for single yeast cells (Chen and Pohl,1974; Crane and Pohl,1978).

When the cell is moving at a constant velocity, the DEP force and the viscous drag forces will be equal. The viscous drag force is given by Stoke's equation,

$$F = 6\pi n a v \tag{12}$$

where n is the viscosity of the medium. The velocity of the cell can be calculated from equations 11 and 12 as

$$v = \frac{a^2 \varepsilon_o K_* \vec{\nabla}(E_o)^2}{3n} \tag{13}$$

The chamber in question has a wire inner electrode centered inside a cylindrical outer electrode. The inner electrode is 0.64 mm. in diameter and the outer electrode has an inner diameter of 11 mm . The potential for this chamber is

$$V = V_o \frac{\ln(r/R_o)}{\ln(r_o)/R_o)} \tag{14}$$

while

$$\vec{\nabla}(E_o)^2 = \frac{2V_o^2}{[\ln(r_o/R_o]^2} \cdot \frac{1}{r^3} \tag{15}$$

Where R_o is the radius of the outer electrode, r_o is the radius of the central wire electrode, r is the current position and V_o is the potential difference applied to

the electrodes. Equation 15 is substituted into equation 13 to give

$$v = \frac{2a^3\varepsilon_o K_\bullet V_o^2}{3n[\ln(r_o/R_o)]^2 r^3} \qquad (16)$$

The aqueous media used to suspend most cells restrict V to a maximum value on the order of 10 volts. The other values chosen for this calculation are:

$a = 4 \times 10^{-6}$ m

$n = 10^{-3}$ Kg·m^{-1}·s^{-1}

$\varepsilon_o = 8.85 \times 10^{-12}$ F·m^{-1}

$r_o = 3.2 \times 10^{-4}$ m

$R_o = 5.5 \times 10^{-3}$ m

$r = 2 \times 10^{-3}$ m

$K_\bullet = 100$

The velocity calculated from equation 16 for this particular chamber using typical values is 1.46×10^{-8} m/s. At this velocity, the cell would take 28 minutes to move a significant distance of 25 μm. It is apparent from these figures that a chamber of this size would be unsuitable for biological DEP. All that remains is to calculate what size electrodes would give sufficient velocity to cells so that their movement is detectable in a reasonable amount of time.

Isomotive electrodes, the desired "ideal shape", will be used as the electrode geometry. For isomotive geometry, the potential has been given by Pohl (1968) as:

$$V = V_0(r/r_{60})^{3/2} \sin(3\theta/2) \qquad (17)$$

Where r_{60} is the critical electrode spacing. The gradient of the square of the field can then be written as:

$$\vec{\nabla}|E_0^2| = 9/4\ V_0^2\ r_{60}^{-3} \qquad (18)$$

Equation 12 can then be used to calculate r_{60}.

$$r_{60} = \left[\frac{3\varepsilon_0 K_e a^2 V_0^2}{4nv} \right]^{1/3} \qquad (19)$$

A reasonable value to expect for the velocity of a cell is 1 μm/s. If the values of the previous calculation are used, then r_{60} = 1.02 mm. The maximum chamber dimension for biological DEP must therefore be on the order of 1 mm..

Electrode Geometries

Certain restrictions are placed on the field produced by the electrodes when a DEP chamber is used as an analyzer or separator. One such restriction is on the electrode configuration. Some electrode configurations produce a field that is too non-uniform. The cylindrical electrodes used successfully as a mineral separator by Pohl and Schwar

(1959, 1960) produce a field whose force varies as r^{-3} with the distance from the central electrode. If a cell is three times farther from the central electrode than an otherwise identical cell, then the force the more distant cell experiences will be 3^3 or 27 times smaller than the closer cell simply because of the difference in their positions. For the present application of a cell separator/analyzer, such a dependence on position is unacceptable. For a chamber to be effective as a separator, it must operate on the sometimes small differences in the polarizabilities of cell types. Any variation with position of the DEP force will tend to mask these differences. Similarly, for a chamber to operate as an analyzer, any variation with position of the DEP force would make it very difficult to observe the action of the polarization mechanisms that will be discussed later in this chapter.

An ideal electrode shape would be one which produced a DEP force on a cell that was constant over the volume of the chamber. Such an electrode configuration, called isomotive electrodes, was used for mineral separations by Pohl and Plymale (1960) and later derived rigorously by Pohl (1968). The ideal isomotive field must be closely approximated in any practical DEP chamber to be used as a separator/analyzer. Appendix C is a study of electrode configurations for various DEP force laws. Electrode configurations producing DEP forces with different dependencies on position are sketched. From the diagrams it

is seen that the form of the dependence on position of the DEP force is very sensitive to the electrode configuration and that to achieve an isomotive field the ideal isomotive electrode configuration must be closely approximated.

The DEP Chamber

The chamber used in Appendix B was a "dry electrode chamber in which there are glass walls between the electrodes and the flow chamber. A "dry" electrode system has a disadvantage in that frequencies below about 100 kHz are greatly attenuated by the glass capillary walls (see figure 5b in Appendix A). A "wet" electrode system eliminates this problem and allows the full frequency range to be studied.

Figure 6 shows the electrode chamber design. The electrodes are cylindrical, gold plated brass 4 mm. in diameter. The electrodes are 200 mm. long with the flow chamber being about .7 mm. in diameter. The electrode holder is plexiglass and encloses the electrodes completely. The holder keeps the electrodes rigidly in place at a spacing of 1mm.

The expression for the gradient of the square of the field for this electrode configuration is given by Appendix A as:

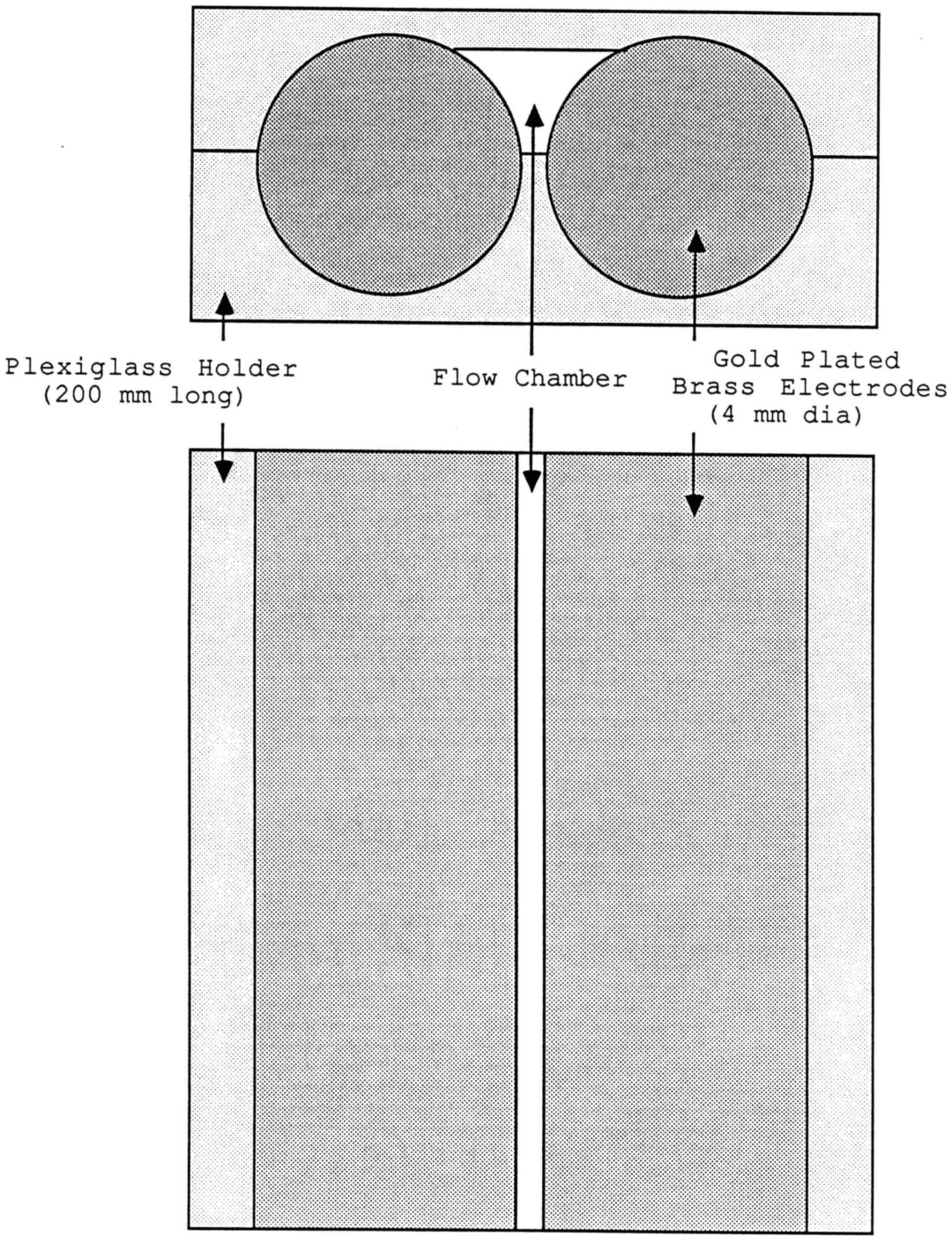

Figure 6. The Continuous DEP Flow Chamber

$$\vec{\nabla}(E_0^2) = 2C_1^2 \left[\left[\frac{-d\cos\theta}{r^2} \right] \left[\frac{2}{r^2} - \frac{2(r-d\cos\theta)^2}{r^4} \right] - \frac{2d^2 \sin^2\theta\,(r-d\cos\theta)}{r^6} \right] \hat{r}$$

$$+ \frac{2C_1^2}{r} \left[\left[\frac{-d\cos\theta}{r^2} \right] \left[\frac{d\sin\theta}{r^2} - \frac{2rd\sin\theta(r-d\cos\theta)}{r^4} \right] + \frac{d^2\sin\theta}{r^4} \left[\cos\theta - \frac{2d\sin^2\theta}{r} \right] \right] \hat{\theta} \quad (20)$$

where $C_1 = \dfrac{\Delta V}{2\ln((d-a)/a)}$

and a is the radius of the electrode, d is the distance between their centers, and r is the distance from the electrodes (figure 3 in Appendix A). The square of the gradient of the field for the chamber, calculated from equation 20, is plotted in figure 7.

As is obvious from the figure, this configuration does not give the ideal isomotive field. But the figure also shows that the force varies little over the active region of the flow chamber. To achieve the true isomotive electrode shape in such small dimensions would be impractical, but it can be seen from the figure that the chosen configuration is adequate.

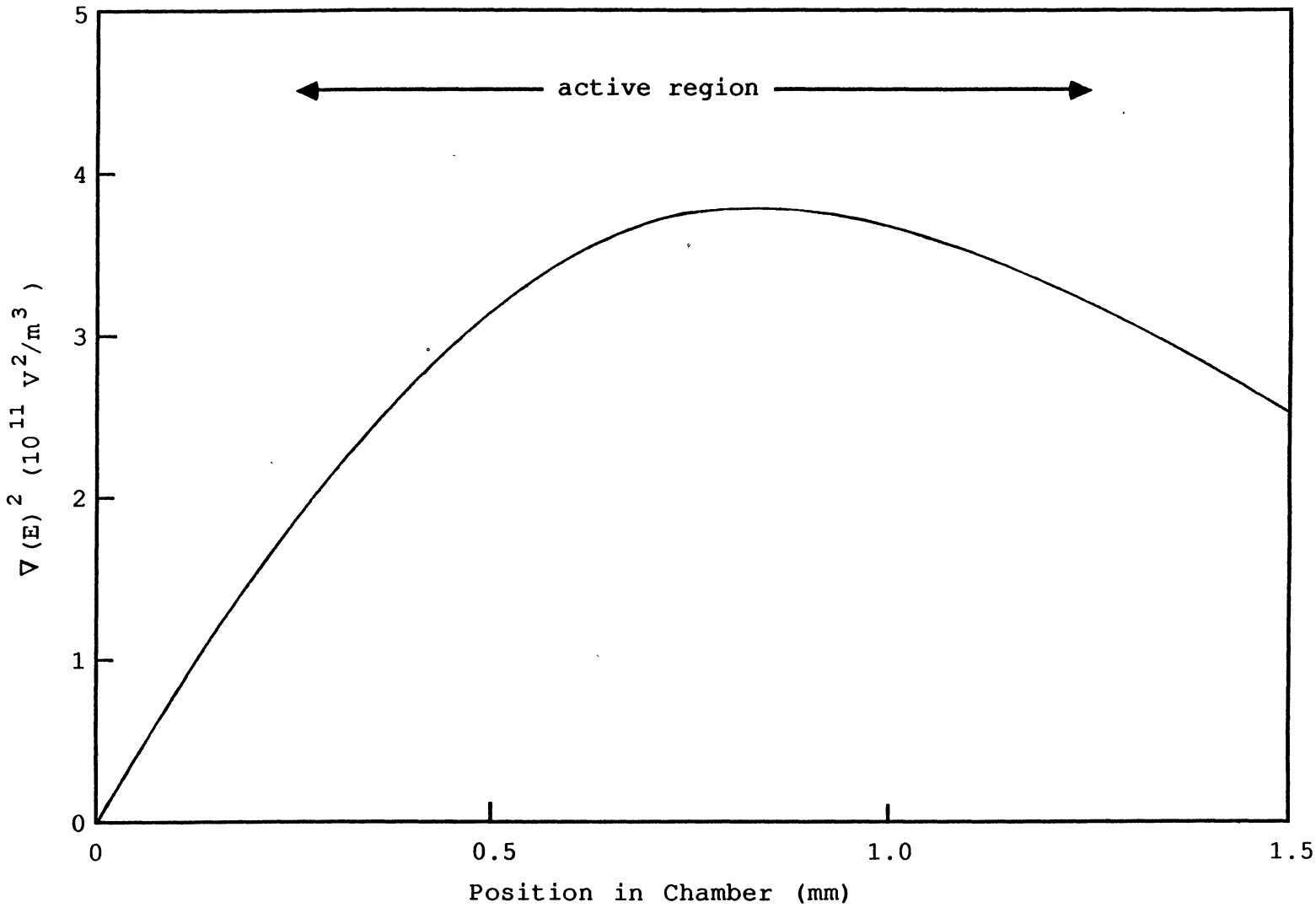

Figure 7. DEP Force Across the Flow Chamber

The Stream Injector

A narrow and stable stream is essential to the continuous DEP system. The key to establishing the stream is the stream injector. Figure 8 shows the design of the stream injector for the chamber. The stream injector used for a previous version is shown in figure 8 of Appendix A.

A stable stream requires the cells flowing out of the center needle to have a lower velocity than the support stream into which they are injected. The velocity of the support stream in the center of the tube is twice the average velocity of the stream, so that:

$$V_c \leq 2V_s$$

or

$$\frac{\text{Volume}_c/\text{Time}}{\text{Area}_c} \leq \frac{2\ \text{Volume}_s/\text{Time}}{\text{Area}_s} \qquad (21)$$

Where V_c denotes the average velocity of the cell stream and V_s denotes the average velocity of the support stream.

An infusion pump (Harvard Apparatus model 975) supplied the two streams that were mixed in the stream injector. A 25 µl. syringe was used for the cell stream and a 5 ml. syringe was used for the support stream. These syringes delivered 10 µl. and 2.58 ml. respectively in the same amount of time. Substituting these values into equation 21 gives:

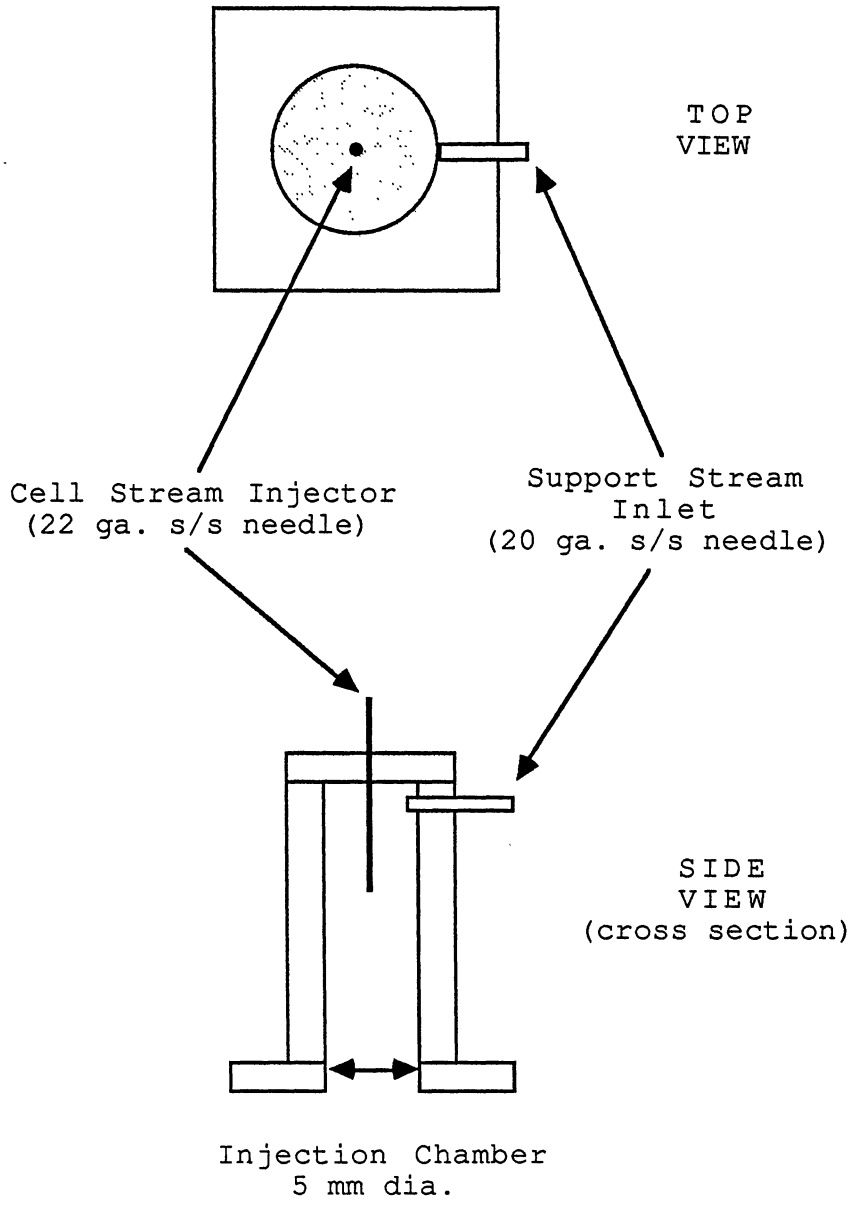

Figure 8. Cell Stream Injection Chamber

$$\frac{10\ \mu l}{\pi r_c^2} \leq \frac{2(2.58\ ml)}{\pi r_s^2} \qquad (22)$$

$$\left[\frac{r_s}{r_c}\right]^2 \leq 516$$

$$\frac{r_s}{r_c} \leq 22.7$$

The needle for the stream injector is a 22 gauge needle inside 5mm chamber which gives a ratio of 15 for their diameters, well within the limit.

Flow Splitter Design

Once the cell stream has been separated into its component parts, the cells must be collected. The splitter design, shown in figure 9, allows two fractions from the original stream to be collected. Counter flow, introduced from the bottom tube, prevents cells from being trapped in the slow moving fluid along the walls of the outlet tubes. Valves in the outlet lines allow the stream split position within the main tube to be selected. The flow tubes are 1.5 mm in diameter.

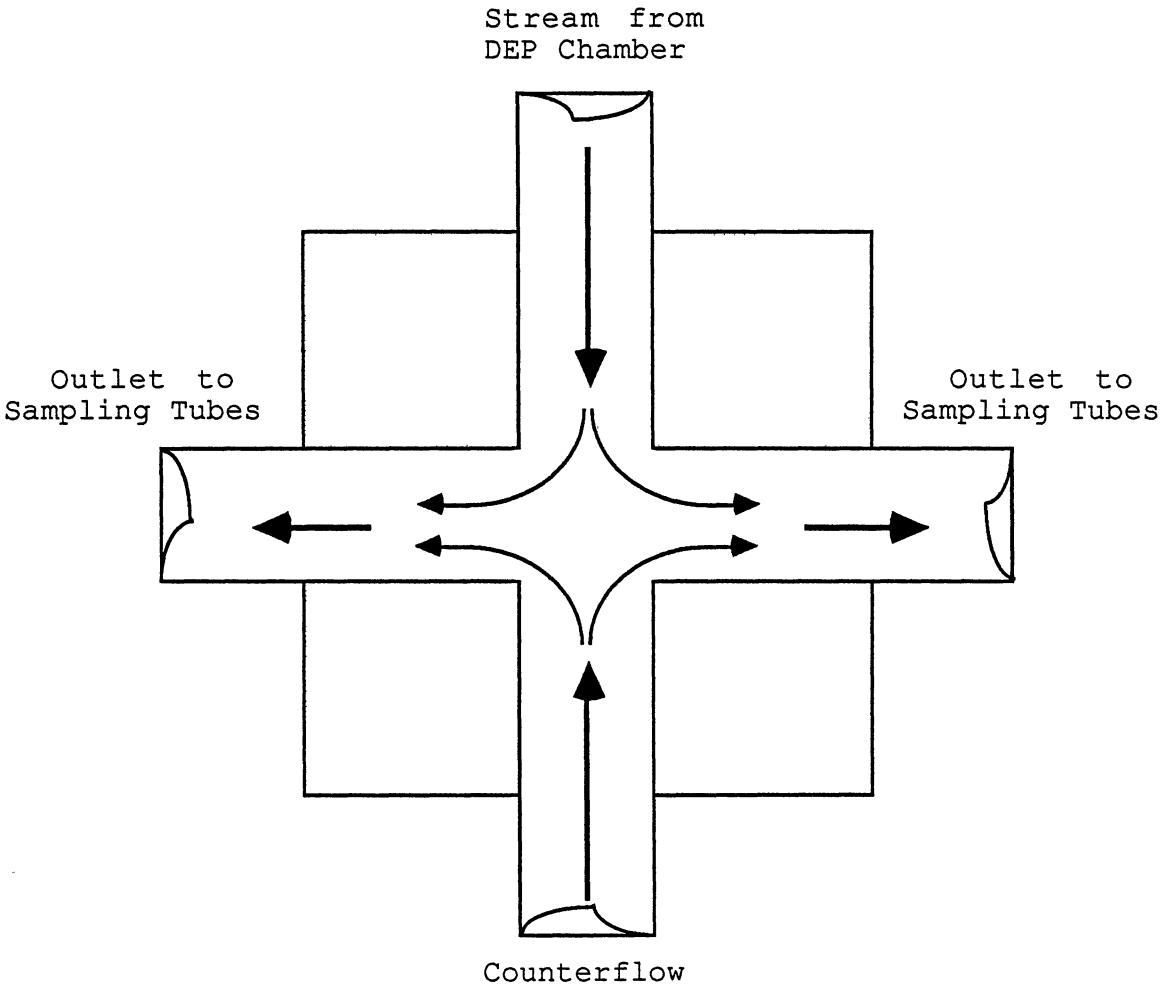

Figure 9. Stream Flow Splitter

The Hydraulic System

Figure 10 is a schematic representation of the continuous DEP sorter/analyzer system. The heart of the mechanical and hydraulic system is the DEP electrode chamber described previously. The electrodes are connected to the Hewlett-Packard frequency synthesizer which supplies the field at various frequencies.

The chamber is connected to the stream splitter by a square capillary of .9 mm. or 1.0 mm. i.d. The whole assembly is then mounted on a microscope stage. The cell stream can be observed either in the square capillary tube or in the flow splitter by a TV camera mounted on one eyepiece of the microscope.

The stream injector is mounted above the electrode chamber to provide a narrow stream flowing down the middle of the chamber. The flow is regulated by an infusion pump (Harvard Apparatus Model 975). Two 5 ml syringes, one providing the support stream, the other providing counterflow for the stream spiltter are used along with a smaller 25 µl syringe used to inject the cells through the central needle into the support stream.

Cells are introduced into the injection line through valve #1. A valve on each outlet port (not shown) allow the position of the stream split to be adjusted within the chamber.

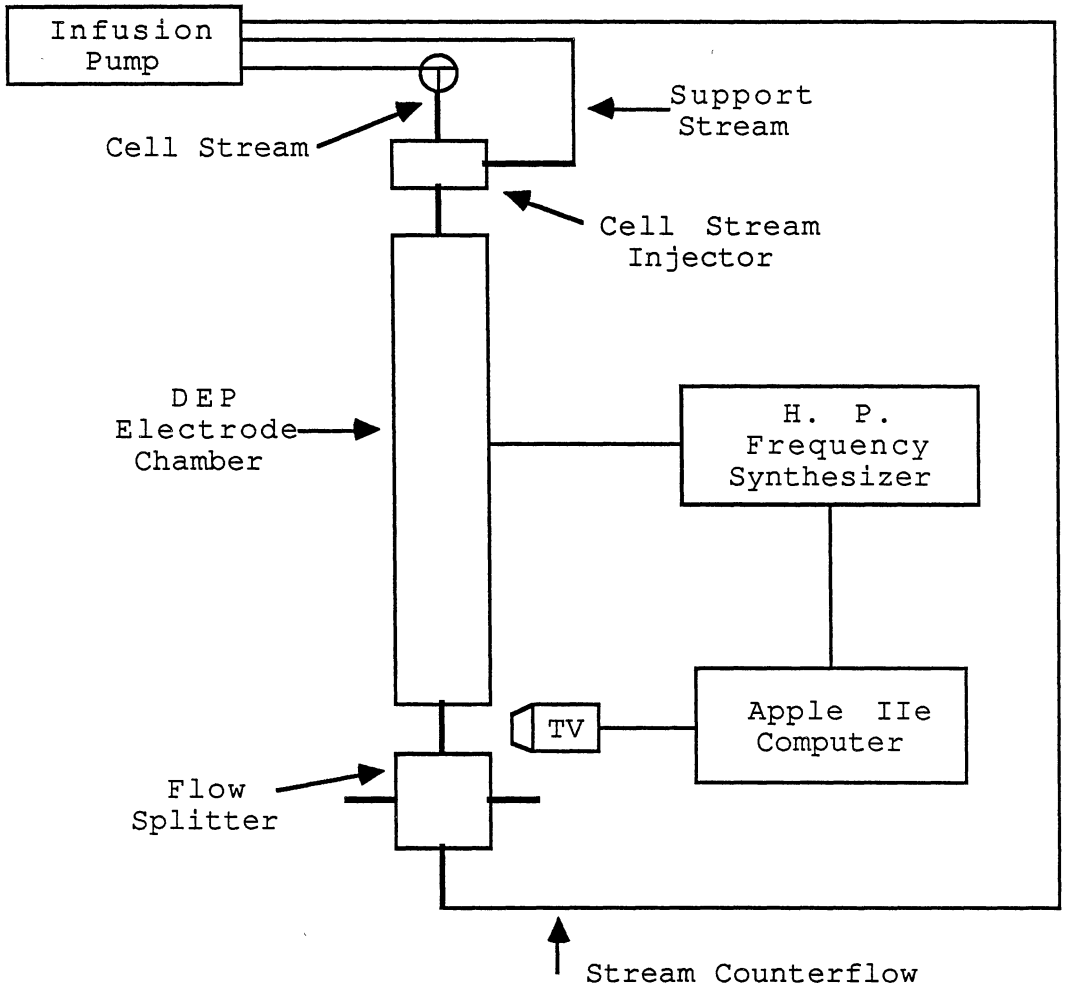

Figure 10. Schematic of Continuous DEP System

Optical Sensing

Optimum viewing in the square glass capillary occurred with cells lit from the side by a 5 mW laser (Spectra Physics), resulting in brightly lit cells in an otherwise dark field. The cells are viewed through a microscope equipped with a TV camera. The video signal is then analyzed by the computer. In separation mode, the cell stream is viewed directly in the flow splitter to allow the operator to adjust the stream split.

The Electronic System

The electronic system is designed to take data from the continuous DEP chamber, display it, and store it for later use. An Apple II+ computer controls the experiment, using software developed for this application (Appendix D), giving commands to the other elements in the system. A Hewlett-Packard (model 3325A) frequency synthesizer supplies the electric field to the DEP chamber. It is capable of producing a 4 Vrms signal with a frequency up to 20 MHz. The synthesizer is controlled by the Apple computer through an IEEE 488 interface.

The Apple computer also receives the signal from the RCA TC1000 TV camera and digitizes it (Microworks DS-68 Digisector board). The cell stream position, width, and distance moved under the influence of the field is calculated. This information is displayed on the screen. The

information, along with the raw scan data, is also stored on disk for later use.

The data from the experiments is analyzed and plotted using a locally written software package ("Curve Analysis" by Jerry Merz, Dept. Biochemistry) and plotted on a dot matrix printer (C.itoh 8510A).

Operation and Typical Curves

Cells used in the sorter/analyzer must be prepared the same as for other DEP experiments. The cells are harvested and washed in a low conductivity solution of an isoosmotic sugar, or simply in low conductivity water for the hardier cells. When a concentrated cell suspension with a conductivity usually less than 300 μS/m is obtained, the DEP chamber and the support stream syringe are loaded with the same solution used to suspend the cells. Care must be taken to have the conductivities of the cell suspension and the support stream equal so there are no polarization differences in the two liquids that might interfere with observing the cell polarization.

After all bubbles have been flushed from the system, a background scan is done of the glass capillary. The background scan will be subtracted from all the cell scans to reduce the noise from light scatter caused by the walls and dirt in the system. A cell stream is then established in the chamber and the computer is given the parameters for the scan. The required parameters are: beginning frequency, stop

frequency, number of points, applied voltage, and length of time between scans. The system will then do a zero field scan to get the initial stream position and then proceed to take the data for the spectrum.

Figures 11 and 12 show typical spectra, of live and dead yeast respectively, taken by the sorter/analyzer. Both spectra contain 25 to 30 points and are more detailed than any spectra recorded by hand.

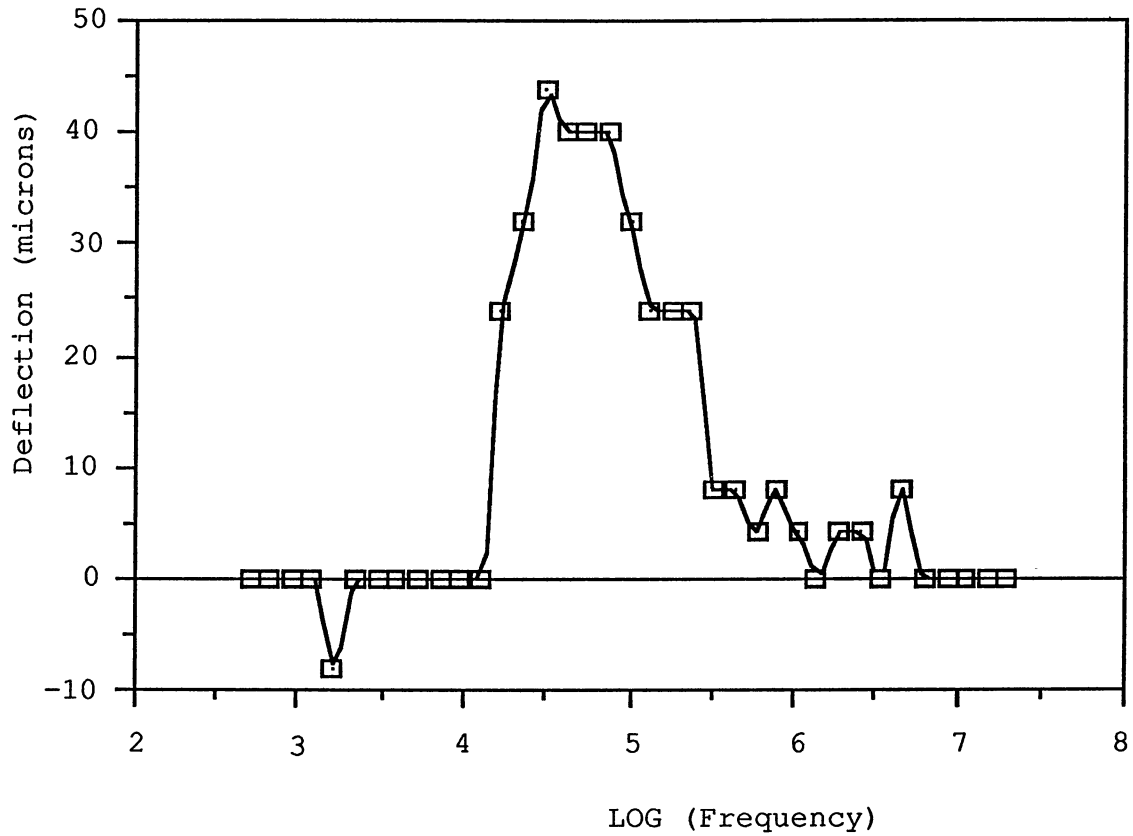

Figure 11. DEP Spectrum for Live Yeast.
(*Saccharomyces cerevisiae*).
Conductivity = 3.3 μ S/cm.
Voltage = 2.5 Vrms

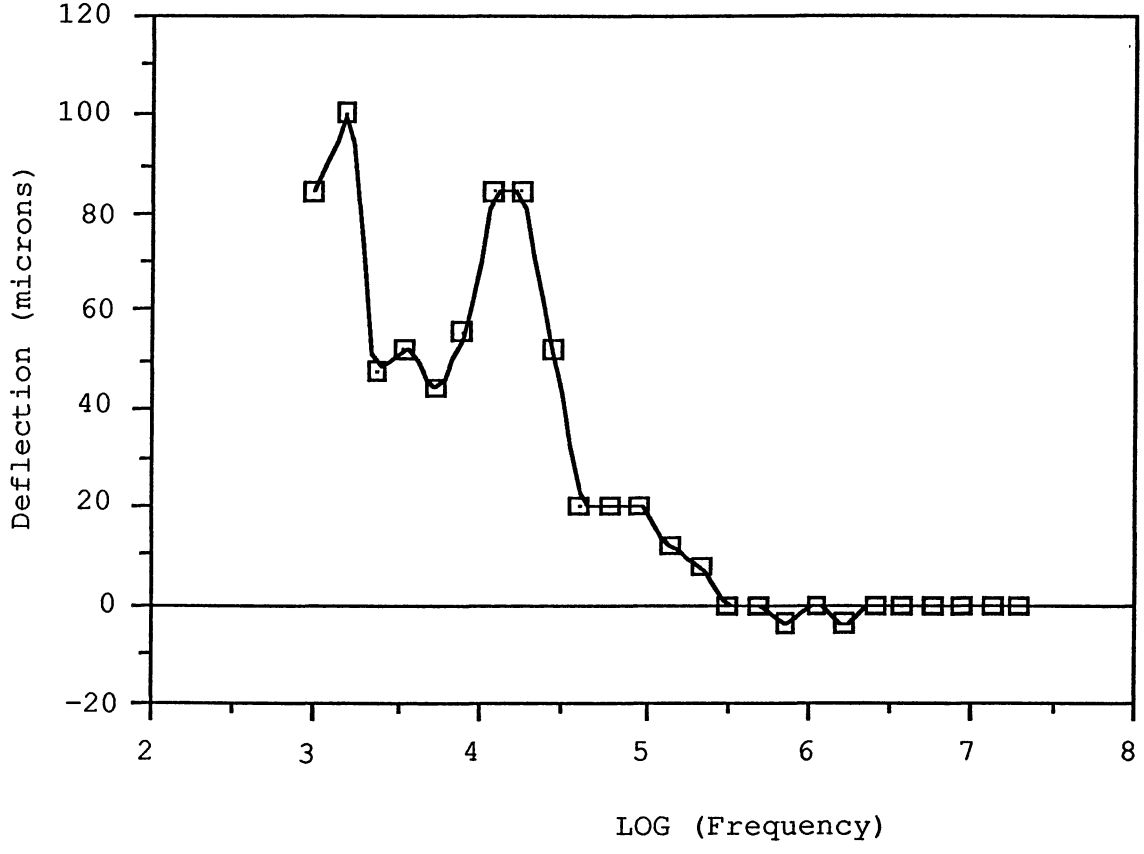

Figure 12. DEP Spectrum for Dead Yeast, (*Saccharomyces cerevisiae*). Conductivity = 83.3 µS/cm. Voltage = 2 Vrms.

CHAPTER IV

CSR STUDIES

Cellular Spin Resonance (CSR) has recently been developed as a way to characterize the electrical properties of cells that is different from standard DEP characterization. That cells respond differently to a rotating electric field can be seen in figure 13. A standard DEP translation curve for yeast is plotted in figure 13 along with a standard CSR curve for the same organism. As can be seen, the translation curve is positive for this frequency range indicating attraction to the strongest field region. The CSR curve, however, shows negative rotation; the cell is rotating opposite to the direction of the field rotation. Since positive DEP translation means that the cell is highly polarized, then the cell would be expected to rotate in the same direction as the field in CSR. Obviously DEP and CSR look at different aspects of cell polarization.

Experimental Methods

To subject cells to a rotating electric field, a CSR chamber with four electrodes was built on a microscope slide. Figure 14 is a diagram showing the four pole chamber design. The electrodes are arranged so that the cells to be

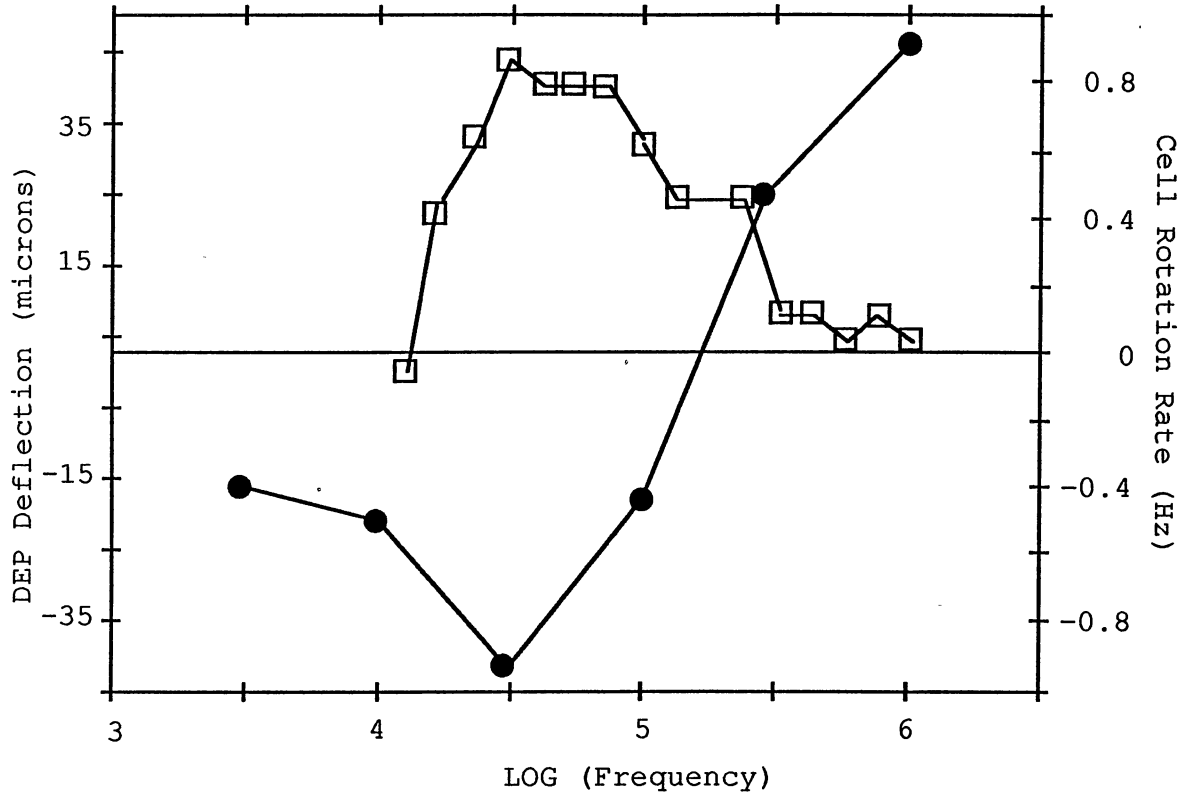

Figure 13. Comparison Between the DEP Deflection Spectrum and the CSR Rotation Spectrum

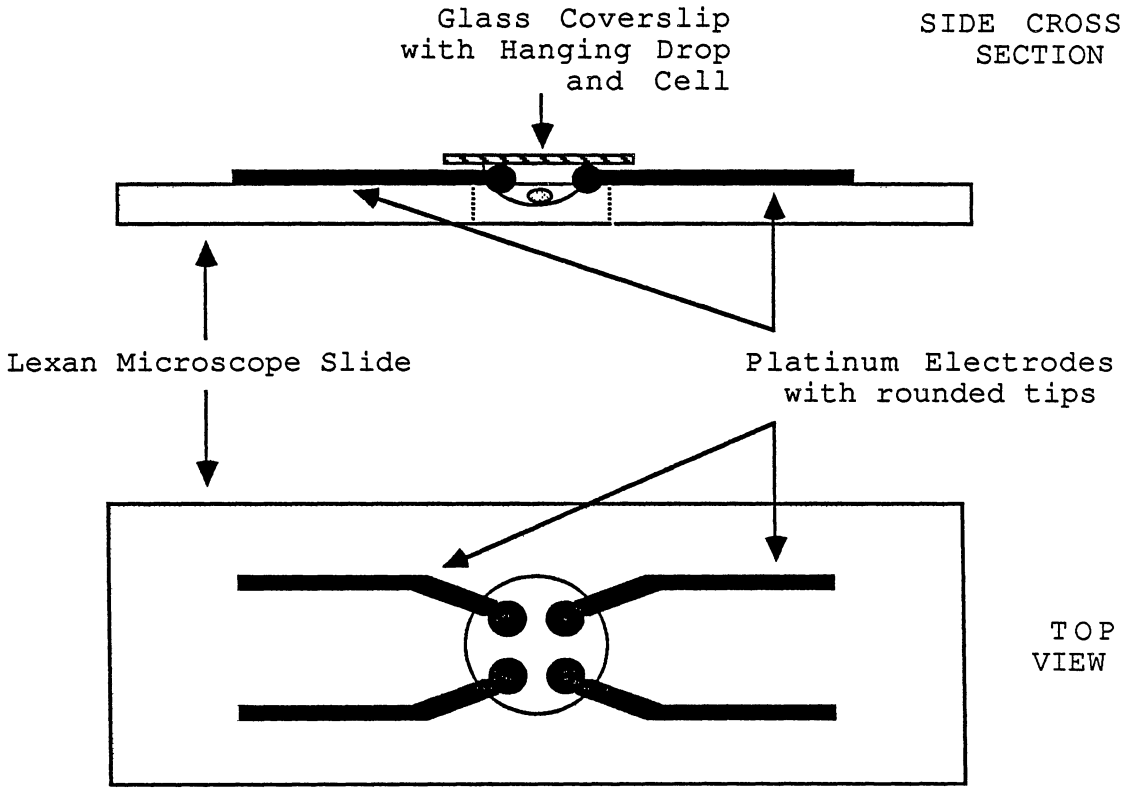

Figure 14. The CSR Electrode Chamber

studied are suspended between in a hanging drop. This allows the cels to spin freely without the friction they would experience resting on a solid surface.

A special circuit producing four output signals, each one lagging in phase by 90° from the previous one, was used to drive the CSR chamber. Figure 15 shows the special circuit, designed by Dr. Karan V. I. S. Kaler, Department of Electrical Engineering, University of Calgary.

To make the recording of data faster, a semi-automated procedure was used. A frequency synthesizer under computer control (Hewlett-Packard model 3325A controlled by an Apple IIe with an IEEE-488 interface card) supplied the driving frequency to the phase shifting circuit. The cells in the chamber were videotaped while the Apple computer stepped through a desired range of frequencies, applying each frequency for 10 to 15 seconds. The videotape was then replayed and the rotation rate of several cells in the field of view was determined for each frequency.

The cell type chosen for study was the yeast *Saccharomyces cerevisiae*. The morphology of this organism through its life cycle has been well characterized (Hartwell et. al., 1973,1974; Reed, 1980; Pringle and Hartwell, 1981) so that the stage in the life cycle of any cell is readily determined by observation of the formation of buds. For the life cycle studies, five stages of development were defined: SC, single cell stage, there is no cell bud; SB, small bud stage, the cell bud diameter is less than 1/5 the diameter

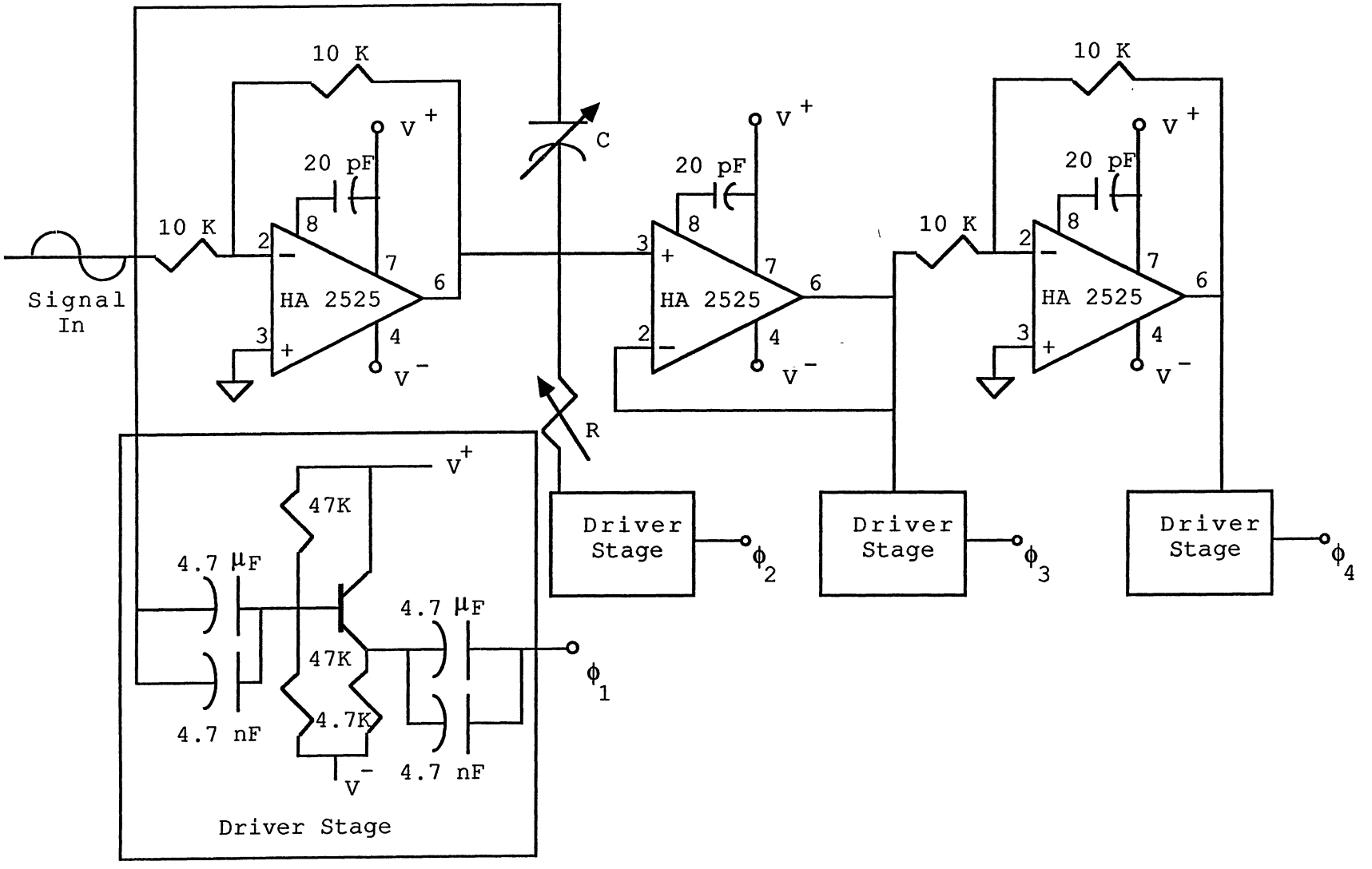

Figure 15. The CSR Phase Shift Circuit

of the mother cell; MB, medium bud stage, the cell bud diameter is between 1/5 and 1/3 the diameter of the mother cell; LB, large bud stage,the cell bud diameter is between 1/3 and 2/3 the diameter of the mother cell; CK, cytokinetic stage, mother and daughter cell are close to the same size. The cell culture procedure has been given in a previous chapter. The procedure to prepare the cells for CSR is the same as that for DEP.

An additional study looking at the differences in the CSR spectra of normal and cancer human lung cells was done. The two cell lines, generously supplied by Dr. M. K. Patterson of the Noble Foundation, Ardmore, Ok, were designated WI-38, normal human lung cell line, and VA-13A, virus transformed human lung cell line. The cells were harvested from culture using trypsin and were prepared for CSR measuremens by washing and final suspension in low conductivity, iso-osmotic mannitol.

Results

Figure 16 shows the CSR spectra for each of the five defined life cycle stages. Figures 17 and 18 show the data in a more interpretable form. In figure 17, the CSR as a function of life cycle stage is shown for 3 kHz, 10 kHz, and 30 kHz. Similar curves for 100 kHz, 300 kHz, and 1 MHz are shown in figure 18.

If it is assumed that the polarization mechanisms discussed in chapter II are present in these cells, that is:

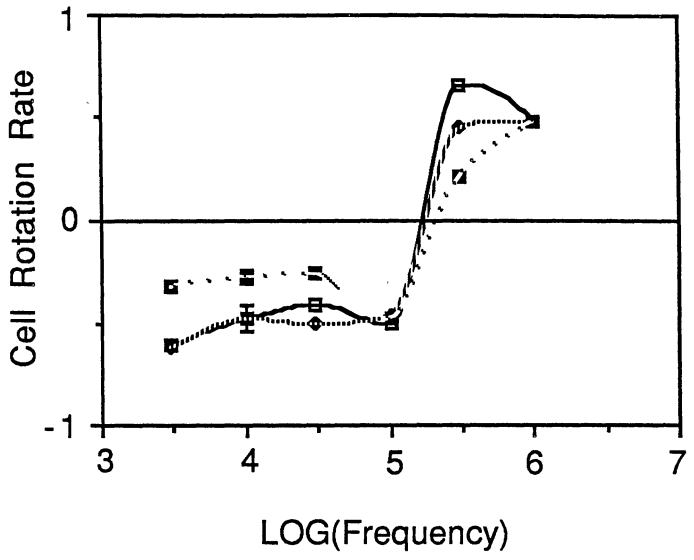

(a)

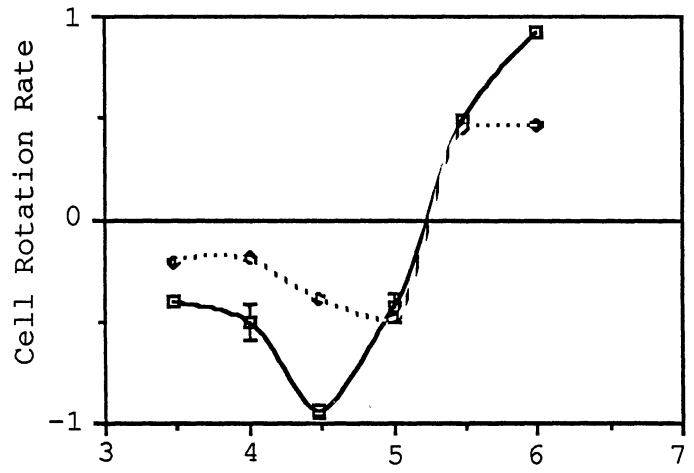

(b)

Figure 16. The CSR Rotation Spectra for Five Stages in the Life Cycle for the Yeast *Saccharomyces cerevisiae*. a) Small Bud, Medium Bud, Large Bud; b) Single Cell, Cytokinesis Stage.

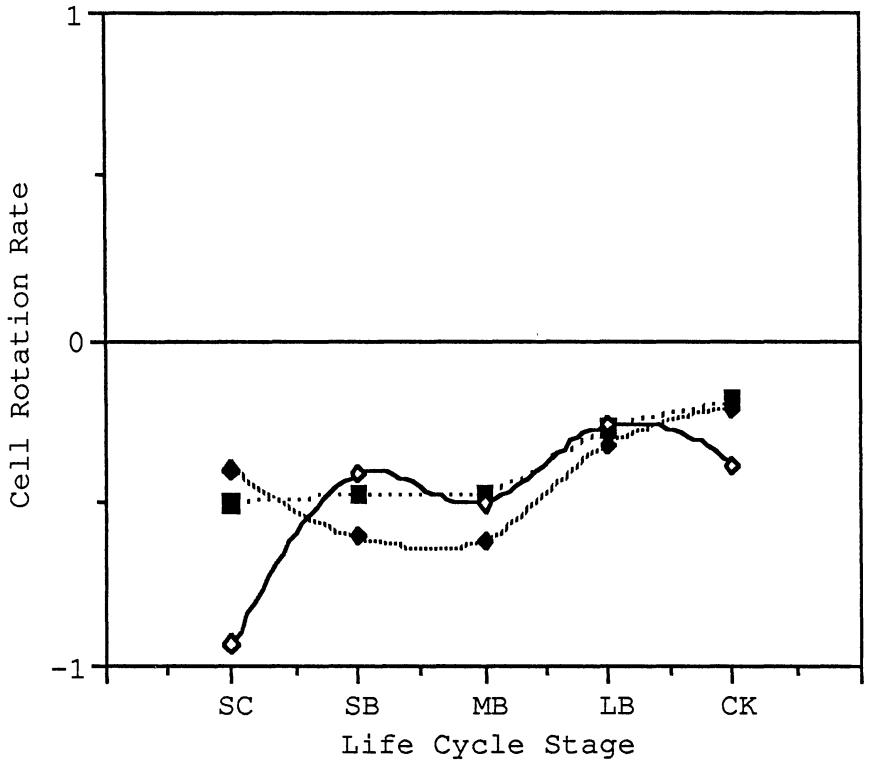

Figure 17. The Cell Rotation Rate vs Life Cycle Stage of *Saccharomyces cerevisiae* at Low Frequencies, ◆·····◆ 3 KHz, ■···■ 10 KHz, ◇—◇ 30 KHz

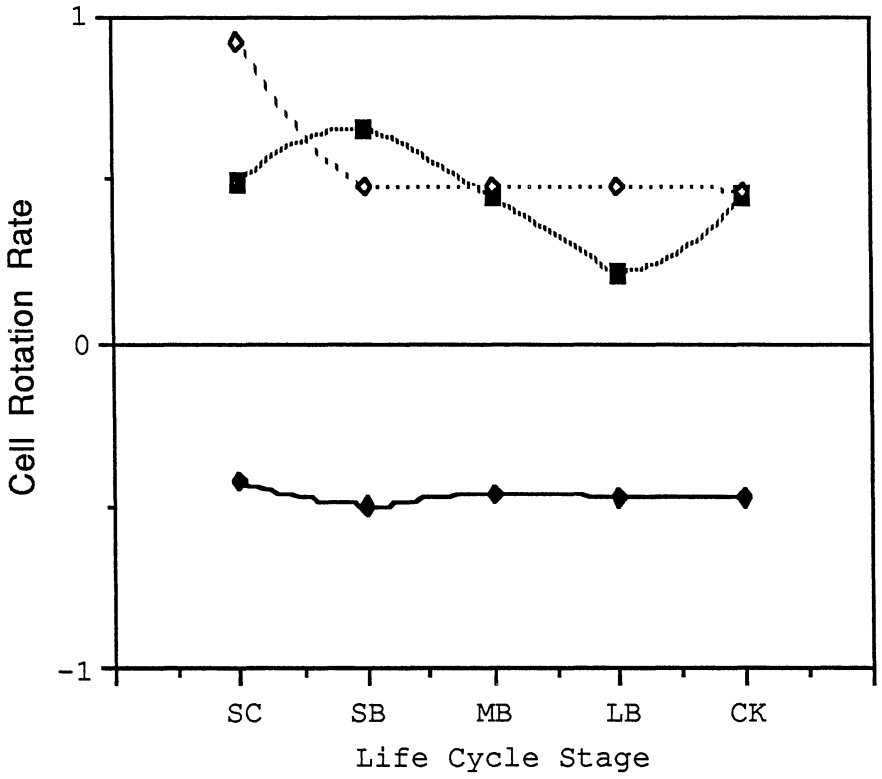

Figure 18. The Cell Rotation Rate vs Life Cycle Stage of *Saccharomyces cerevisiae* at High Frequencies, ◆—◆ 100 KHz, ■·····■ 300 KHz, ◇···◇ 1 MHz

a) loose ion polarization (Dukhin,1973) is the dominant mode at frequencies from 1 to 10kHz.

b) the polarization at 10 kHz is primarily due to plasmoidal polarization (Carstensen and Marquis,1974).

c) the polarization at 30 kHz is primarily due to the tightly held ions of the ionic double layer (Schwarz,1962).

d) polarization of the tightly held ions of the ionic double layer and Maxwell-Wagner polarization are equally responsible for the cell polarization at 100 kHz.

e) Maxwell-Wagner polarization is the dominant mode of polarization at 300 kHz.

f) the polarization at 1 MHz is due to Maxwell-Wagner polarization and to another mechanism such as dipolar polarization

Then the following interpretations can be made for the data:

a) The Dukhin diffuse double layer polarization and plasmoid-type polarization is greatest in the single cell and large bud stage.

b) The Schwarz tight-ion polarization is at a minimum in the single cell and cytokinetic stages.

c) The Maxwell-Wagner polarization varies slowly through the life cycle, and is maximal at the small bud stage, and minimal at the large bud stage

In other words, in the single cell stage (SC), the diffuse ion mode of polarizaton predominates and the tight ion mode is repressed. The budding stages show a gradual increase in the tight ion polarization until the cytokinetic stage where a slight decrease is again seen and the ratio of loose ion to tight ion polarization approximates that of the single cell stage. In general, the ionic double layer gradually tightens through the progression through the life cycle.

Figure 19 shows a comparison between normal human lung cells, line WI-38, and cancer human lung cells, line VA-13A. The main difference in the two lines occurs in the frequency region in which the tight ion polarization is at a maximum. It can be concluded from the electrical studies that the difference between the normal and cancer cell lines occurs on the membrane surface and in the tightly held ions of the double layer.

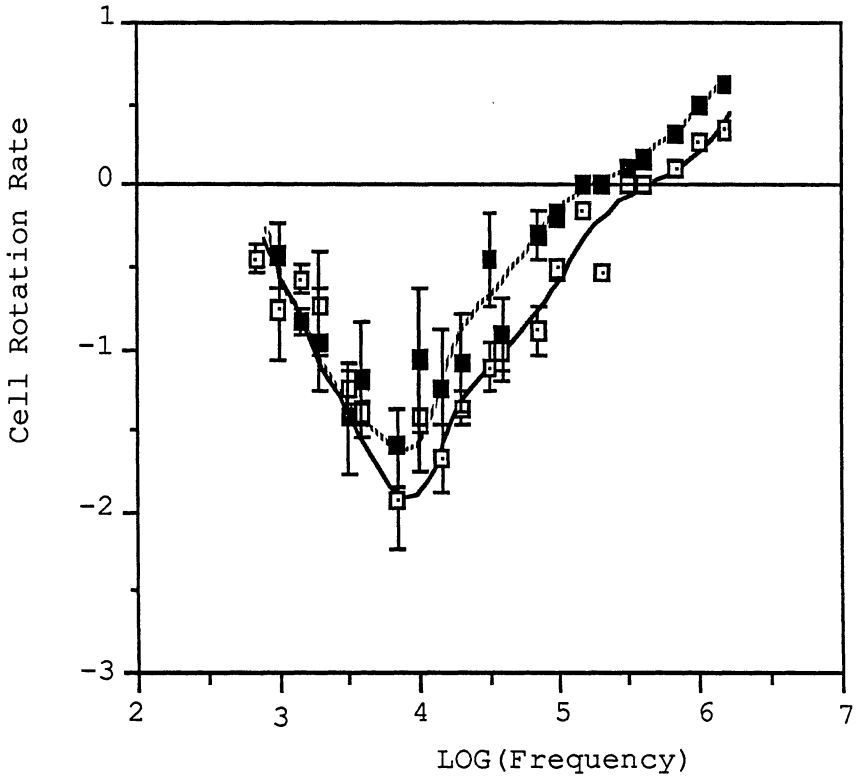

Figure 19. Comparison of CSR Spectra for Normal Human Lung Cell Line (WI-38) and Cancer Human lung Cell Line (VA-13A). Medium: iso-osmotic dextrose, conductivity: $\sigma = 15\ \mu S/cm$, —⊡— WI-38 ·····■····· VA-13A

CHAPTER V

PATTERNS: EVIDENCE FOR CELLULAR AC FIELDS

It has long been known that cells produce static electric fields. The presence of oscillating fields produced by cells has only recently been postulated and reported. Pohl et. al. (1981) showed that small particles with high dielectric constants were attracted to cells in preference over particles with low dielectric constants. The cause of this attraction was assumed to be ac fields produced by the cells. This chapter will report on further evidence for such fields.

Methods and Procedures

The hanging drop technique used in this study was developed from the μ-DEP technique of Pohl (Pohl et. al.,1981). Instead of counting particles attached to the cells, as in μ-DEP, the cells are suspended in a hanging drop that also contains a large number of particles in suspension. As the small, ~1 μm, particles settle around the cells, the fields produced by the cells affect the pattern that the particles assume. Recall from chapt r II that low dielectric constant particles should be repelled from the cells and that high dielectric constant particles should be

attracted towards the cells.

The particles used in these experiments are shown in Table III. Notice that the high dielectric constant particles all have relative dielectric constants greater than water (78) and should be attracted towards strong electric field regions, while all the low dielectric constant particles have dielectric constants lower than water and should be repelled under the same circumstances. All the particles were ground on a roller mill (Fisher Scientific portable roller mill, catalog #08-381). The desired 1 to 2 μm diameter size was selected by sedimentation through thin aqueous layers. The particles were suspended in de-ionized water or, in the case of use with mammalian cells, in de-ionized, iso-osmotic solutions of alanine, mannitol, or dextrose.

The following types of cells were studied: Two African green monkey kidney lines (BSC-1 and VERO), a feline lung line (AK-D), fetal bovine kidney cells (primary culture), and the algae *Netrium digitus* and *Closterium acerosum*. Two types of fertilized egg were also studied: *Zenopus laevis* (African clawed frog) and *Monochoides changii* (nematode). The mammalian cells were supplied by Mrs. Jill Dotson, OSU School of Veterinary Medicine. The algae and the frog eggs were obtained from Carolina Biological Supply. The nematode eggs were supplied by Professor Charles Russell, OSU Department of Plant Pathology.

The mammalian cells were cultured in RPMI-1640 medium

with 10% FBS and gentamycin and l-glutamine added. The cells were detached with 0.25% trypsin and resuspended in the growth medium to neutralize the remaining trypsin.

TABLE III

Dielectric Particles Used and Their Relative Dielectric Constants

Particle	Relative Dielectric Constant at 1 KHz
$BaTiO_3$	~2000
$SrTiO_3$	~5000
$NaNbO_3$	~650
$BaSO_4$	11.5
SiO_2	3.8
Al_2O_3	7.5

The algae were cultured on Alga-Gro medium (Carolina Biological Supply) under fluorescent lamps and harvested directly from the growth medium.

The procedure for preparing hanging drops consisted of placing 5 µl of suspension containing the desired particle on a cover slip. The chosen cells were harvested by centrifugation and resuspension in the appropriate de-ionized medium. A particular cell was then selected from the suspension by a micropipette and placed in the drop on

the coverslip. In the case of the smaller mammalian cells, up to ten cells would be put in a single drop. The coverslip was then turned over and placed on a pocketed microscope slide. Patterns developed within 10 to 30 minutes. The patterns were viewed with a microscope fitted with a videocamera. the patterns were also videotaped for later study.

There are several precautions to take for the proper development and interpretation of powder patterns. Mechanical vibration of the hanging drop can disrupt the developing pattern and must be minimized. The presence of clumps or particle agglomerates or detritus can distort or destroy the pattern and must be avoided. Actively lysing cells can also disturb the pattern. In mammalian cells, the presence of exudates or pericellular zones has been reported (Clarris and Fraser,1968; McBride and Bard,1979; Underhill and Toole,1982). These exudates, consisting primarily of hyaluronic acid, can act as a physical barrier to particles and magnify a repulsion pattern and reduce an attraction pattern.

Results

Figures 20 through 24 show attraction patterns for various types of cells and particles having a high dielectric constant. The large algae cells, *Closterium acerosum*, a long (~500 μm), spindle shaped cell, and *Netrium digitus*, a long (~700 μm), cigar shaped cell, seem to reveal

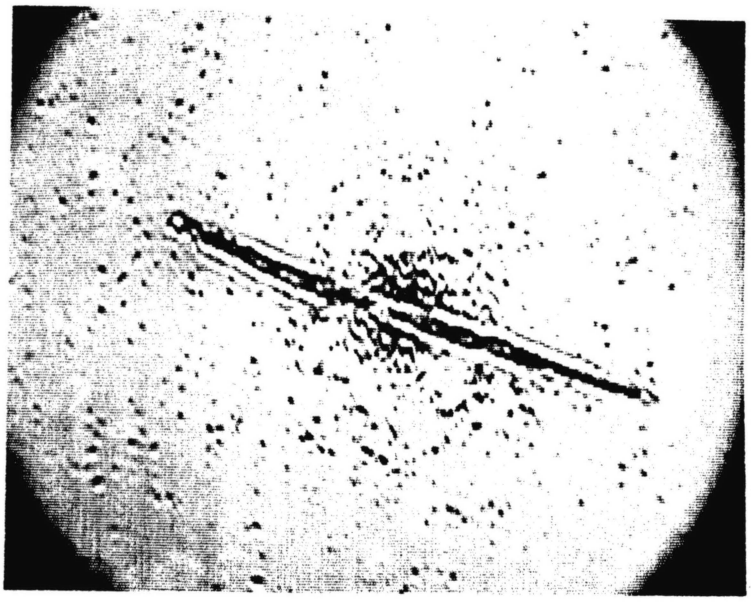

(a)

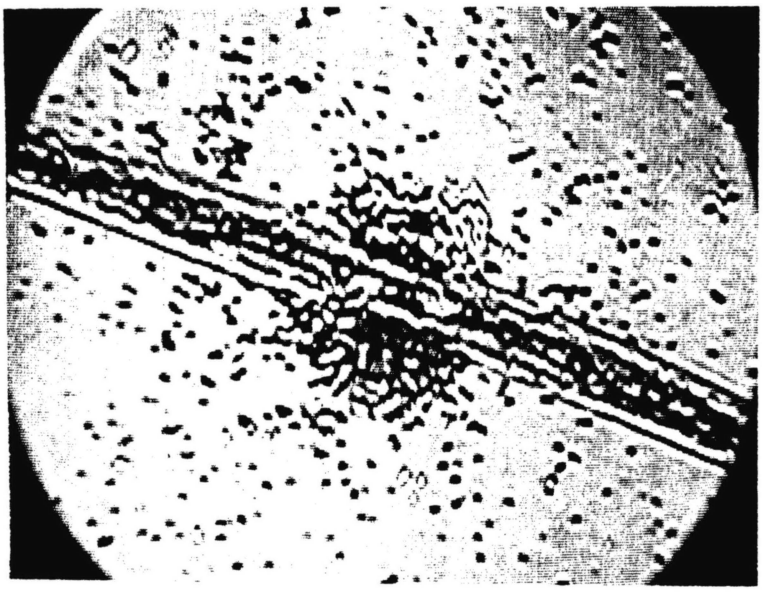

(b)

Figure 20. Dipolar attraction pattern: *Closterium acerosum* and barium titanate particles, b) Closeup of the pattern in part a

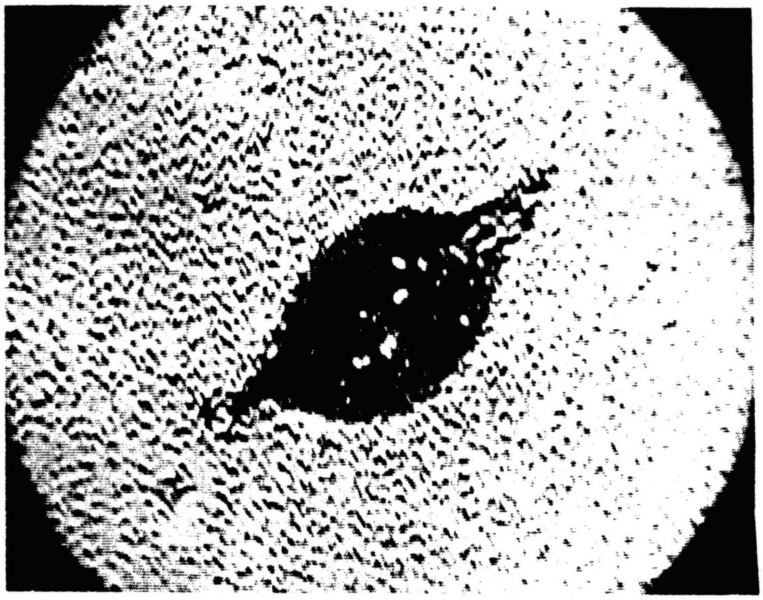

(a)

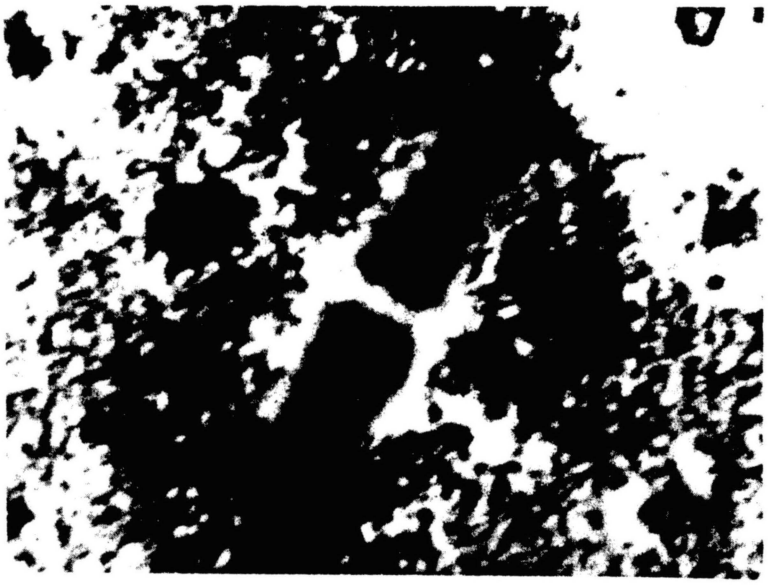

(b)

Figure 21 a) Dipolar attraction pattern: *Closterium acerosum* and strontium titanate particles.
b) Quadripolar attraction pattern: *Netrium digitus* and barium titanate particles.

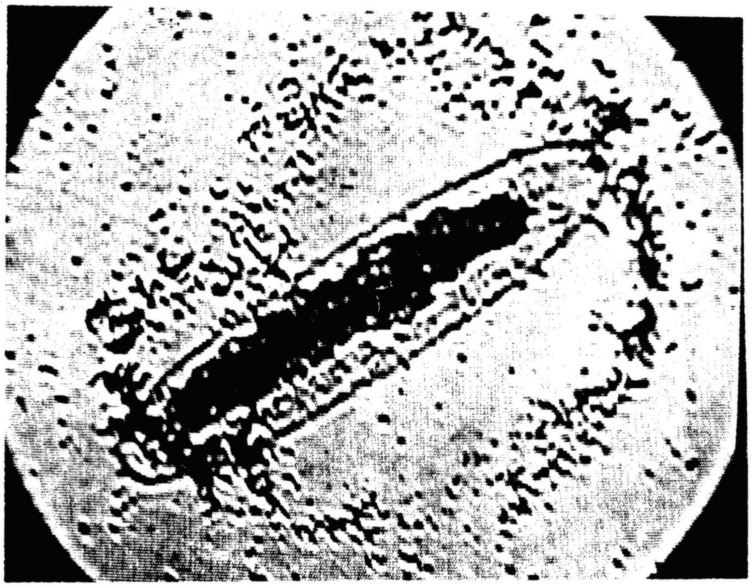

(a)

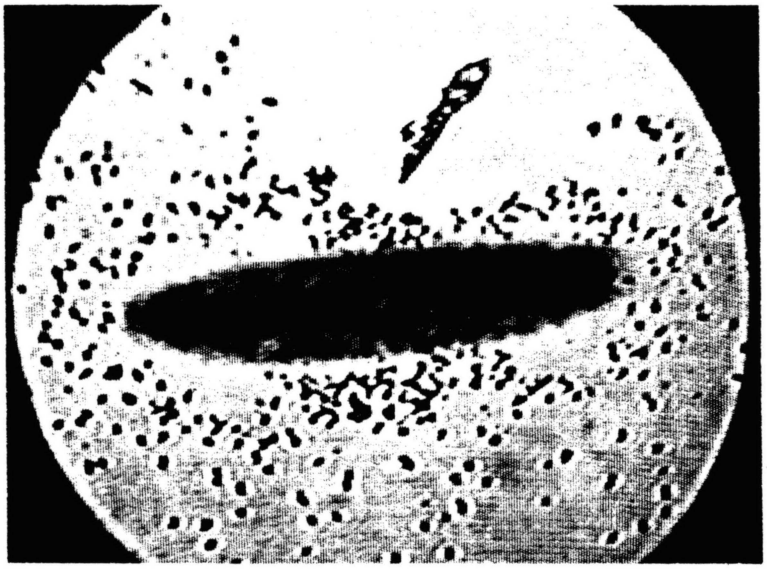

(b)

Figure 22 a) Quadripolar attraction pattern: *Netrium digitus* and strontium titanate particles.
b) Quadripolar attraction pattern: *Netrium digitus* and calcium zirconate particles.

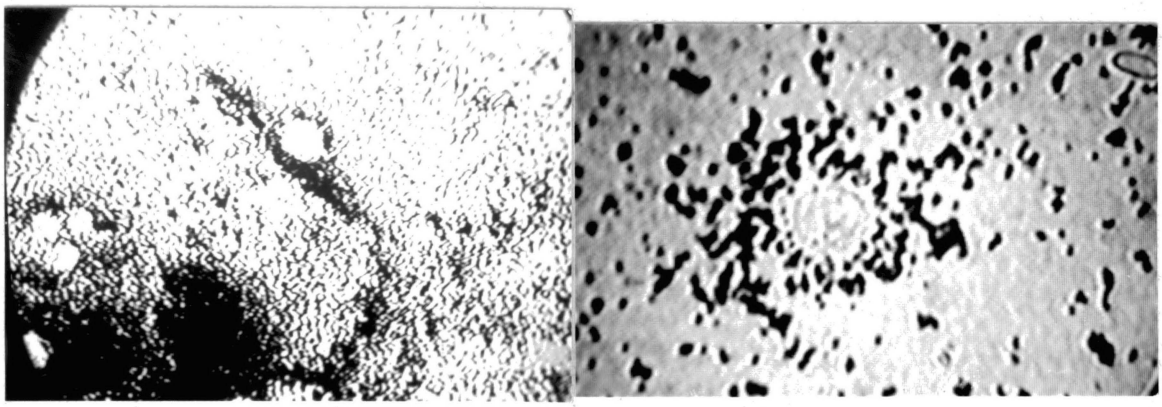

(a) (b)

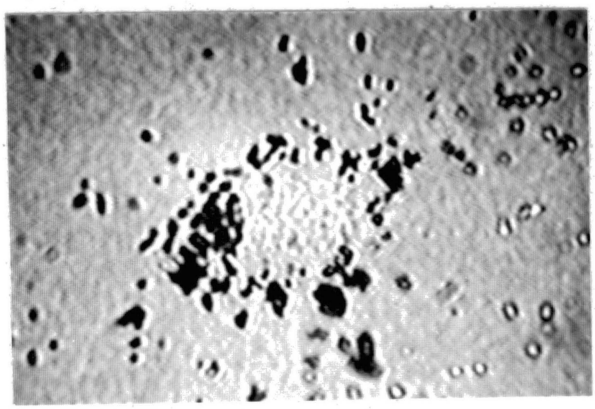

(c)

Figure 23 a) Attraction pattern: AK-D (Feline lung cell line) and strontium titanate particles, Medium: Isoosmolar Alanine, Conductivity σ=15 µS/cm.
b) Attraction pattern: BFK (Bovine Fetal Kidney cells) and strontium titanate particles, Medium: Isoosmolar Dextrose, Conductivity σ=10 µS/cm.
c) Attraction pattern: Vero (African green monkey kidney cell line) and barium titanate particles, Medium: Isoosmolar Dextrose, Conductivity σ=10 µS/cm.

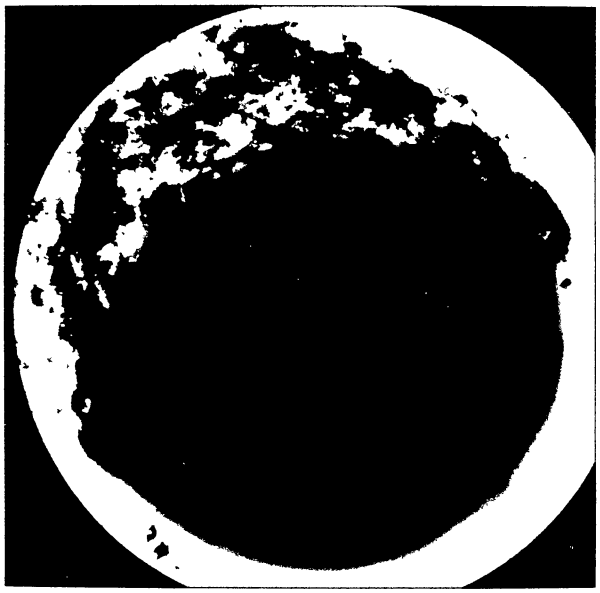

Figure 24 Dipolar attraction pattern, fertilized egg of *Zenopus laevis* (African clawed frog), and barium titanate particles.

something about the shape of their fields. The *Closterium* collects particles about its middle in a dipole pattern, while the *Netrium* shows a quadripole field, collecting particles at its middle and at the tips of the cell. The much smaller mammalian cells, AK-D (feline lung) and BKF (Bovine Fetal Kidney cells) are too small (10μm) to show much detail, but collect cells all over their surfaces. The fertilized egg of the african clawed frog was enormous (~2 mm diameter) and attracted particles in a dipole pattern, forming clumps of particles on opposite ends of the cell.

Figures 25 and 26 show repulsion patterns for algae and mammalian cells and particles of low dielectric constant. The same type of algae cells were used, and an additional African green monkey cell line, BSC-1, was used for the mammalian cell type. The existence of an exudate around the mammalian cells, particularly the Vero cells, increased the particle free zone and exaggerated the repulsion pattern.

Figures 27 and 28 show neutral patterns for both live and dead cells where the particles are unaffected by the cell's presence. The live *Closterium* is in a solution in which the conductivity has been adjusted so that the DEP force is much reduced and the particles are no longer attracted. The dead *Netrium* and BSC-1 cells are no longer producing fields.

Figure 29 shows the effect of increasing solution conductivity on the patterns formed by $SrTiO_3$ particles about BFK (bovine fetal kidney) cells. Part a shows

(a)

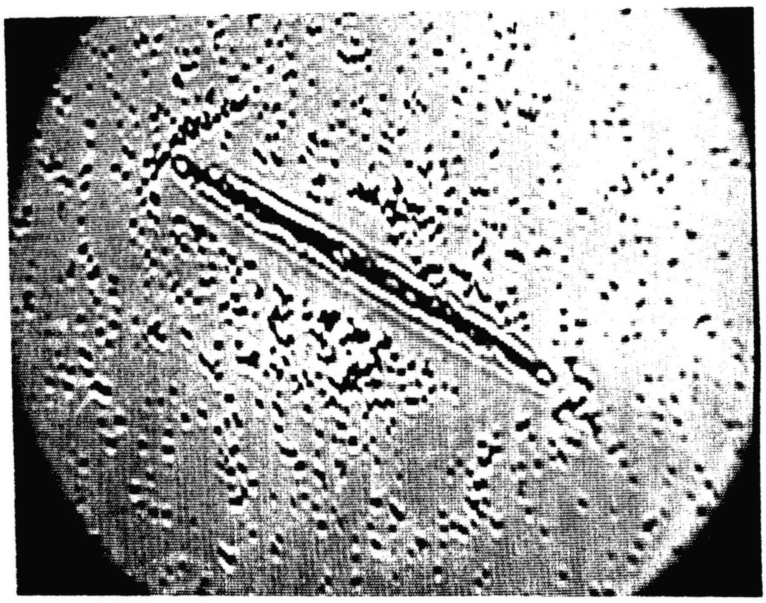

(b)

Figure 25 a) Repulsion pattern: *Netrium digitus* and barium sulfate particles.
b) Repulsion pattern: *Closterium acerosum* and barium sulfate particles.

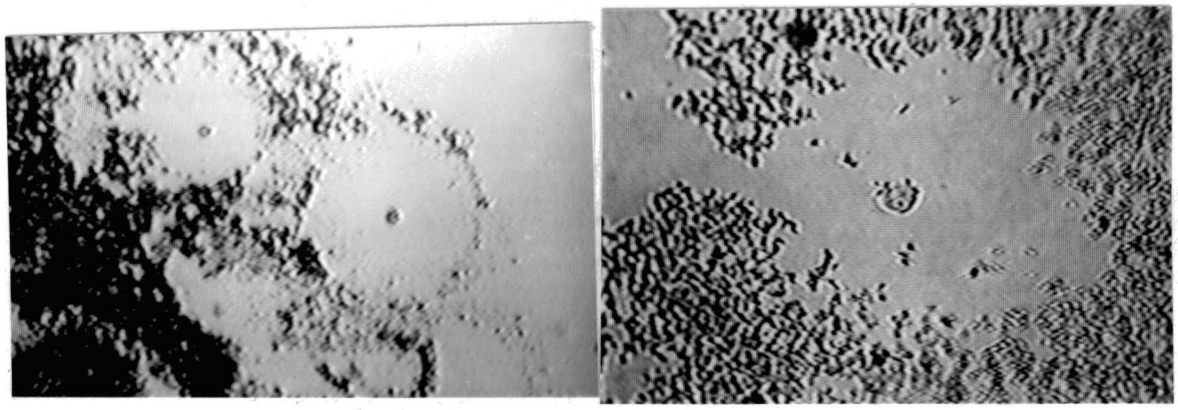

(a) (b)

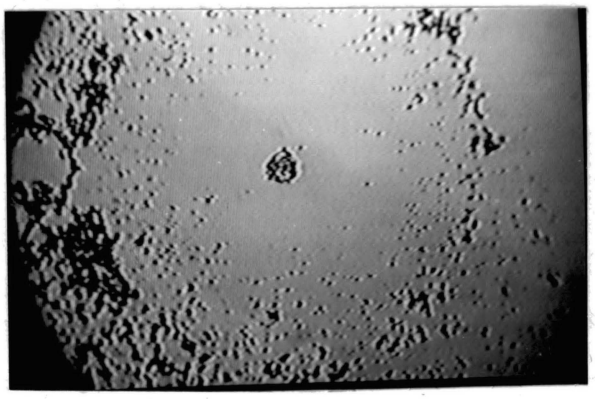

(c)

Figure 26 a) Repulsion pattern: BFK (Bovine Fetal Kidney cells) and barium sulfate particles, Medium: Isoosmolar Dextrose Conductivity σ = 10 μS/cm.
b) Repulsion pattern: Vero (African green monkey kidney cell line) and barium sulfate particles, medium and conductivity, same as in part a.
c) Repulsion pattern: BSC-1 (African green monkey kidney cell line) and barium sulfate particles, medium and conductivity, same as in part a.

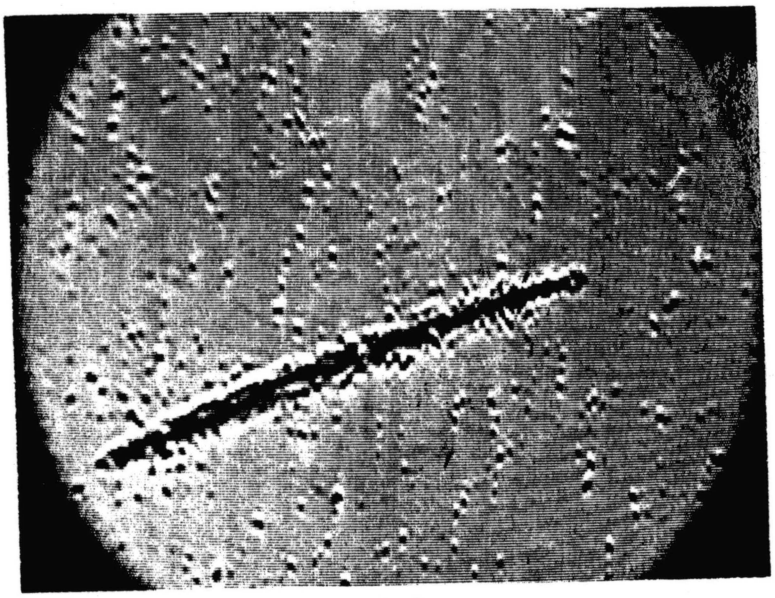

(a)

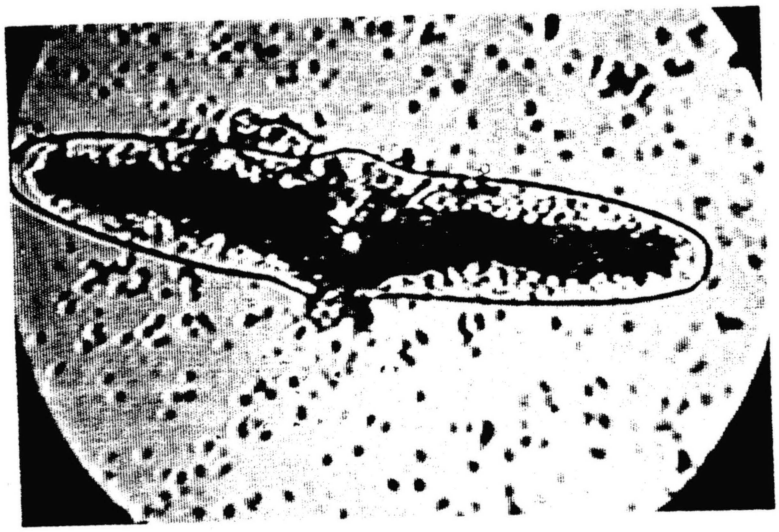

(b)

Figure 27 a) Neutral pattern: live *Closterium acerosum* and barium titanate particles.
b) Neutral pattern: dead *Netrium digitus* and strontium titanate particles.

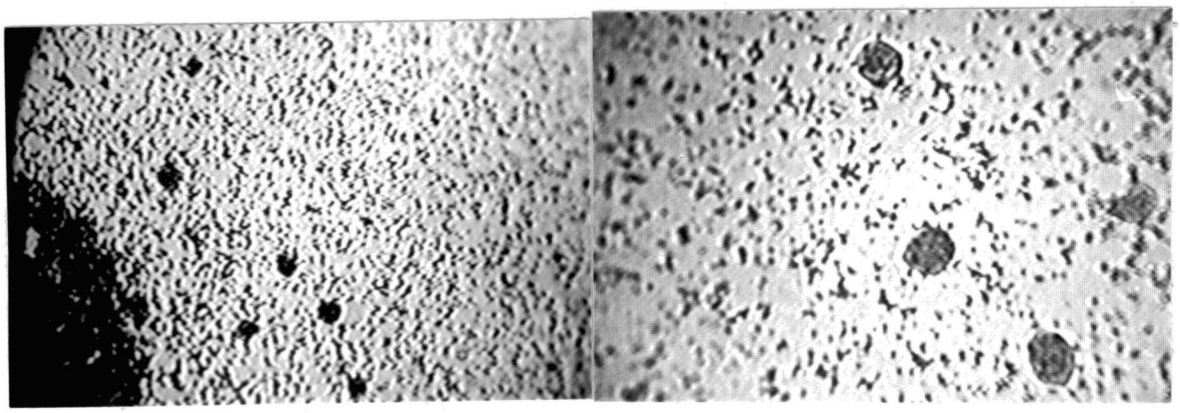

(a) (b)

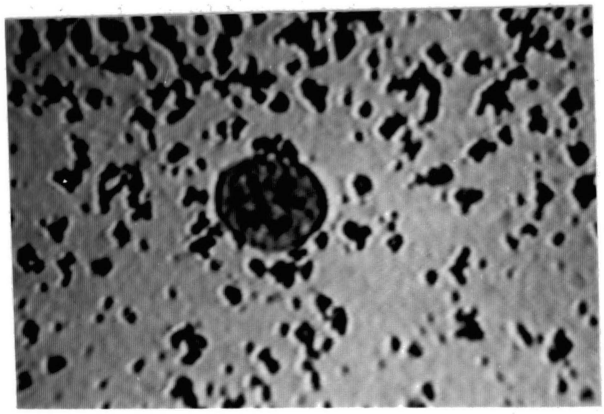

(c)

Figure 28 a) Neutral pattern: heat killed BSC-1 (African green monkey kidney cell line) and strontium titanate particles, Medium: Isoosmolar Dextrose, Conductivity σ=10 μS/cm.
b) Higher magnification of part a.
c) Higher magnification of part b.

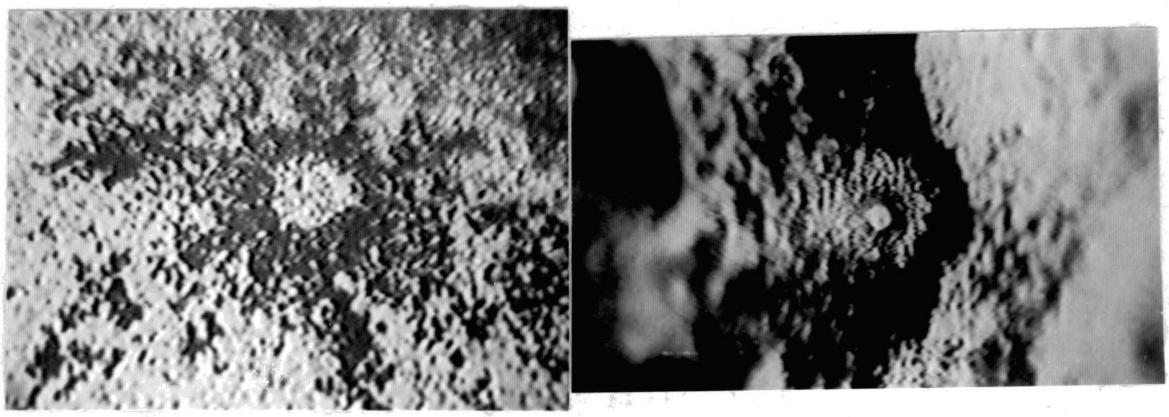

(a) (b)

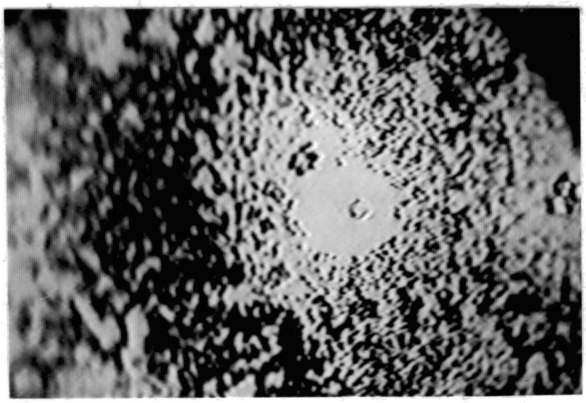

(c)

Figure 29 a) Bovine fetal kidney cells and strontium titanate particles, Medium: Isoosmolar Dextrose, Conductivity σ=30 µS/cm.
b) As in part a, except Conductivity σ=200 µS/cm.
c) As in part a, except Conductivity σ=3000 µS/cm.

particles strongly attracted to the cell. Part b shows the cell surrounded by a halo of particles that is not as dense as the particles further away from the cell. In this case, the higher conductivity of the solution reduces the DEP force on the particles and allows the cell exudate to exclude most of the particles from around the cell. A few particles are still drawn up over this exuded film and attracted to the cell. In part c, the even higher conductivity reduces the DEP force to zero or even to negative and all particles are excluded from around the cell.

Electrophoresis experiments were done to determine the charge of the cells and particles used in these experiments. All cells and particles showed a slight net negative charge. In spite of this and in spite of the pericellular zone of the mammalian cells, both attraction and repulsion patterns appeared when the proper electrical conditions of particle dielectric constant and solution conductivity were met.

The results of these experiments are consistent with the assumption that the cells are producing ac fields. To summarize:

a) Live cells in low conductivity water attract high dielectric constant particles to themselves.
b) Live cells repel low dielectric constant particles from themselves.
c) Dead cells have little or no affect on particles, regardless of the dielectric constant of the

particles.

d) Attraction patterns become less evident as the solution conductivity increases. Increasing solution conductivity increases the effective dielectric constant of the water so that even particles of high dielectric constant are repeled from cells.

Other explanations do not seem as likely. Chemical effects, such as cell chemotaxis, would seem to be improbable as a cause for these observations, as the particles used vary widely in chemical composition, with their only common characteristic being a high or low dielectric constant. The presence of surface effects on the drop surface in the hanging drop experiments seems to not alter the results, since the patterns developed in a predictable way, consistent with the μ-DEP experiments (Pohl et. al.,1981) which were done in the bulk liquid, away from the air-water interface.

CHAPTER VI

SUMMARY

The electrical properties of cells have been investigated using three different techniques. An automated DEP sorter/analyzer has been developed capable of measuring the translational DEP spectra of different cells in detail. A semi-automated CSR spectrometer was used to measure the change in cellular polarizability through the life cycle and differences in normal and cancer cells. A hanging drop μ-DEP technique was used to detect ac fields produced by cells.

The development of the sorter/analyzer involved calculating the correct size and shape of the electrodes, and developing a method to produce and control a steady cell stream in the middle of a flow chamber. The sorter/analyzer first successfully demonstrated positive and negative DEP force in cells (Appendix A), and to separate cells an appreciable distance (Pohl and Kaler,1979). The automated system allows the taking of detailed spectra with a speed not previously acheived.

The CSR studies followed the yeast *S. cerevisiae* through its life cycle and measured the changes in its polarizability. The CSR spectra of normal human lung cells and cancer human lung cells was found to differ in a

frequency region associated with Schwarz type tight ion polarization. A proposed CSR equation was qualitatively correct: the spin rate varies as the square of the applied field, the spin rate can be either in the direction of the applied field rotation or in the opposite direction depending on the frequency of the applied field, and the spin rate is much slower than the frequency of rotation of the applied field. The theory fails quantitatively however. If reasonable values are assumed for the quantities in equation 10, the cell rotation frequency calculated is of the order of 10^{-6} Hz instead of the observed frequency of 1 Hz to 10 Hz. A reasonable value for the rotation frequency would require a cell effective dielectric constant many orders of magnitude higher than has been observed (Crane and Pohl,1978).

The hanging drop experiments revealed ac fields produced by a wide range of cells: algal, amphibian, and mammalian, indicating a process that could be fundamental to life. The patterns behave in a way consistant with DEP theory.

Suggestions for Further Study

There are two main areas for continued study in this area:

1) Develop an electrical model of a living cell using data from both DEP translational spectra and CSR spectra. A new technique, laser doppler velocimetry, can provide rapid, detailed spectra of both techniques. The eventual

goal would be to correlate cell structure with specific polarization mechanisms.

2) Determine if the patterns formed in the hanging drop experiment depends upon the cells metabolism, and if so, to what extent. Modify the cells to try and determine what cell structures produce the fields. Try to detect the fields from cells directly.

Optimally, the work suggested above would involve close collaboration between life scientists and physical scientists.

A SELECTED BIBLIOGRAPHY

Carstensen, E. L. and R. E. Marquis, Spores VI, P. Gerhardt, R. N. Costilow, and H. L. Sadoff eds., p. 563 (1974).

Chen, C. S., "On the Nature and Origins of Biological Dielectrophoresis", (unpublished Ph.D. thesis, Oklahoma State University, 1972).

Chen, C. S. and H. A. Pohl, Trans. N. Y. Acad. Sci. 238, 176 (1974).

Chen, K. W. L., "Dielectrophoresis of Solids in Aqueous Solutions", (unpublished M.S. thesis, Oklahoma State University, 1969).

Clarris, B. J. and J. R. E. Fraser, Exp. Cell Res. 49, 181 (1968).

Cole, K. S., R. H. Cole, and H. J. Curts, J. Gen. Physiol. 18, 877 (1935).

Cole, K. S., R. H. Cole, and H. J. Curtis, J. Gen. Physiol. 19, 609 (1936).

Cole, K. S., R. H. Cole, and H. J. Curtis, J. Gen. Physiol. 21, 591 (1938).

Crane, J. S., "The Dielectrophoresis of Cells", (unpublished Ph.D. thesis, Oklahoma State University, 1970).

Crane, J. S. and H. A. Pohl, J. Electrochem. Soc. 115, 584 (1968).

Crane, J. S. and H. A. Pohl, J. Biol. Phys. 5, 49 (1977).

Crane, J. S. and H. A. Pohl, J. Electrostatics 5, 11 (1978).

Dekker, A. J., Electromagnetic Theory, p. 141 Macmillan, London (1962).

Dukhin, S. S., Surface and Colloid Science 3, 83 (1973).

Dukhin, S. S. and V. N. Shilov, Colloid J. (USSR) 31, 564 (1970a).

Dukhin, S. S. and V. N. Shilov, Colloid J. (USSR) 32, 245 (1970b).

Dukhin, S. S. and V. N. Shilov, Colloid J. (USSR) 32, 90 (1970c).

Dukhin, S. S. and V. N. Shilov, Dielectric Phenomona and the Double Layer in Disperse Systems and Polyelectrolytes, John Wiley and Sons, N. Y. (1974).

Denner, V. and H. A. Pohl, J. Electrostatics 13, 167 (1982).

Feeley, C. M., "Dielectrophoresis of Solids in Liquids of Differing Dielectric Constant and Conductivity", (unpublished M.S. thesis, Oklahoma State University, 1969).

Fricke, H. and H. J. Curtis, J. Phys. Chem. 41, 729 (1937).

Fröhlich, H., Theory of Dielectrics, Oxford Press, London, (1949).

Fröhlich, H., Int. J. Quantum Chem. 2, 641 (1968).

Fröhlich, H., Adv. Electron. Electron Physics 53, 85 (1980).

Griffin, J. L. and C. D. Ferris, Nature 226, 152 (1970).

Griffin, J. L. and R. E. Stowell, Exp. Cell Res. 44, 648 (1966).

Grimley, T. B. and N. F. Mott, Discuss. Faraday Soc. 1, 3 (1947).

Hartwell, L. H., R. K. Mortimer, J. Culotti, and M. Culotti, Genetics 74, 267 (1973).

Hartwell, L. H., J. Culotti, J. R. Pringle, and B. J. Reid, Science 183, 46 (1974).

Heller, J. H., Digest of 12th Annual Conference on Techniques in Medicine and Biology, p. 56, IRE-AIEEE-ISA (Nov. 1959).

Jones, T. B., J. Electrostatics 6, 69 (1979).

Jones, T. B., IEEE-IAS Ann. Meeting, 1136 (1984).

Jones, T. B. and G. W. Bliss, J. Appl. Phys. 48, 1412 (1977).

Jones, T. B. and G. A. Kallio, J. Electrostatics 6, 207 (1979).

Kaler, K. and H. A. Pohl, J. Biol. Phys. 8, 18 (1980).

Kallio, G. A. and T. B. Jones, I.E.E.E. Trans. Industrial Applic. IA-16, 69 (1980).

Kittel, C., Elementary Solid State Physics, John Wiley and Sons, N. Y. (1973).

Liebesny, P., Arch. Phys. Ther. 19, 763 (1939).

Manegold, E., Kolloid-Z 111, 11 (1950).

Mason, B. D. and P. M. Townsley, Can. J. Microbiol. 17, 879 (1971).

McBride, W. H. and J. B. L. Bard, J. Exp. Med. 149, 507 (1979).

Meyer, P. I. and W. E. Vaughan, Biophys. Chem. 12, 329 (1980).

Minakata, A. and N. Imai, Biopolymers 11, 329 (1972a).

Minakata, A. N. Imai, and F. Oosawa, Biopolymers 11, 347 (1972b).

Mischel, M. and H. A. Pohl, J. Biol. Phys. 11, 98 (1983).

Mischel, M., A. Voss, and H. A. Pohl, J. Biol. Phys. 10, 223 (1982).

Mognaschi, E. R. and A.Savini, IEEE-IAS Ann. Meeting, 1120 (1984).

Morgan J. R. and R. Pethig, J. Phys. E.: Sci. Instrum. 12, 1132 (1979).

Muth, E., Kolloid Z. 41, 97 (1927).

Paul, R., R. Chatterjee, J. A. Tuszynski, and O. G. Fritz, J. Theor. Biol., 104, 169 (1983).

Pethig, R., Dielectric and Electronic Properties of Biological Materials, John Wiley and Sons, N. Y. (1979).

Pohl, H. A., J. Appl. Phys. 22, 869 (1951).

Pohl, H. A., J. Appl. Phys. 29, 1182 (1958).

Pohl, H. A., J. Electrochem. Soc. 107, 386 (1960).

Pohl, H. A., J. Electrochem. Soc. 115, 155c (1968).

Pohl, H. A., J. Colloid Interface Sci. 39, 437 (1972).

Pohl, H. A., Dielectrophoresis, Cambridge University Press, Cambridge (1978).

Pohl, H. A., J. Bioenerg. Biomembr. 13, 149 (1981).

Pohl, H. A. and T. Braden, J. Biol. Phys. 10, 17 (1982).

Pohl, H. A., T. Braden, S. Robinson, J. Piclardi, and D. G. Pohl, J. Biol. Phys. 9, 133 (1981).

Pohl, H. A. and J. S. Crane, Biophys. J. 11, 711 (1971).

Pohl, H. A. and J. S. Crane, J. Theor. Biol. 37, 1 (1972).

Pohl, H. A. and I. Hawk, Science 152, 647 (1966).

Pohl, H. A. and K. Kaler, Cell Biophys. 1, 15 (1979).

Pohl, H. A., K. Kaler, and K. Pollock, J. Biol. Phys. 9, 67 (1981).

Pohl, H. A. and R. Pethig, J. Phys. E. 10, 190 (1977).

Pohl, H. A. and C. E. Plymale, J. Electrochem. Soc. 107, 390 (1960).

Pohl, H. A. and M. Pollak, J. Chem. Phys. 66, 4031 (1977).

Pohl, H. A., K. Pollock, and J. S. Crane, J. Biol. Phys. 6, 133 (1978).

Pohl, H. A. and J. P. Schwar, J. Appl. Phys. 30, 69 (1959).

Pohl, H. A. and J. P. Schwar, J. Electrochem.. Soc. 107, 386 (1960).

Pohl,H. A., P. S. Vijayakumar, L. Dunn, and W. T. Ford, IEEE-CEIDP, p. 486 (1983).

Polk, C., personal communication, (1985).

Pollak, M. and H. A. Pohl, J. Chem. Phys. 63, 2980 (1975).

Pringle, J. R. and L. H. Hartwell, Molecular Biology of the Yeast Saccharomyces, ed. J. N. Strathern, E. W. Jones, and J. R. Broach, Cold Spring Harbor Laboratory, N. Y. (1981).

Reed, S. I., Genetics 95, 561 (1980).

Rhoads, J. E., R. E. Buckner, and H. A. Pohl, J. Biol. Phys. 4, 93 (1976).

Rivera, H., "Cellular Spin Resonance", (unpublished M.S. thesis, Oklahoma State University, 1984).

Rowlands, S., L. S. Sewchand, R. E. Lovlin, and E. G. Ennis, Phys. Lett. 82A, 436 (1981).

Rowlands, S., L. S. Sewchand, and E. G. Ennis, Phys. Lett. 87A, 256 (1982a).

Rowlands, S., L. S. Sewchand, and E. G. Ennis, Can. J. Physiol. Pharm. 60, 52 (1982b).

Saito, M., H. P. Schwan, and G. Schwarz, Biophys. J. 6, 313 (1966).

Sauer, F. A., Coherent Excitations in Biological Systems, H. Fröhlich and F. Kremer eds., p. 134, Springer-Verlag, N. Y. (1983).

Scrimager, C. G., "Dielectrophoresis of Inorganic Suspensions", (unpublished M.S. thesis, Oklahoma State University, 1974).

Schwan, H. P., Adv. Biol. Med. Phys. 4, 147 (1957).

Schwan, H. P., G. Schwarz, J. Maczuk, and H. Pauly, J. Phys. Chem. 66, 2626 (1962).

Schwarz, G., J. Phys. Chem. 66, 2636 (1962).

Schwarz, G., J. Phys. Chem. 39, 2387 (1963).

Sewchand, L. S., D. Roberts, and S. Rowlands, Cell Biophysics 4, 253 (1982).

Sher, L. D., Nature 220, 695 (1968).

Takashima, S., Biopolymers 5, 899 (1967).

Teixera-Pinto, A. A., L. L. Nejelski, J. L. Cutler, and J. H. Heller, Exp. Cell Res. 20, 548 (1960).

Ting, I. P., K. Jolley, C. A. Beasley, and H. A. Pohl, Biochim. Biophys. Acta 234, 324 (1971).

Underhill, C. B. and B. P. Toole, J. Cellular Phys. 110, 123 (1982).

Verschure, R. H. and L. Ijlst, Nature 211, 619 (1966).

von Hippel, A. H., Dielectrics and Waves, p. 39. John Wiley and Sons, N. Y. (1954).

Wiley, K. L., "A Comparison of Normal and Abnormal Cells Using Dielectrophoresis", (unpublished M.S. thesis, Oklahoma State University, 1970).

APPENDIXES

APPENDIX A

THE CONTINUOUS POSITIVE AND NEGATIVE DIELECTROPHORESIS OF MICROORGANISMS

COPYRIGHT © 1981 by Forum Press, Inc. All Rights Reserved.

THE CONTINUOUS POSITIVE AND NEGATIVE DIELECTROPHORESIS OF MICROORGANISMS

H. A. Pohl, Karan Kaler, and Kent Pollock
Department of Physics, Oklahoma State University, Stillwater, OK 74074

ABSTRACT: The continuous dielectrophoresis of living cells is described. The technique uses stream-centered transport of suspended microorganisms through an especially shaped nonuniform electric field. The cells can be given a positive or negative displacement, i.e., can be pushed into or out of the region of higher field intensity, depending upon the frequency of the applied ac field, and upon the relative permittivities of the cells and the suspending medium. Yeast (*Saccharomyces cerevisiae*) and algal cells (*Chlorella vulgaris*) were found to provide spectra of dielectrophoretic responses varying with the applied frequency (10 to 600 kHz) and conductivity.

INTRODUCTION

It is well established that nonuniform electrical fields can induce translational and rotational motions of cells in suspension, and that these motions can be used to characterize and even usefully separate living cells and their parts. The nonuniform field, it may be pictured, acts by aligning or inducing a dipole moment in the particle, which is then impelled by the field nonuniformity usually towards the region of greatest field intensity. The force is known as the dielectrophoretic force, and the resulting motion is known as dielectrophoresis (Pohl, 1951, 1958, 1960, 1978). In the event the body being acted upon is suspended in a polarizable medium, the net polarization of the whole may be such as to evoke a dielectrophoretic force in favor of pushing the body either into or away from the region of higher field intensity.

The body is said then to experience 'positive' dielectrophoresis or 'negative' dielectrophoresis respectively. Positive dielectrophoresis has been observed far more frequently than negative dielectrophoresis. This is because the electrode shapes and the field distributions usually used produce dielectrophoretic forces which vary strongly with the position in the field, i.e., as for example, F_d = constant x r^{-n}, where F_d is the dielectrophoretic force, r is some radial coordinate, and n is a dimensionless exponent in the order of 3 to 5. As can be seen, attractive forces will tend to pull particles into a small region of higher and higher attractiveness, whereas repulsive forces will repel the particles into large regions where the field rapidly becomes ineffective and the negative dielectrophoretic effect is soon dissipated to the difficultly observable level.

Negative dielectrophoresis, that is, the repulsion of suspended particles away from the region of highest field intensity, has not been much studied. This is probably because of the considerable experimental difficulties associated with obtaining it. It was discussed briefly by Pohl (1960) in connection with the dielectrophoretic precipitation of polyethylene particles suspended in benzene, and by Black and Hammond (1965a, 1965b) in treating the dielectrophoretic separation of biological particles from hydrocarbon fluids. Negative dielectrophoresis was studied by C. Feeley and by K. Chen using spheres of various dielectrics suspended by fine glass fibers between a wire and plate electrode pair in various dielectric liquids (Pohl, 1978). Negative dielectrophoresis is the basis of the levitation of bubbles in insulating liquids, and was recently studied at length by Jones and Bliss (1977) and by Parmar and Jalaluddin (1974). At the molecular level, negative dielectrophoresis is used in the ammonia maser. Molecules in paraelectric (attracted) states, especially those in the ground state, are separated from those in an apoelectric (repelled) excited state by passage through a region of intense nonuniform electric field (Pohl, 1973).

With the existence of both positive and negative dielectrophoresis well established on both experimental and theoretical grounds, at least for molecules and for systems of simple dielectrics, it is of considerable interest to ask whether or not the much more complicated systems involving living cells or their parts can be made to usefully show both types of dielectrophoresis. There is already some evidence for the occurrence of negative dielectrophoresis in suspensions of cells and organelles. When one examines dielectrophoretic collection rate (or 'yield') as a function of the applied frequency, one obtains a spectrum of the response of the suspended particles to the applied nonuniform field. In some regions of the frequency, the collection rate is zero (see Fig. 1). Clear cases of this occurrence were observed by

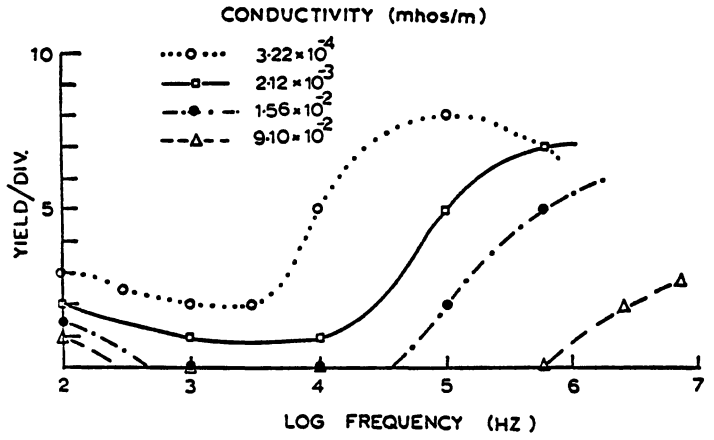

Fig. 1. Dielectrophoretic collection rate (or 'yield') spectra for yeast cells (*Saccharomyces cerevisiae*) as typically observed using pin-pin electrodes. The variations in the rate of collection of yeast cells with the frequency of the applied field, and by the conductivity of the suspension, are evident. Note the large regions over which no collection occurs, indicating the probable presence of negative dielectrophoresis at the higher conductivities. The data are those of Crane and Pohl (1974).

Pohl and Crane (1971) for yeast cells (*Saccharomyces cerevisiae*), by Rhoads, Pohl, and Buckner (1976) on canine thrombocytes, by Pohl and Crane (1973) on human erythrocytes, and by Ting et al. on spinach chloroplasts (1971). Mason and Townsley (1971) were able to obtain near-zero values for the dielectrophoretic collection rate of yeast cells (*S. cerevisiae* var. *ellipsoideus*) in a narrow region near 10 kHz while exploring the frequency range of approximately 2 kHz to 600 kHz. We can conclude, then, that quite complicated dielectric systems such as suspensions of living cells and organelles should indeed exhibit negative dielectrophoresis and in a potentially useful way. It remains for this to be demonstrated by direct observation. Such is the principal aim of the present study.

THEORETICAL ASPECTS

It was shown previously (Pohl and Crane, 1972) that the time-averaged force $\vec{F}$ on a body of complex permittivity ε_2 in a medium of complex permittivity ε_1 placed in a nonuniform electric field originally of strength $\vec{E}_o$ is given by the expression

$$\vec{F}_d = -\tfrac{1}{4}\int_{body} Re\ \nabla\left(\varepsilon_1^* \left(1 - \frac{\varepsilon_2}{\varepsilon_1}\right) \vec{E}_o^* \cdot \vec{E}\right) dv \qquad (1)$$

The asterisk indicates the complex conjugate, and $\vec{E}$ is the resultant field throughout the body. For a spherical body, this reduces to the simpler expression (Sher, 1968; Pohl, 1978):

$$\vec{F}_d = 2\pi a^3\ Re \left\{\varepsilon_1^* \frac{(\varepsilon_2 - \varepsilon_1)}{(\varepsilon_2 + 2\varepsilon_1)}\right\} \nabla (E_o)^2 \qquad (2)$$

where a is the particle radius. The complex (frequency-dependent) permittivity is given by

$$\varepsilon = \varepsilon_o (K' - iK'') = \varepsilon_o K' - i\sigma/\omega \qquad (3)$$

where K' and K" are the in-phase and out-of-phase relative dielectric constants, σ is the conductivity, ω is the angular frequency of the applied field, and i is the square root of minus one.

The dielectric constant and the conductivity of a real material are "constants" of the material only at a particular frequency, and reflect the slope of the polarization versus field strength relation at that frequency. Normally, the dielectric constants and conductivities are monotonically varying functions of the frequency. The interplay of these variations between the suspended body and the surrounding medium gives rise to a net polarization of the body in the medium which can have rather complicated shapes over the frequency range. This was discussed at length in an earlier paper (Pohl and Crane, 1972), and need not be repeated here except to say that the effective net polarization given by the quantity in curly brackets in Eq. 2 can have positive and negative values over the frequency range. It is this feature of the net polarization of real systems which gives rise to the complicated dielectrophoretic collection rate spectra. Where the net polarization of the system is negative, negative dielectrophoresis is to be expected upon the application of a nonuniform electric field.

The Polarizability

In order to evaluate the probable magnitude of the dielectrophoretic force on a living cell, such as a single yeast cell, one needs to have the values of the physically realizable parameters. For simplicity, let us designate the effective net polarizability as K_e, where

$$\varepsilon_o K_e = Re \left\{ \frac{\varepsilon_1^* (\varepsilon_2 - \varepsilon_1)}{(\varepsilon_2 + 2\varepsilon_1)} \right\} \tag{4}$$

and ε_o is the permittivity of free space, so that

$$\vec{F}_d = 2\pi a^3 \varepsilon_o K_e \nabla (E_o)^2 \tag{5}$$

For frequencies in the range of interest, it was observed earlier (Chen and Pohl, 1974; Crane and Pohl, 1978) that values of K_e ranged from zero to about 100 for single yeast cells.

The Field Gradient

It now remains to evaluate the practical magnitude for the field gradient term, $\nabla (E_o)^2$. Ideally this should be done for particles in an *isomotive* field (Pohl, 1968, 1969, 1978; Pohl and Pethig, 1977), where the magnitude of the dielectrophoretic force, $|F| = kr^o$, is independent of the position coordinate r, so that all particles present are subject to identical forces, no matter what their positions in the electrode confines (see Fig. 2). In practice, this ideal cannot quite

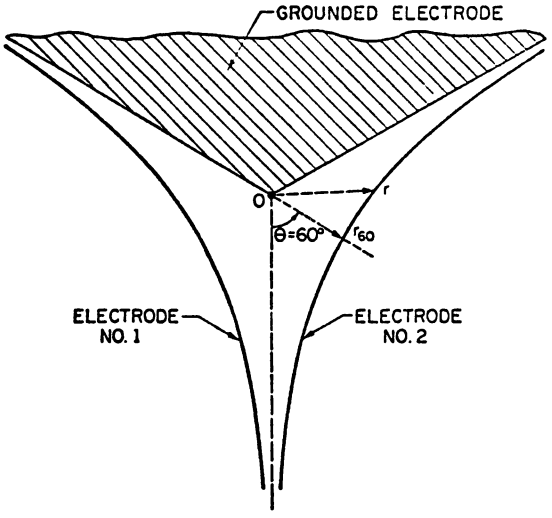

Fig. 2. The isomotive electrode configuration. The field produced by applying equal but oppositely signed voltages on curved electrodes 1 and 2, and by grounding the angular electrode, produces a force upon neutral objects within the electrode confines which is independent of the radial coordinate, r. The sketch implies that the electrodes continue on to infinity, but reduction to practice requires compromise such as cutting short the electrodes and fairing off the edges.

be met for very large regions because of the limitations of geometry, and of practically useful field strengths which may be applied without excessive heat generation in conductive dielectrics such as the watery suspensions of cells. One can, however, approximate the isomotive configuration in practice to a reasonable degree and obtain the benefits of having a practically uniform force operating over short regions.

How big the practical region can be for the operation of nonuniform field forces on biological particles in aqueous media is a necessary datum for the successful application of dielectrophoresis to biological systems. In such applications, a biological particle such as a cell must be made to respond to the applied nonuniform field at a reasonable rate. A velocity at least of about 1.0 $\mu m\ s^{-1}$ is usually required. Stokes' relation for the velocity of spherical particles can be used to estimate the necessary gradient of the square of the applied nonuniform electric field.

$$\vec{F}_v = 6\pi\eta a\vec{v} \tag{6}$$

When the particle is moving in a steady state under the influence of the applied field, the dielectrophoretic and the drag forces will be in balance,

$$\vec{F}_d = \vec{F}_v \tag{7}$$

from which we find on equating Eqs. 5 and 6 that

$$\nabla(E_o)^2 = 3\eta v\ \hat{r} / (a^2\varepsilon_o K_e) \tag{8}$$

where $\hat{r}$ is the unit radial vector in the cylindrical geometry. Upon inserting reasonable values for the several parameters as known for yeast cells, i.e. a = 4 μm, and η = 0.010 poise = 0.0010 kg $m^{-1}s^{-1}$ for the viscosity of water, we can calculate that a conditional value of the necessary gradient magnitude is

$$|\nabla(E_o)^2| = 2.12 \times 10^{11}\ \ v^2\ m^{-3}$$

If we have isomotive field conditions, the dielectrophoretic force is constant along a radial direction and the above value of $|\nabla(\vec{E}\cdot\vec{E})|$ can be used to evaluate the necessary electrode spacing as follows.

Electrode Dimensions and Spacing

The field in the charge-free region between the electrodes shown in the diagram of Fig. 2 is described by the Laplace equation for the potential, V,

$$\nabla^2 V = 0 \tag{9}$$

subject to the boundary condition that the force on the small spherical body, $\vec{F}_e$, is constant in a given radial direction. Eq. 5 for simplicity is rewritten as

$$\vec{F}_e = 2\pi a^3\varepsilon_o K_e\nabla(E_o)^2 = F_r(r^0)\hat{r} \tag{5'}$$

where $F_r(r^0)$ is a constant along the radial coordinate. The solution of the Laplacian in cylindrical coordinates, assuming constancy of the potential surfaces in the z-direction, is

$$V = Ar^n \sin(n\theta) \tag{10}$$

from which one obtains

$$\vec{E}_o = -nAr^{n-1} \left(\hat{r} \sin(n\theta) + \hat{\theta} \cos(n\theta)\right) \tag{11}$$

and

$$E_o^2 = n^2A^2 r^{2n-2} \tag{12}$$

and

$$\nabla(E_o)^2 = 2(n-1)n^2A^2r^{2n-3}\hat{r} \tag{13}$$

For the force to be independent of the radial coordinate, this requires that

$n = 3/2$, so

$$\nabla(\vec{E}\cdot\vec{E}) = 9\, A^2\hat{r}/4 \tag{14}$$

Accordingly,

$$V = Ar^{3/2}\sin(3/2\theta) = A(r_{60})^{3/2}; \tag{15}$$

where r_{60} is the value of the radial distance coordinate at $\theta = 60^o$, hence

$$r^{3/2} = (r_{60})^{3/2}\left(\sin(3/2\theta)\right)^{-1} \tag{16}$$

and

$$A = V(r_{60})^{-3/2} \tag{17}$$

so

$$\nabla(\vec{E}\cdot\vec{E}) = \frac{9}{4}V^2r(r_{60})^{-3} \tag{18}$$

Combining this with Eq. 5, we have

$$F_r = \frac{9}{2}\pi a^3V^2(r_{60})^{-3}\varepsilon_o K_e \tag{19}$$

or

$$F_r = \frac{9}{2}a^3V^2(r_{60})^{-3}Re\left\{\frac{\varepsilon_1^*(\varepsilon_2-\varepsilon_1)}{\varepsilon_2 + 2\varepsilon_1}\right\} \tag{20}$$

On inserting the conditional value for the gradient obtained earlier (following Eq. 8), and assuming an impressed voltage of 10 V across the electrode pair, as is reasonable for use in aqueous media, we find from Eq. 18 that the value for r_{60} is

$$r_{60} = \left[\frac{9\ V^2}{\nabla(\vec{E}\cdot\vec{E})}\right]^{1/3} = \left[\frac{9x10x10}{4x2.12x10^{11}}\right]^{1/3} = 1.02 \text{ mm} \tag{21}$$

This small value of the required distance, about 1 mm, for the critical spacing of electrodes in dielectrophoresis chambers to be applied to aqueous suspensions is quite restrictive. It severely limits the size of the regions in which one can expect to maintain reasonable control over suspended biological material. We have been guided by this consideration in the construction and use of operable dielectrophoretic systems for biological particles.

The Electrode Configuration

Fig. 3 shows the electrode configuration used in this study. It gives only an approximation of the desired isomotive field, but the quantity $\vec{\nabla}(E_o)^2$ does not change unreasonably over the volume of interest.

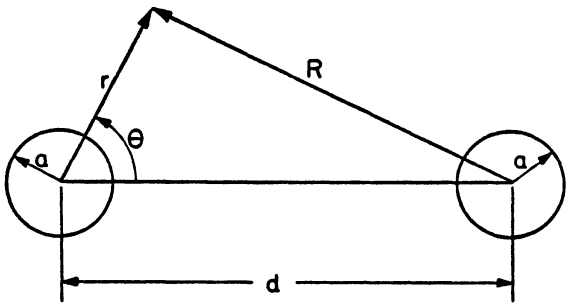

Fig. 3. Geometry of the wire-wire electrode system.

The quantity $\vec{\nabla}(E_o)^2$ has been given for this electrode system previously as (Crane and Pohl, 1978)

$$\vec{\nabla}(E_o)^2 = 2C_1^2 \left[\left(\frac{r-d\cos\theta}{R^2} - \frac{1}{r}\right)\left(\frac{1}{R^2} - \frac{2(r-d\cos\theta)^2}{R^4} \quad 1/r^2\right)\right.$$

$$\left. - \frac{2d^2\sin^2\theta(r-d\cos\theta)}{R^6}\right] \hat{r} + \frac{\theta 2C_1^2}{r}\left[\left(\frac{r-d\cos\theta}{R^2} - \frac{1}{r}\right)\right.$$

$$\left.\left(\frac{d\sin\theta}{R^2} - \frac{2(r-d\cos\theta)\ (rd\sin\theta)}{R^4}\right) + \frac{d^2\sin\theta}{R^4}\left(\cos\theta - \frac{2rd\sin^2\theta}{R^2}\right)\right]$$

$$\text{where } C_1 = \frac{\Delta V}{2\ell n\left[\frac{d-a}{a}\right]} \qquad (22)$$

ΔV is the potential difference between the electrodes, θ, d, a, R, and r are as shown in Fig. 3, and the potential is assumed to be zero midway between the conductors.

For the present analysis, $\vec{\nabla}(E_o)^2$ can be simplified by setting r = R, which gives

$$\vec{\nabla}(E_o)^2 = 2C_1^2\left[\left(\frac{-d\cos\theta}{r^2}\right)\left(\frac{2}{r^2} - \frac{2\ (r-d\cos\theta)^2}{r^4}\right) - \frac{2d^2\sin^2\theta\ (r-d\cos\theta)}{r^6}\right]\hat{r}$$

$$+ \frac{2C_1^2}{r}\left[\left(\frac{-d\cos\theta}{r^2}\right)\left(\frac{d\sin\theta}{r^2} - \frac{2(r-d\cos\theta)\ rd\sin\theta}{r^4}\right) + \frac{d^2\sin\theta}{r^4}\left(\cos\theta - \right.\right.$$

$$\left.\left.\frac{2d\sin^2\theta}{r}\right)\right]\hat{\theta} \qquad (23)$$

Fig. 4 shows the variation of $\vec{\nabla}(E_o)^2$ with position. The numerical values used in this calculation were: $\Delta V = 10$ V, $d = 3.26$ mm, $a = 1.00$ mm, $r = (d^2 + y^2)^{\frac{1}{2}}$, $\Theta = \sin^{-1}\left(\frac{y}{n}\right)$. The value y is the abscissa in Fig. 4 and ranges from 0 to 0.9 mm. y is measured along the perpendicular bisector of the line of centers of the two electrodes.

It can be seen that $\vec{\nabla}(E_o)^2$ does not vary strongly in the region of our interest (y = 300 μm to 900 μm).

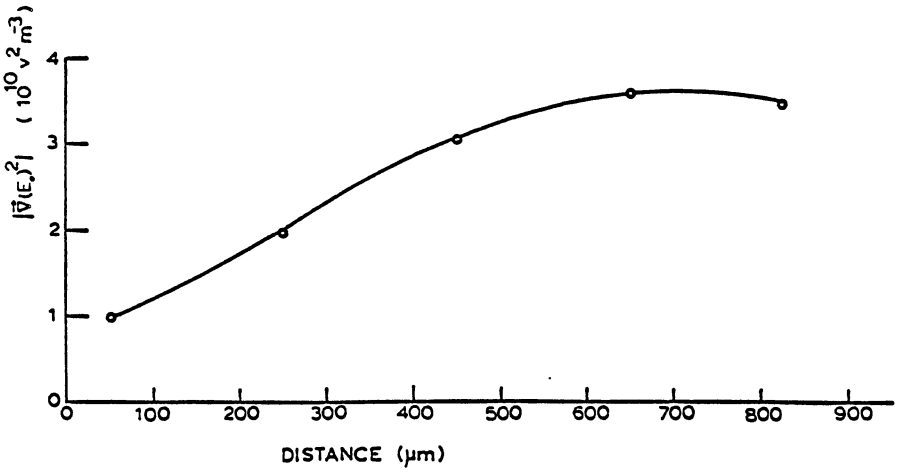

Fig. 4. The computed variation of the gradient of the field-squared along the perpendicular bisector of two parallel cylindrical electrodes. As an imitator of the isomotive field, this electrode system is seen to give no great variation of $\vec{\nabla}(E)^2$ over the distance range 300 to 800 μm.

Potential and Field Distribution in Insulator - Isolated Aqueous Media

By way of emphasizing the importance of real versus ideal dielectrics in dealing with cellular dielectrophoresis, let us see how effective the voltage applied on metallic electrodes *external* to a glass-contained water stream is in producing a voltage drop in the water phase. For simplicity, let us consider the dielectrophoresis chamber as merely consisting of three dielectric layers situated between ohmic electrodes. The two outer layers are glass, the inner layer is the aqueous phase, as shown in Fig. 5a. Using the network laws, one arrives at the voltage drop across the water phase as

$$\frac{V_w}{V_o} = \left(\frac{R_w}{1 + j\omega R_w C_w}\right) \left\{ \frac{1}{\frac{R_w}{1+j\omega C_w R_w} + \frac{2R_g}{1+j\omega C_g R_g}} \right\} \tag{24}$$

from which one finds the real part of the expected voltage drop in the water phase as

$$V_w = \frac{V_o R_w \{R_w + 2R_g + \omega^2 C_g R_g (R_w C_g R_g + 2R_g C_w R_w)\}}{(R_w + 2R_g)^2 + \omega^2 (R_w C_g R_g + 2R_g C_w R_w)^2} \tag{25}$$

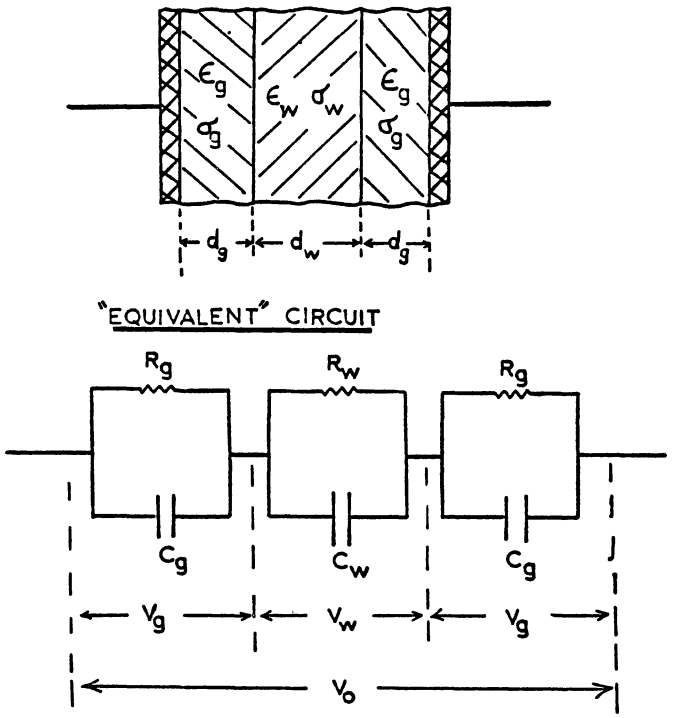

Fig. 5a. Diagram of the dielectric situation for an aqueous medium held by glass between metallic electrodes. The equivalent circuit is shown.

where R_g and R_w are the resistances of the glass and water phases respectively, C_g and C_w are the corresponding capacitances, V_w is the voltage drop in the water phase, and V_o is that across the total system, while ω is the angular frequency of the applied electrical field. The above equations, it is emphasized, apply only as an approximation to the actual and geometrically much more complicated real system, and describe only the steady state situation during the application of a sinusoidal voltage, $V = V_o e^{j\omega t}$. Upon assuming unit cross-sectional dimensions for the construction, for example, and values therefore of $C_w = 80\ \epsilon_o/d_w$ and $C_g = 7.5\ \epsilon_o/d_g$ for the water and glass phases respectively, R_w = (140; 750; and 3000 ohm-m) $\div$ (i_w) (corresponding to the actual resistivities used experimentally), and $R_g = 10^{13}$ ohm, the V_w/V_o ratios computed are shown in Fig. 5b for d_w = 900 μm and d_g = 180 μm. It is instructive to note that the effective voltage rapidly falls to experimentally insignificant values in the frequency range 10^3 to 10^5 Hz, depending upon the resistivity of the aqueous medium. The actual dielectrophoretic force is, moreover dependent upon the square of the effective local field, so the situation is perhaps even more critical. It is apparent that the dielectrophoretic force will probably be negligible in aqueous suspensions held between glass walls at frequencies below about 10^3 to 10^4 Hz.

EXPERIMENTAL

To study both positive and negative biological dielectrophoresis, a continuous-flow chamber with stream-centered flow was used. The

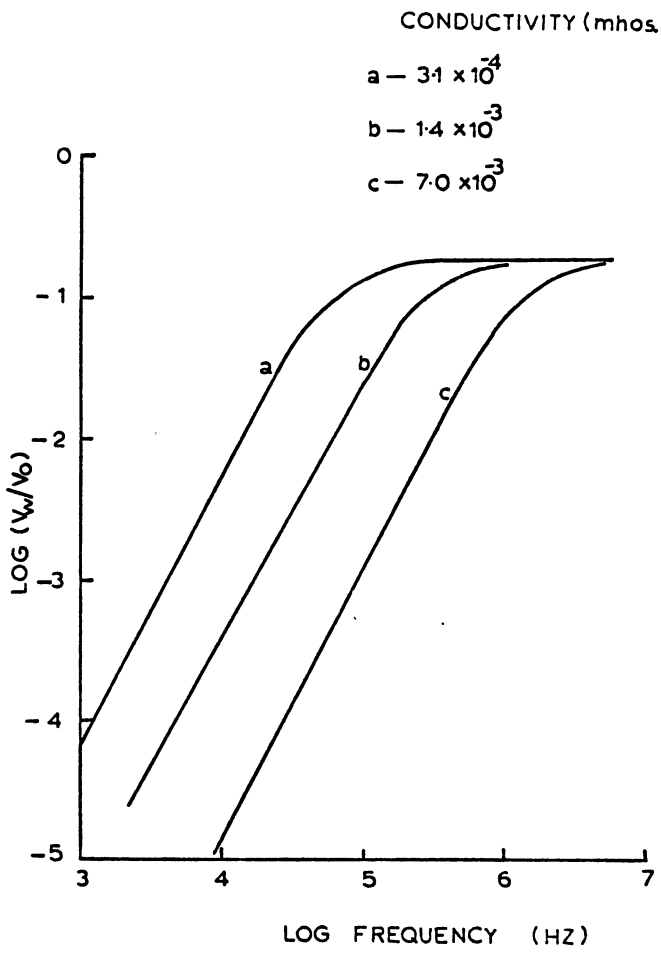

Fig. 5b. Plot of computed voltage ratio V_w/V_o versus frequency for the potential across a water layer V_w between glass walls, all subject to an applied potential of V.

flow chamber, shown in Fig. 6, consisted of a square capillary Microcell (Vitro Dynamics Inc.), 0.9-mm I.D., mounted on a microscope slide. Two cylindrical copper electrodes, 2 mm in diameter, (see exploded view in Fig. 7) were placed closely on either side of the Microcell to provide the nonuniform field. An injector consisting of an arrangement of a #31 gauge 0.25-mm O.D., 0.13-mm i.d., gas chromatograph syringe needle centered in a #20 gauge (0.58-mm i.d.) hypodermic needle was used (see Fig. 8) to inject a concentrated cell suspension into the center of a support liquid stream to provide stream-centered flow in the cells. This arrangement gave a narrow stream of cells in the center of the flow chamber. The diameter of the central cell stream was observed to typically be in the order of 25 to 100 μm in a flow chamber of 900 μm, as the half-widths of the traces shown in Figs. 14a and 14b show.

A schematic representation of the experimental set-up is shown in Fig. 9. The two liquids were supplied from syringes mounted in an infusion pump (Harvard Apparatus model 975). The support stream was supplied from a 5-mℓ syringe at a flow rate of 9.6 x 10^{-3}mℓ/min. The

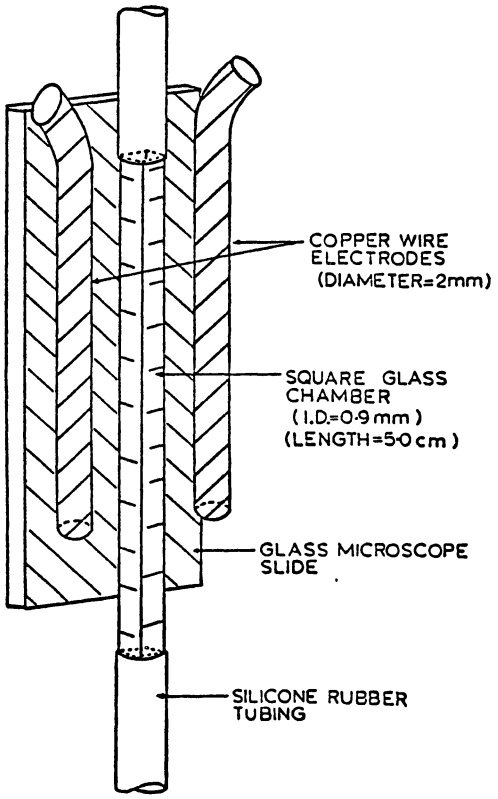

Fig. 6. Exploded view of the continuous-flow chamber for dielectrophoretic analysis and separation of microorganisms.

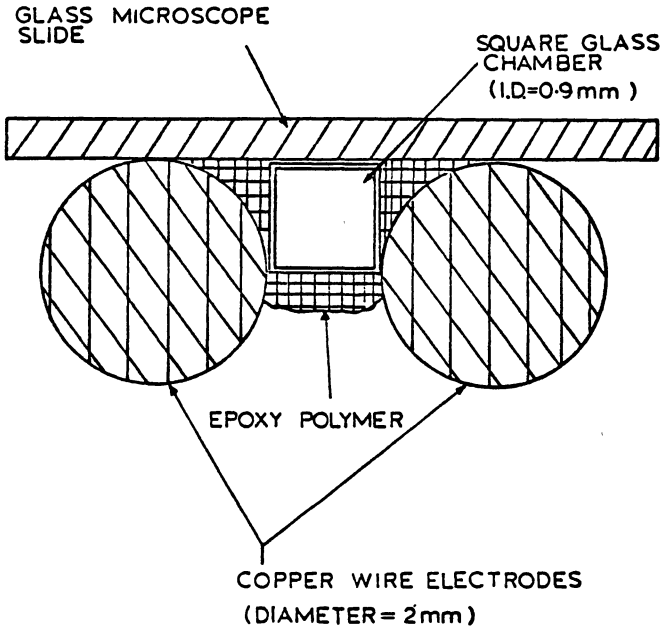

Fig. 7. Cross-sectional view of the continuous-flow chamber showing the square capillary in cross-section.

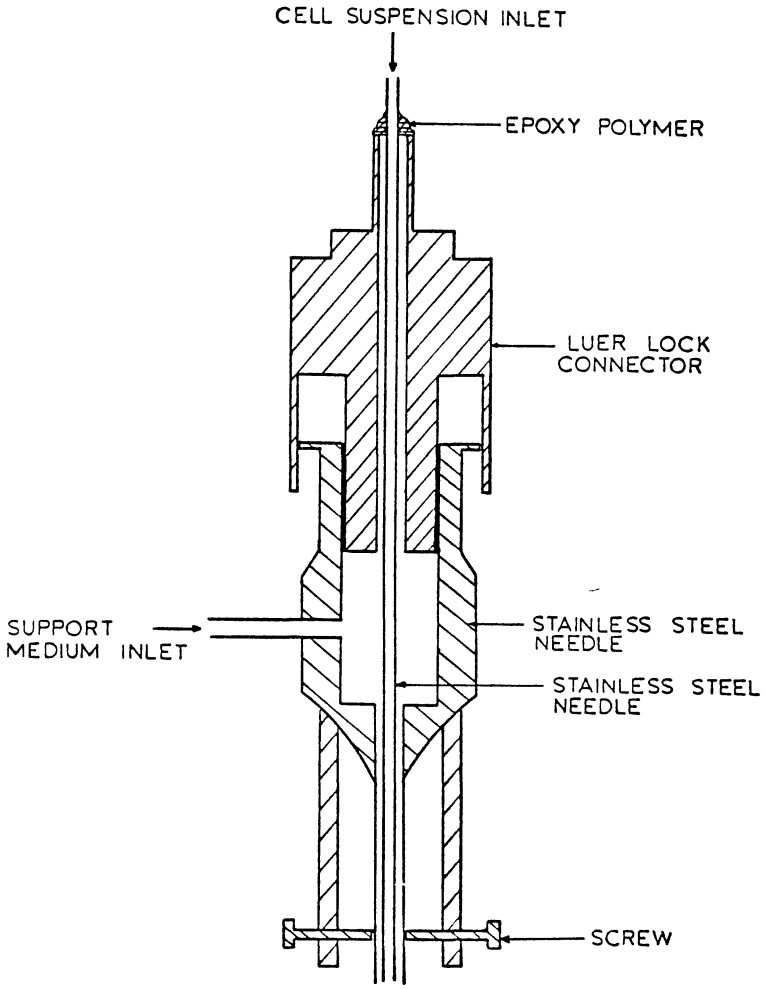

Fig. 8. Injector for producing stream-centered flow of the cells in a supporting medium.

cell suspension was injected from a 50-μℓ syringe. This gave the cells an average velocity through the flow chamber of approximately 200 μm/s; thus they were subjected to the field for approximately 100 s. The incorporation of an in-line conductivity cell in each stream enabled the conductivity of each stream to be measured. It is important to insure that the streams have the same conductivity so as to minimize bulk polarization effects masking the polarization of the cells.

Each conductivity cell (shown in Fig. 10) consisted of a flow chamber containing two parallel platinum black wires 2.5 cm long and 0.25 mm in diameter. The center (cell supply) stream also had a small glass supply chamber of about 1-mℓ volume in the line. The supply chamber (shown in Fig. 11) contained a magnetic stirrer to keep the cells in suspension during the course of an experiment.

The dielectrophoresis chamber was mounted on a microscope stage for observation. The microscope (Bausch & Lomb Model PB152) was set on its back so that the chamber was held vertically upright. An RCA Model TC1000 video camera was used to display the chamber contents on

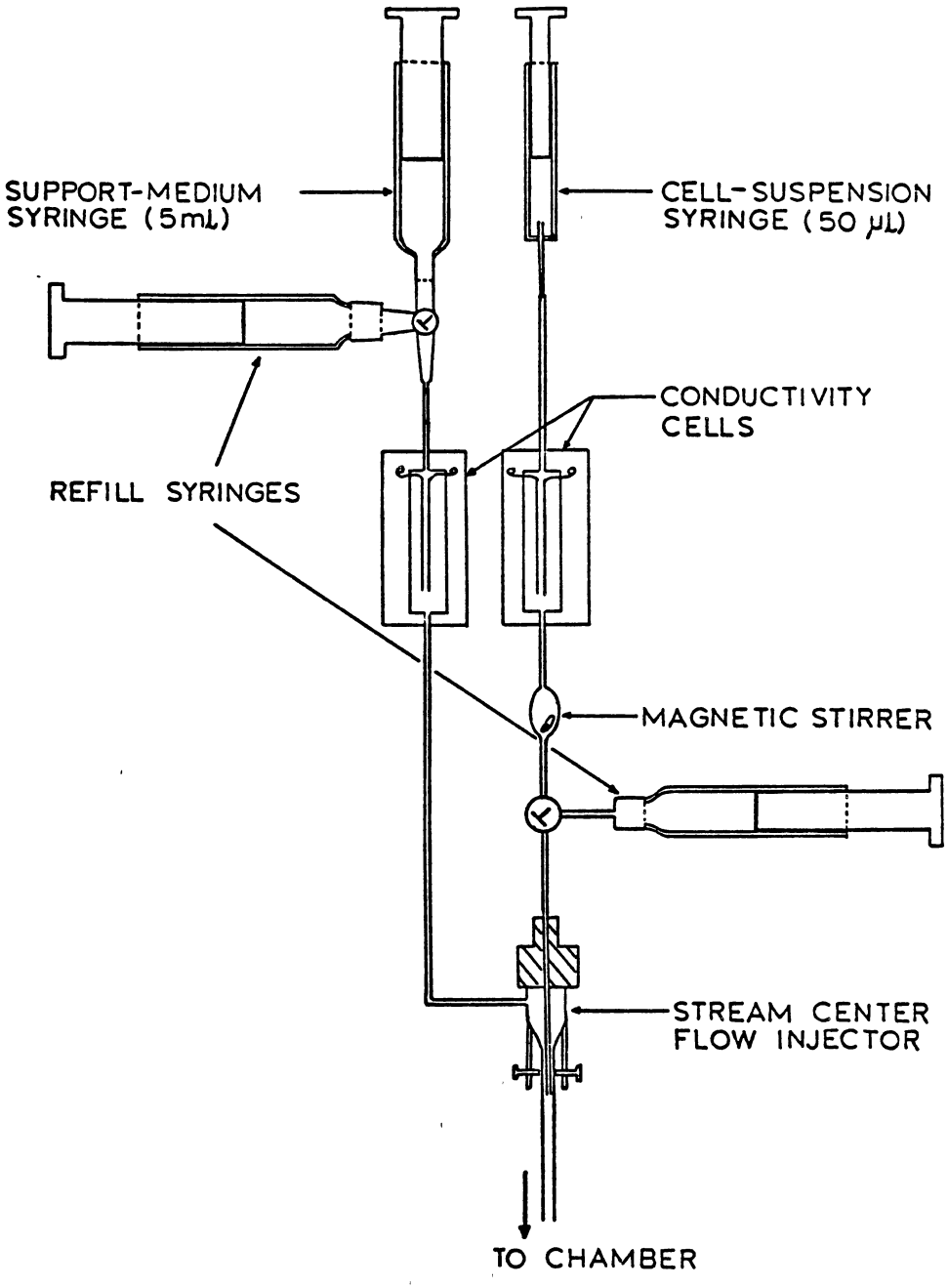

Fig. 9. Schematic diagram of the apparatus for supplying stream-centered cells to the dielectrophoresis chamber.

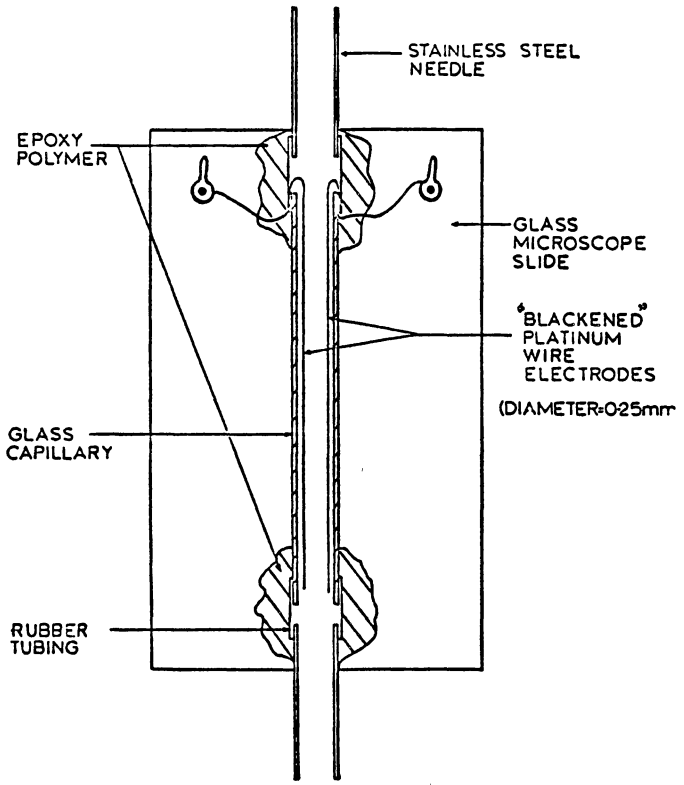

Fig. 10. Diagram of the in-line conductivity cell. It contains two parallel Pt wires having Pt-black surfaces.

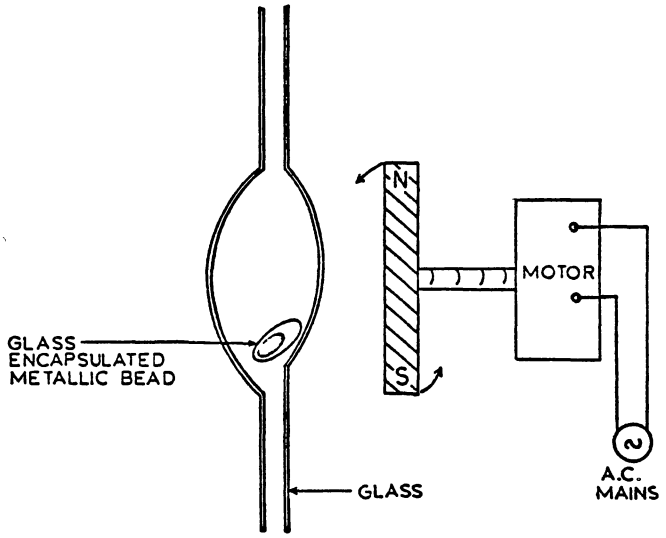

Fig. 11. Cell supply chamber.

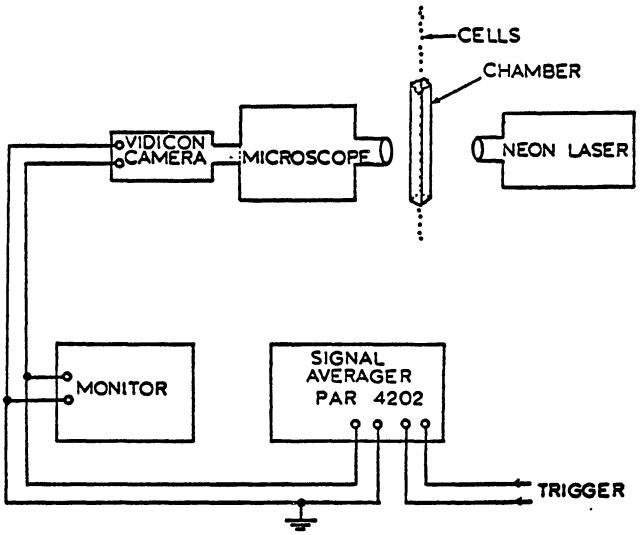

Fig. 12. Block diagram of the optical and electronic arrangements for determining the deflection of microorganisms by dielectrophoresis.

a HaRco MV-10A monitor. The chamber was illuminated at right angles to the side by a 2-mW Metrologic laser focused by a lens of 20 cm focal length to provide dark field illumination (see Fig. 12).

The video output was fed to a PAR 4202 signal averager used in the multichannel scaling (MCS) mode and triggered by a 1.5-V 60-Hz signal. The signal averager in the MCS mode allowed a threshold voltage to be set so that only the voltage peaks of the illuminated cells were counted and registered while the background noise was filtered out. Two memories (A and B) were available in the signal averager. A dual memory store enabled a comparison of the position of the deflected stream to be made with respect to the undeflected stream.

Voltages (50 to 150 V r.m.s. at 10^2 Hz to 6 x 10^5 Hz) were supplied across the dielectrophoresis chamber with a Hewlett-Packard 200CD audio oscillator and a Krohn-Hite Model DCA wide-band amplifier. The voltages were measured with a Hewlett-Packard 410B voltmeter. A block diagram of the electrical system is shown in Fig. 13.

Conductivity measurements were made with a General Radio 165A impedance bridge at 1 KHz. In addition to the in-line conductivity cells, a Yellow Springs Instruments 3403 dipping-type electrode was used as an occasional check on the in-line cells. Conductivities were adjusted with KCℓ.

The cells used in this study were yeast (*Saccharomyces cerevisiae*) and algae (*Chlorella vulgaris*). The yeast cells were cultured in malt extract broth (Difco) with shaking to minimize clumping. The *Chlorella* was grown in large stirred 4-ℓ aspirator bottles on Chu No. 10 medium (Nichols, 1973). Both of the above cell species were harvested, then subjected to repeated washing using centrifugation and resuspension in deionized water. The cells were then resuspended in water of the desired conductivity for the final preparation on which the measurements were made.

After the cells were thus resuspended, the cell suspension and

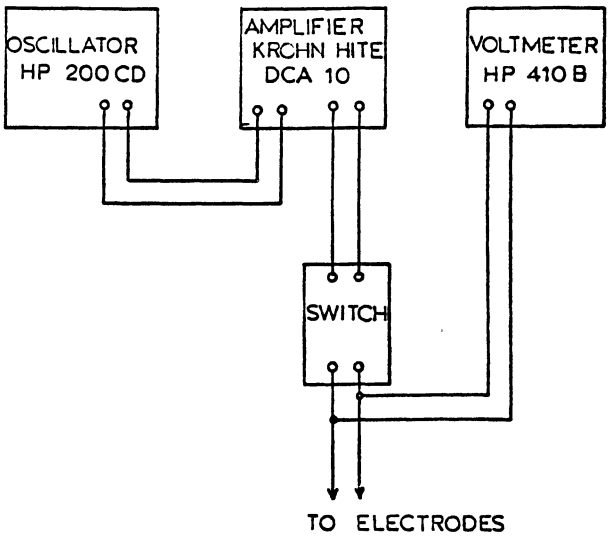

Fig. 13. Block diagram of the high field supply to the dielectrophoresis chamber.

support liquid were loaded into the pumping syringes and a steady stream flow was established in the chamber.

With the stream established, a count was made on channel A of the signal averager to determine the original position of the stream. The voltage at a desired frequency was applied and, after 2 min, a count was made on channel B of the signal averager. The positions of the two peaks could then be compared and the deflection determined.

The photographs in Fig. 14 show some typical positive and negative deflections of *C. vulgaris* cells. Fig. 14a shown the deflections of such cells when subjected to a voltage of 50 V r.m.s. at 600 KHz. The upper trace (Channel A) shows the reference position of the stream with zero applied voltage. The lower trace (Channel B) represents the cell stream position after having being subjected to the nonuniform field for two min, showing a positive displacement (to the right) of 90 μm.

The next photograph (Fig. 14b) shows the displacement of the same stream under the influence of 50 V r.m.s. at 20 KHz. As in the first photograph, the top trace (Channel A) shows the original position of the stream without a field, while the bottom trace (Channel B) shows the now steady-state position of the stream after two min of applied field. At this frequency there is a *negative* displacement (to the left) of 30 μm in the cell stream.

Photograph 14c shown the same result as photograph 14b, but in the difference form of (A-B). In this form the negative displacement of the cell stream is clearly visible.

RESULTS

The results illustrate a useful method for observing continuous dielectrophoresis and perhaps more importantly, demonstrate the existence of negative as well as positive dielectrophoresis in suspensions of living cells.

The two unicellular organisms were studied at different conductivities ($\sigma = 7.1 \times 10^{-3}$, 3.1×10^{-4}, and $1.4 \times 10^{-3} \Omega^{-1} \cdot m^{-1}$ for *S.*

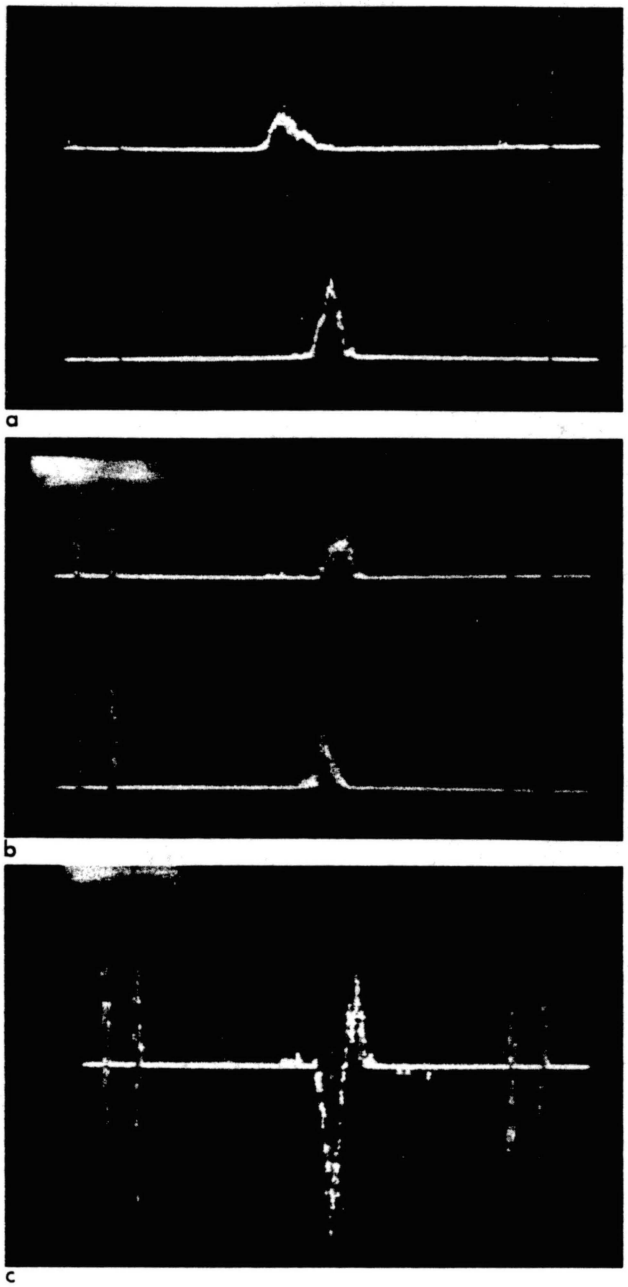

Fig. 14. Signal-averaged recordings of the deflection of *Chlorella vulgaris* cells in a nonuniform electric field. The cells were suspended in water adjusted to a resistivity of 130 K ohm-cm by the addition of KCl, and subject to 50 V r.m.s. at the frequencies shown below. 1 division = 100 μm.
(a) Positive dielectrophoresis: top trace = control (zero field); bottom trace = positive deflection (steady value after two min).
(b) Negative dielectrophoresis: top trace = control (zero field); bottom trace = negative deflection (steady state after two min).
(c) Negative dielectrophoresis: Shown is (A-B), the difference of the recorded traces where A = control and B = deflected cells' trace.

cerevisiae; σ = 7.1 x 10^{-3}, and 7.7 x $10^{-4}\Omega^{-1}\cdot m^{-1}$ for *C. vulgaris*) and at frequencies from 6 x 10^{2} Hz to 6 x 10^{5} Hz. The magnitudes of the applied voltages were chosen so that the largest diflections were still measurable and the cells were not pulled against the chamber wall.

Fig. 15 shows the dielectrophoretic displacement curves for *S. cerevisiae* for the three cell suspension conductivities. All the curves show both positive and negative displacements, with the largest displacements occurring at a frequency of 10^{5} Hz or higher. It is of interest that the curve for the largest conductivity shows displacements that are reversed from those of the lower conductivity curves.

Fig. 16 shows the dielectrophoretic displacement curves for *C. vulgaris* at the two conductivity values used. Both of these curves exhibit positive as well as negative displacements with the maximum displacements occurring at or above 10^{5} Hz. The above plots show response characteriscics similar to those of *S. cerevisiae* in that for a particular frequency, the displacement at low conductivity is the opposite of that for high conductivity. In view of the expected low intensity with which externally applied electric potentials create a field in such insulator-isolated aqueous regions, the observed dielectrophoresis is small at low frequencies. That presently observed at 10^{3} to 10^{4} Hz is probably within experimental error. The technique of stream-centered dielectrophoresis is a delicate one requiring careful control of several experimental parameters. To obtain measurable dis-

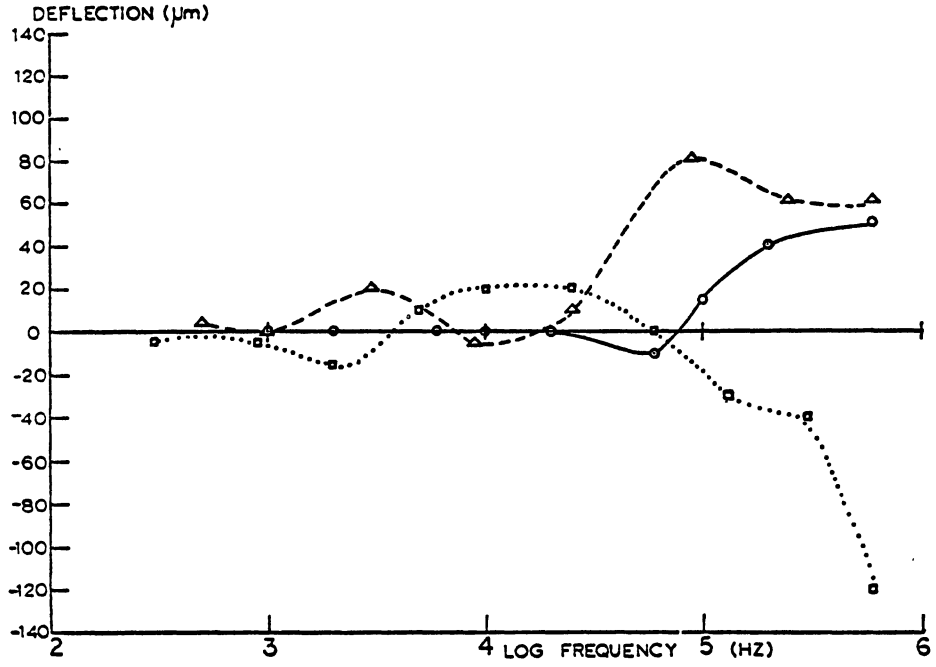

Fig. 15. Dielectrophoretic displacement versus log frequency plot for yeast cells (*Saccharomyces cerevisiae*) obtained using the continuous stream-centered dielectrophoresis technique.

□ ·····; Resistivity = 14 k ohm-cm, $V_{applied}$ = 100 V r.m.s., except at 300 Hz where V = 85 V.

⊙ ————; Resistivity = 75 k ohm-cm, $V_{applied}$ = 30 V r.m.s.

Δ----------; Resistivity = 320 k ohm-cm, $V_{applied}$ = 75 V r.m.s.

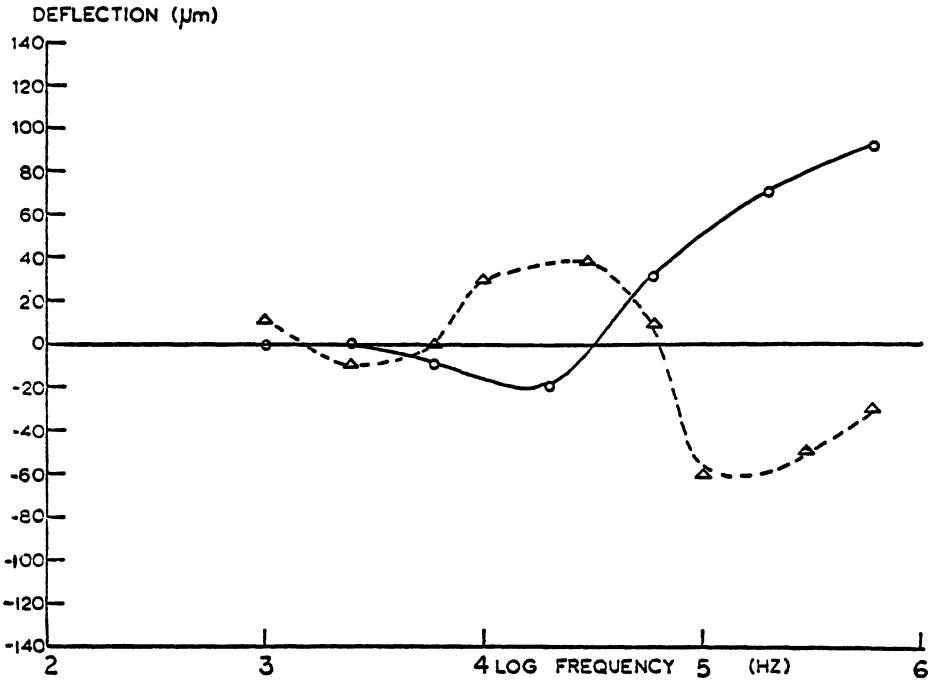

Fig. 16. Dielectrophoretic displacement spectrum of *Chlorella vulgaris* obtained using stream-centered continuous dielectrophoresis.

⊙ _____ ; Resistivity = 130 k ohm-cm, $V_{applied}$ = 50 V r.m.s.

Δ----------; Resistivity = 13 k ohm-cm, $V_{applied}$ = 100 V r.m.s.

placements of the cell stream, considerable care must be exercised in preparing the cell suspensions, preserving the laminar flow characteristics of the cell stream, and establishing the center stream. Both the direction and magnitude of the displacements were observed to be sensitive to changes in the conductivity of the suspensions and the frequency of the applied field.

SUMMARY

We conclude that measurable dielectrophoretic displacements in both positive and negative directions have been demonstrated using a stream-centered continuous-flow chamber. Displacements in agreement with theory and of up to 100 μm were readily observed for both cells of *Saccharomyces cerevisiae* and *Chlorella vulgaris*.

Dielectrophoretic studies using this technique have the advantage of allowing both positive and negative dielectrophoretic forces to be studied and applied. The wider range of dielectric response available to stream-centered dielectrophoresis indicates that it may be preferred in many applications, such as cell separations, over previously developed dielectrophoretic techniques, particularly in the study of living cells.

ACKNOWLEDGEMENT

The authors acknowledge with appreciation the stimulus and support given to this research by the National Science Foundation through Grant No. NSF PCM76-21467.

REFERENCES

Black, B. C.; Hammond, E. G. 1965a. J. Am. Oil Chem. Soc. 42, 931.

Black, B. C.; Hammond, E. G. 1965b. J. Am. Oil Chem. Soc. 42, 936.

Chen, C. S.; Pohl, H. A. 1974. Trans. N. Y. Acad. Sci. 238, 176.

Crane, J. S. 1970. "The Dielectrophoresis of Cells", Ph.D. Dissertation, Oklahoma State University.

Crane, J. S.; Pohl, H. A. 1978. J. Biol. Phys 6, 45.

Jones, T. B.; Bliss, G. W. 1977. J. Appl. Phys. 48, 1412.

Mason, B. D.; Townsley, P. M. 1971. Can. J. Microbiol. 17, 879.

Nichols, H. Wayne. 1973. "Growth media--fresh water", in HANDBOOK OF PHYCOLOGICAL METHODS (Janet R. Stein, ed). Cambridge University Press, Cambridge, p. 15.

Parmar, D. S.; Jalaluddin, A. K. 1974. Jap. J. Appl. Phys. 13, 793.

Pohl, H. A. 1951. J. Appl. Phys. 22, 869.

Pohl, H. A. 1958. J. Appl. Phys. 29, 1182.

Pohl, H. A. 1960. Sci. Am. 203, 107.

Pohl, H. A. 1968. J. Electrochem. Soc. 115, 155c.

Pohl, H. A. 1969. In DIELECTROPHORETIC AND ELECTROPHORETIC SEPARATION, (H. A. Pohl and W. F. Pickard, eds.). The Electrochemical Society, New York, p. 12.

Pohl, H. A.; Crane, J. S. 1971. Biophys. J. 11, 711.

Pohl, H. A.; Crane, J. S. 1972. J. Theor. Biol. 37, 1.

Pohl, H. A. 1973. In ELECTROSTATICS AND ITS APPLICATIONS, (A. D. Moore, ed.). Wiley-Interscience, N.Y., pp. 342-3.

Pohl, H. A.; Crane, J. S. 1973. In ELECTROSTATICS AND ITS APPLICATIONS, (A. D. Moore, ed.). Wiley-Interscience, N.Y. pp. 368-70.

Pohl, H. A.; Pethig, R. 1977. J. Phys. E. 10, 190.

Pohl, H. A. 1978. DIELECTROPHORESIS. Cambridge University Press, Cambridge, England.

Rhoads, J. E.; Pohl, H. A.; Buckner, R. G. 1976. J. Biol. Phys. 4, 93.

Sher, L. 1968. Nature (London) 220, 695.

Ting, I. P.; Jolley, K.; Beasley, C. A.; Pohl, H. A. 1971. Biochim. Biophys. Acta 234, 324.

APPENDIX B

DIELECTROPHORETIC FORCE: A COMPARISON OF THEORY AND EXPERIMENT

COPYRIGHT © 1979 by Physical Biological Sciences Ltd. All Rights Reserved.

Dielectrophoretic Force: A Comparison of Theory and Experiment

H. A. Pohl, K. Pollock
Department of Physics
Oklahoma State University
Stillwater, OK 74074

J. S. Crane
Department of Physical Sciences
Cameron University
Lawton, OK 73501

ABSTRACT Because of the increasing use of dielectrophoresis in the dielectric characterization and sorting of living cells or their parts, it has become important to establish carefully the theoretical backgrounds for this effect. A comparison with experiment is made of the several versions of the theory for the dielectrophoretic force exerted by nonuniform electric fields upon a neutral object. The three fundamental approaches: the Maxwell-Strattonstress tensor, the effective dipole moment, and the 'Helmholtz' energy approach are presented along with the general solution given earlier by Pohl and Crane. These are found to agree closely with experiment in predicting the dielectrophoretic force upon various rods hung in specially shaped (isomotive) field distributions. On the other hand, an alternative formulation based upon a debatable assignment of fields local to the dipoles gave a good fit to the experimental data only for materials of very low permittivity, and fitted poorly in the case of highly polarizable materials.

An improved derivation of the theory for stable dielectrophoretic levitation is also presented. This phenomenon is of particular interest in that it is based upon an apparent violation of the Earnshaw's theorem, and is useful in the study of the dielectric properties of individual living cells.

Introduction

When a neutral object is subjected to an nonuniform electric field, $\vec{E}$, a translational force, $\vec{F}$, is produced which is proportional to E^2. In some cases, a torque tending to produce rotation also arises, but that torque is not the immediate object of our discussion. Instead we shall inquire as to the proper relation between $\vec{F}$ and E^2 as it depends upon the dielectric properties of the object and its surrounding medium, and show experimental evidence deciding for the more correct of several postulatable theoretical relationships. The precise relationship between $\vec{F}$ and E^2 has been in question for some years. Because of the growing usefulness of nonuniform field effects in various applications, it has become crucial to establish the best possible theoretical background.

The translational motion of objects subject to this force arising in nonuniform electric fields is known as dielectrophoresis.[1] Dielectrophoretic methods of particle separation and analysis, especially that of biological materials such as living cells, are becoming increasingly useful. The principles of the operation are straightfor-

ward. The results can yield much information as to the electrical makeup of the systems studied. The action of a nonuniform electric field (ac or dc) upon a small, polarizable, neutral body is usually such as to create a dipole oriented along the line of the applied field. Since the charges of the (induced or re-aligned) dipole are of equal but opposite sign, but lie in field regions of differing strength, there is a net translational force upon the particle. Dielectrophoresis is to be distinguished from electrophoresis, the motion caused by the action of an electric field (whether uniform or nonuniform) upon a charged object. The dielectrophoretic force, then, is a measure of the net polarizability of the object sitting in the surrounding medium: electrophoretic force is a measure of the charge on an object.

The present problem of the precise relationship between $\vec{F}$ and E^2 during particulate dielectrophoresis is analogous in some ways to the problem of the (electrostrictive) pressure, p, which arises in fluids subject to electric fields. It is somewhat more complex, however, because dielectrophoresis deals with systems having several dielectrics present, adding both material parameters and geometrical factors to the more straightforward pressure problem. Because of the similarities, however, it will be useful here to touch upon the resolution of the $p:E^2$ relationship for fluids before resolving the $\vec{F}:E^2$ relationship for dielectrophoresis.

The $p:E^2$ problem for fluids has had an interesting history. An analysis of the volume forces on a fluid in an electric field done along the lines suggested by Korteweg[1] and by Helmholtz[2], and developed further by Abraham and Becker[3], by Stratton[4], and by Durand[5] showed that the vector force acting on any volume element, dv, inside the dielectric fluid is

$$\vec{F}=\int_v \nabla\left(\frac{E^2}{2}\rho\frac{\partial\varepsilon}{\partial\rho}\right)dv-\int_v\frac{E^2}{2}\nabla\varepsilon\,dv \tag{1}$$

where ρ is the density of the dielectric fluid, ε is its permittivity, and v is its total volume.

The energy method of Helmholtz for the theory of the mechanical action in dielectrics subject to electric fields was criticized by Larmour[6] and later by Livens[7]. From the polarization of the dielectric, Livens derived the expression

$$\vec{F}=\int_v(\vec{P}\cdot\nabla)\vec{E}\,dv \tag{2}$$

where $\vec{P}$ is the polarization, and $\vec{E}$ is taken to be the *local* electric field in the volume element, dv. However, Cade[8] has argued that this formula does not take into account the fact that the volume element at the position of E does itself provide a contribution to the field, one of the same order of magnitude as that of E, so that in computing the force upon the volume element this contribution must be subtracted. Hakim analysed the problem theoretically, concluding that Eq. 1 was valid and that Eq. 2 was false. The problem appeared to be settled when Hakim and Higham[10] showed experimentally upon using Schlieren optics to examine the effect of pressure upon the refractive index of non-polar liquids that Eq. 1 and not Eq. 2 predicted the correct results. Although the knotty problem of

the proper $p:E^2$ relationship fluids may now be considered to be resolved in favor of the energy approach as suggested by Helmholtz, it will be appreciated that the preferred answer was not easy to arrive at. An analogous situation has arisen regarding dielectrophoretic forces, a matter to which we now return.

Overview

The dielectrophoretic force exerted by a nonuniform electric field acting upon a particle situated in a surrounding medium can be considered to be made up of three factors, one determined by the nature of the several dielectrics, one determined by their geometrical distribution, and the third determined by the distribution of the electric field. We shall here be concerned with the first, the polarization factor in the $\vec{F}:E^2$ relationship. The analysis will proceed along several possible theoretical lines and the results will be compared with experiment. The theoretical analyses will proceed using three distinct approaches. In the first, the Maxwell-Stratton stress analysis is used. In it the stress, or force per unit area on a surface enclosing the body of interest is used to find the total force by integration over the surface. Here, one must know the field intensity, $\vec{E}$, and the dielectric displacement, $\vec{D}$, at all points on the surface. The theoretical background and its applications are well described in standard texts.[4, 5, 17, 21]

The second theoretical approach, which we shall refer to for brevity as the 'effective dipole moment' approach, computes the total force resulting from the action of the field upon the dipole moments of each volume element. A dipole moment is attributed to each volume element as a result of the polarization, $\vec{P}$, caused by the action of the field. Through the interaction of the dipole moment with the electric field, a force per unit volume is obtained. The total force is computed by integration over the volume of the body. In this case there is some question as to which field may be used ($\vec{E}_{\text{local}}$ or $\vec{E}_{\text{external}}$) and also a question as to how the dipole moment is to be calculated when the body is in a material medium. A knowledge of $\vec{P}$ and $\vec{E}$ for every volume element is required. Here, the force, $\vec{F}$, is given by [21, 36]

$$\vec{F}=\int_v(\vec{P}\cdot\nabla)\vec{E}\,dv \tag{3}$$

The expression has been applied to the calculation of the force upon a spherical dielectric body in a fluid medium by von Hippel[12] and by Pohl[11, 13, 36] with the effective field chosen to be that external to the body, $\vec{E}_{\text{ext}}$. On the other hand, Lorain and Corson[19] compute the dielectrophoretic force using $\vec{E}$ as the local field, $\vec{E}_{\text{loc}}$.

In the third approach, which we shall refer to for brevity as the Helmholtz 'energy' approach, one computes the energy of the body in the field with a volume integration, and relates the force to the change in energy resulting from a small displacement. A knowledge of $\vec{D}$ and $\vec{E}$ at all points in the volume to be occupied by the body is necessary both before and after the introduction of the body. The

Helmholtz energy approach used for a wide variety of problems[4, 5, 20, 21, 27] is well discussed in the cited texts. The method has recently been questioned by Neufeld[18, 22]. The Helmholtz approach has been used for the calculation of the energy and force of a body in a nonuniform electric field by Schwartz[24], and by Pohl and Crane[15, 16]. Adaptation to the very useful case of a lossy sphere in a lossy medium was made by Sher[14]. Experimental verification of a general sort for the theory concerning lossy spherical particles in a lossy fluid medium was obtained by Crane and Pohl[16] on studying the dielectrophoretic collection rate of yeast cells, and on studying the dielectrophoretic force on single yeast cells[25]. Experiments on the levitation of bubbles by Jones and Bliss[26] also tend to confirm this approach. Greinacher[28] experimentally examined the electrostrictive rise of liquids in capacitors held at high potential, in a method analogous to the Quincke method for the measurement of magnetic susceptibility, and found good agreement with the theory based upon the energy argument. A still sharper experimental check is needed, however.

The details of the theoretical analysis comparing the dielectrophoretic force as calculated by the several assumptions outlined above, and done with several system shapes chosen for ease of calculation are given in Appendix A. Since we shall wish to make an experimental comparison of the several theoretical postulates, and such an experiment is rather conveniently done with objects of cylindrical shape, a brief derivation of the relevant equations is presented below.

Theoretical Calculations of the Dielectrophoretic Force for Various Model Systems

In this section we discuss the results of various calculations for the dielectrophoretic force expected to arise upon various uniformly polarizable and homogenous bodies when subject to a nonuniform electric field.

A. Small sphere. Upon using the "effective dipole moment" approach, (cf. Eq. 3) a number of authors[11, 12, 13–16, 36] arrive at the expression

$$\vec{F}=2\pi a^3\varepsilon_1\frac{(\varepsilon_2-\varepsilon_1)}{\varepsilon_2+2\varepsilon_1}\nabla(E_0^2) \tag{4}$$

where $\vec{F}$ is the total net force exerted along the x-direction, a is the radius of the sphere, ε_1 and ε_2 are the absolute permittivities of the fluid medium and sphere respectively, and E_0 is the (x-directed) electric field intensity of the *original* field present before the sphere was inserted.

An alternative expression was derived by Lorrain and Corson[19] which may be put as

$$F=\frac{2}{3}\pi a^3\frac{(\varepsilon_2-\varepsilon_1)}{(\varepsilon_2+2\varepsilon_1)^2}\left[\varepsilon_1(4\varepsilon_1+5\varepsilon_0)-\varepsilon_2(\varepsilon_1-\varepsilon_0)\right]\nabla(E_0^2) \tag{5}$$

The differences between Eqs. 4 and 5 arise primarily because of the assumptions as to the identity of the E term in Eq. 3, as noted earlier. In view of the two differing results obtained in Eqs. 4 and 5 through the use of the effective dipole moment approach (Eq. 3) it is of considerable interest to see what result is obtained by an alternate approach. In this case, the energy approach[14, 15] is readily usable and gives the same result as Eq. 4. The argument is readily extended to the case of lossy dielectrics, where

$$\varepsilon_j = \varepsilon_j' - i\varepsilon_j'' = \varepsilon_j' - i\sigma_j'/\omega \tag{6}$$

The result, analogous to Eq. 4, is[16, 36]

$$\vec{F} = 2\pi a^3 \operatorname{Re}\left\{ \varepsilon_1^* \frac{(\varepsilon_2 - \varepsilon_1)}{(\varepsilon_2 + 2\varepsilon_1)} \right\} \nabla (E_0)^2 \tag{7}$$

and $j = 1, 2$ refers to the surrounding medium and the particle respectively, and the symbols Re, *, ε_j', and ε_j'' denote the real part of the time mean, the complex conjugate, the real in-phase permittivity and the out-of-phase dielectric permittivity (loss) respectively. The in-phase conductivity and the angular frequency are denoted by σ_j' and ω. Stratton[4] derives the result for loss-free dielectrics only. The validity of replacing the real by the complex dielectric constant is discussed by Fano et al.[13], and by von Hippel[12]. In general, it can be done for any particular solution of Maxwell's equations for the sinusoidal steady state in a source-free region.

B. Small cylinders and plates. The force exerted by a nonuniform field upon small isotropic, homogeneous objects of spherical, cylindrical, or plate-like shape can be evaluated readily using the 'effective dipole moment' approach, Eq. 3. The induced net polarization or moment per unit volume, $\vec{P}$, in the volume is

$$\vec{P} = (\varepsilon_2 - \varepsilon_1)\vec{E}_i \tag{8}$$

where ε_2 and ε_1 are the permittivities of the body and the surrounding medium, as before, and E_i is the internal field within the body. The induced moment of the body, $\vec{\mu}$, is given by

$$\vec{\mu} = v\vec{P} = \alpha v \vec{E}_0 \tag{9}$$

where V is the volume of the body and α is the effective polarizability.

$$\alpha = \vec{P}/\vec{E}_0 = (\varepsilon_2 - \varepsilon_1)\vec{E}_i/\vec{E}_0 \tag{10}$$

For ellipsoidal bodies in general, having major axes a, b, and c, the uniform field E_a within the ellipsoid, when the external field $E_0 = |E_0|$ is applied along the a-axis, is given as

$$E_a = \varepsilon_1 E_0/[\varepsilon_1 + A(\varepsilon_2 - \varepsilon_1)] \tag{11}$$

where A is called the depolarization factor. It follows from Eqs. 10 and 11 that for ellipsoidal bodies

$$\alpha = \varepsilon_1(\varepsilon_2 - \varepsilon_1)/[\varepsilon_1 + A(\varepsilon_2 - \varepsilon_1)] \tag{12}$$

For the case of sphere, $a = b = c =$ radius, and $A = 1/3$, so that

$$\alpha = 3\varepsilon_1(\varepsilon_2 - \varepsilon_1)/(\varepsilon_2 + 2\varepsilon_1) \tag{12}$$

Equation 3 may be written as

$$\vec{F} = (\vec{\mu}\cdot\nabla)\vec{E}_0 = \alpha v(\vec{E}_0\cdot\nabla)\vec{E}_0 = \tfrac{1}{2}\alpha v\nabla(E_0)^2 \tag{13}$$

Upon insertion of Eq. 12, the result for the dielectrophoretic force upon small spherical objects, Eq. 4, is then readily obtained.

For a long thin cylindrical rod of radius r, with E_0 perpendicular to its length L, and for $A = \frac{1}{2}$, then

$$\alpha = 2\varepsilon_1(\varepsilon_2 - \varepsilon_1)/(\varepsilon_2 + \varepsilon_1) \tag{14}$$

and

$$\vec{F}_{\text{rod}} = \pi r^2 L\,\mathrm{Re}\{\varepsilon_1^*(\varepsilon_2 - \varepsilon_1)/(\varepsilon_2 + \varepsilon_1)\}\nabla(E_0)^2 \tag{15}$$

Similarly for a thin plate of length L, height h, and thickness d, with $L \gg d$, $h \gg d$, and with E_0 perpendicular to the major face, then $A = 1$, and

$$\alpha = \varepsilon_1(\varepsilon_2 - \varepsilon_1)/\varepsilon_2 \tag{16}$$

giving

$$\vec{F}_{\text{plate}} = \tfrac{1}{2}hdL\,\mathrm{Re}\{\varepsilon_1^*(\varepsilon_2 - \varepsilon_1)/\varepsilon_2\}\nabla(E_0)^2 \tag{17}$$

For other shapes, Pohl and Crane[15] derived a generalized equation which gives the dielectrophoretic force as

$$F = \tfrac{1}{2}\int_{\text{body}} \mathrm{Re}\left\{\nabla\left[\xi_1^*\left(1 - \frac{\xi_2}{\xi_1}\right)E_0^* E_i\right]\right\} dv \tag{18}$$

where ξ denotes the complex dielectric factor, $K/i\omega$, with $K = \sigma + i\omega\varepsilon$.

The alternative result, analogous to that of Lorrain and Corson (Eq. 5) but for rods, and assuming the effective field acting to produce the dielectrophoretic force is the *internal* field, E_i, may be obtained using the equation for the net force $\dot{F}'$ per unit volume as (ref. 19, p. 126)

$$\dot{F}'_{\text{net}} = \dot{F}_{\text{body}} - \dot{F}_{\text{fluid}} \tag{19}$$

$$\dot{F}'_{\text{net}} = \left(\frac{\varepsilon_2 - \varepsilon_0}{2}\right)\nabla(E_i)^2 - \left(\frac{\varepsilon_1 - \varepsilon_0}{2}\right)\nabla(E_0)^2; \tag{20}$$

where $\vec{E}$ is the field within the body and E_0 is the external field. Using Eq. 14, Eq. 20 becomes

$$\vec{F}'_{net} = \frac{\pi r L}{2}\left[(\varepsilon_2 - \varepsilon_0)\left(\frac{2\varepsilon_1}{\varepsilon_2 + \varepsilon_1}\right)^2 - (\varepsilon_1 - \varepsilon_0)\right]\nabla(E_0)^2; \tag{21}$$

It remains for experiment to test and compare the predictions of Eqs. 15 vs. 21.

An interesting sidelight on the application of dielectrophoretic forces on small particles or voids in fluid media in which the particle or void (bubble, e.g.) is of lower permittivity than the surrounding medium shows that stable levitation can be obtained in a nonuniform field.

The levitation of bubbles in liquids has been studied by Parmar and Jalaluddin[32] and by Jones and Bliss.[26] The former used a ring-shaped electrode to hold down bubbles in insulating liquids, and also observed that surface tension was reduced at the vapor-liquid interface. The latter effect modifies the particles size of escaping droplets, and has been known since 1748 through the studies of Winckler. It is much used nowadays as in spray painting, but the details of the phenomena are yet in need of clarification. Jones and Bliss used disc-and-ring electrodes to obtain strong stabilization of the levitation of bubbles in three dimensions, and gave a penetrating analysis of the forces. This type of stable confinement using principally electrical forces is, at first sight, an apparent violation of Earnshaw's theorem.

Earnshaw's theorem states that an electrical charge cannot be stably confined in an electrostatic potential well.[34] As discussed by Epstein,[35] an extension of this theorem can be used to show that a dipole also cannot be stably confined by any nonuniform electric field. It is an interesting apparent contradiction, however, that a dipole which results from a particle (or void volume) of low dielectric constant can be suspended stably in a fluid of higher dielectric constant. One proof of this corollary theorem is given in Appendix B.

Experimental

The following experiments were done to help decide between the several theoretical equations (Eq. 15 and 21) offered as correctly descriptive of the force on objects in a nonuniform field. It proved adequate to measure the force upon cylinders of various dielectrics hung in a nonuniform electric field.

The apparatus used in this experiment was an isomotive electrode chamber similar to that devised by Pohl and Pethig[31] for the measurement of dielectric constants. The isomotive chamber is so named because the force an object experiences is independent of the position of the object lying on the median plane within the chamber. The electrodes were shaped according to the equation[36]

$$r = r_{60}\left[\sin\left(\frac{3\Theta}{2}\right)\right]^{-2/3}. \tag{22}$$

The constant, r_{60}, is the smallest distance between the electrode and the coordinate center. Any experimentally convenient distance can be chosen for the parameter r_{60} but having r_{60} small eases voltage supply and maintainance problems. The ideal electrode configuration from Eq. (22) is shown in Fig. 1, while Fig. 2 shows the experimental apparatus.

The electrode chamber is in effect a metallic cube forming a Faraday cage 14.5 cm on a side with a radial distance at $\Theta = 60°$ of 1.8 cm. The chamber was placed beneath an analytical balance so that test objects hung from the balance were positioned between the electrodes of the chamber. The force exerted on the object by the applied field was measured by the balance as a function of voltage.

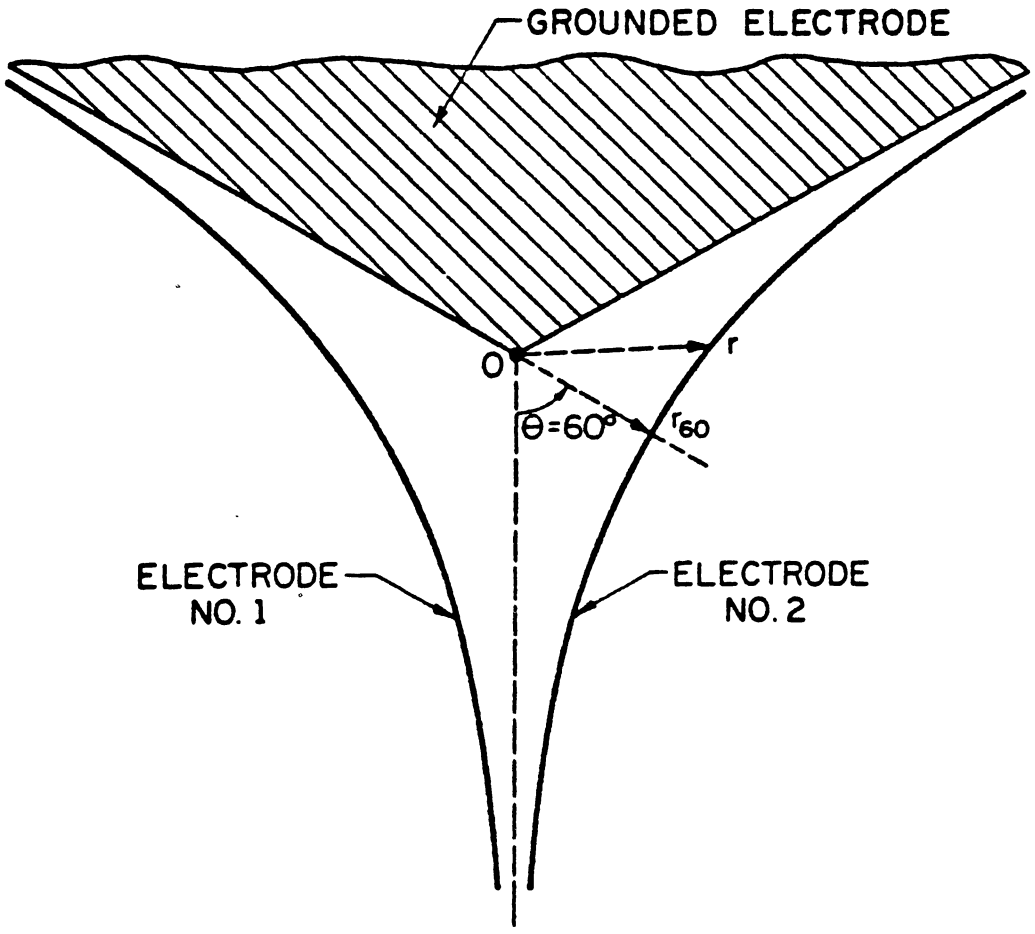

Fig. 1. Sketch of the ideal isomotive electrode configuration. The potential at the electrodes goes as kV = constant along the curve $r^{3/2} = r_{60}^{3/2} \times (\sin(30/2))^{-1}$.

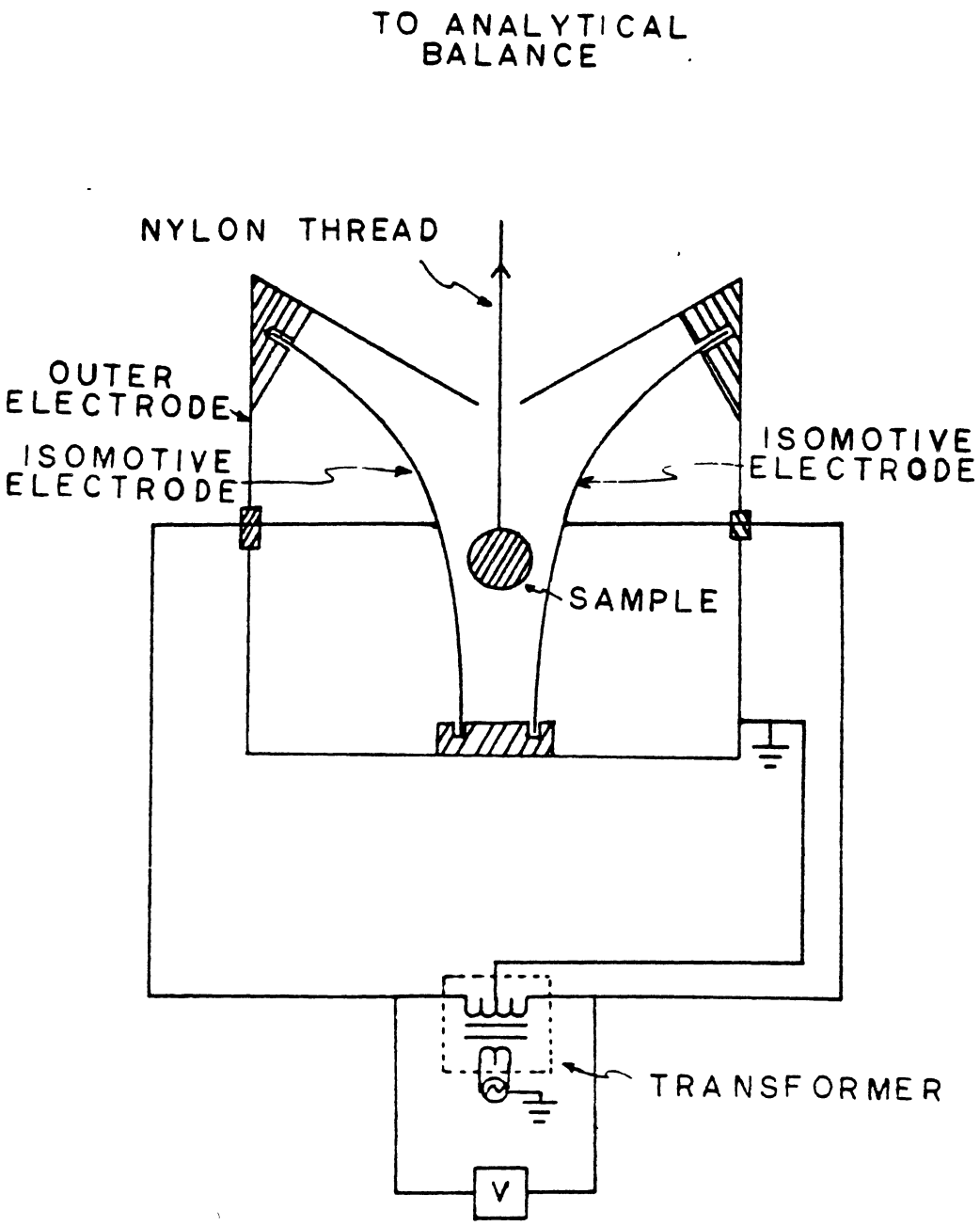

Fig 2. Practical configuration of an isomotive electrode system showing how the dielectrophoretic force upon a sample body (in air) is determined.

The voltage (0–4 Kv, 60 Hz) was supplied by a center-tap transformer (the outer electrode being grounded to the center tap). Voltage was varied by a variable transformer supply and measured by an appropriate voltmeter.

The test objects used were long thin cylinders oriented with their long axes perpendicular to the applied field. The dimensions of the cylinders and their relative dielectric constants are given in Table 1.

TABLE 1

Experimental Dielectrophoretic Force Parameters for Cylinders in an Isomotive Field.

Sample	ϵ_r^a	Volume (cm^3)	Force/Voltage^2 ($\times 10^{12}$ N/V^2)	Obs. K_ϵ	Calc. K_ϵ	K_ϵ'
Teflon	2.1	2.55	3.2	0.35	0.35	0.23
Polystyrene	2.56	7.02	13.7	0.55	0.44	0.25
PMMA	3.4	28.39	24.5[b]	0.68	0.56	0.25
SiO_2	3.78	3.17	6.8	0.61	0.58	0.24
Pyrex	5.02	1.21	3.0			
		1.21	2.9			
		3.02	8.5			
		2.61	7.9	0.77	0.67	0.22
		8.72	8.5[b]			
		4.01	4.4[b]			
		2.61	2.2[b]			
		2.61	2.8[b]			
Al_2O_3	$\perp$ 8.6	2.46	6.7	0.77	$\perp$0.79	0.16
	$\parallel$10.55	1.98	5.8	0.83	$\parallel$0.83	0 14

a. A. R. Von Hippel, *Dielectric Materials and Applications*, John Wiley & Sons, N.Y., 1954
b. $r_{60} = 2.5$ cm, all others $r_{60} = 1.8$ cm.

Results

The two force equations to be compared for this case as derived earlier (Eqs. 15 and 21) are simplified for the case of air and of relatively loss free dielectrics to:

$$\vec{F} = \epsilon_0(\text{volume})\frac{(\epsilon_r - 1)}{(\epsilon_r + 1)}\vec{\nabla}|E_0|^2 \tag{23}$$

and

$$\vec{F}' = \epsilon_0(\text{volume})\frac{2(\epsilon_r - 1)}{(\epsilon_r + 1)^2}\vec{\nabla}|E_0|^2 \tag{24}$$

The potential within the chamber is

$$V = Ar^{3/2}\sin\left(\frac{3\Theta}{2}\right). \tag{25}$$

Since

$$\vec{E} = -\vec{\nabla} V = -\hat{a}_r \frac{\partial V}{\partial r} - \hat{a}_\Theta \frac{1}{r} \frac{\partial v}{\partial \Theta}. \tag{26}$$

the field is then

$$\vec{E}_0 = \frac{3}{2} A r^{1/2} \left[\sin\left(\frac{3\Theta}{2}\right) \hat{a}_r + \cos\left(\frac{3\Theta}{2}\right) \hat{a}_\Theta \right] \tag{27}$$

and

$$\vec{\nabla} |E_0|^2 = (9/4) A^2 \hat{a}_r. \tag{28}$$

At $\Theta = 60°$

$$V = A r_{60}^{3/2} \tag{29}$$

and

$$A = V r_{60}^{-3/2} \tag{30}$$

Then

$$\vec{\nabla} |E_0|^2 = \frac{g V^2}{4 r_{60}^3} \hat{a}_r, \tag{31}$$

and the force equations become

$$\vec{F} = \frac{9\varepsilon_0 (\text{volume})}{4 r_{60}^3} \frac{(\varepsilon_r - 1)}{(\varepsilon_r + 1)} V^2 \hat{a}_r \tag{32}$$

$$\vec{F}' = \frac{9\varepsilon_0 (\text{volume})}{4 r_{60}^3} \frac{2(\varepsilon_r - 1)}{(\varepsilon_r + 1)^2} V^2 \hat{a}_r. \tag{33}$$

In this case $r_{60} = 1.8$ cm. The latter two force equations differ only in the term containing the relative dielectric constant. This term will be called the "excess" effective dielectric constant so that

$$K_e = \frac{(\varepsilon_r - 1)}{(\varepsilon_r + 1)} = \left[\frac{\text{Force}}{(\text{Voltage})^2} \right] \frac{4 r_{60}^3}{9\varepsilon_0 (\text{volume})} \tag{34}$$

and

$$K_e' = \frac{2(\varepsilon_r - 1)}{(\varepsilon_r + 1)^2} = \left[\frac{\text{Force}}{(\text{Voltage})^2} \right] \frac{4 r_{60}^3}{9\varepsilon_0 (\text{volume})}. \tag{35}$$

Experimental values for the "excess" effective dielectric constant were computed using the above equations. The slopes of the experimental curves of force vs. Voltage^2 were obtained by a least squares calculation. Typical values of the change in weight due to the potential are: 3.0 mg. at 3.0 Kv for teflon, 5.6 mg. at 2.0 Kv for polystyrene, and 4.4 mg. at 2.5 Kv for SiO_2. Table 1 shows the force vs. Voltage^2 slopes for each sample along with the calculated experimental values of K_e and the theoretical values (from Eqs. 34 and 35) for K_e and K_e'. The graph of Fig. 3 shows the theoretical curves of the excess effective dielectric constant (K_e and K_e') plotted against relative dielectric constant. The experimental values of excess effective dielectric constant for the samples are also plotted in Fig. 3 and lie along the theoretical curve of K_e. [Eq. 34]

The experimental values of K_e were observed to be reproducible to within $\pm 5\%$ except for the case of pyrex glass ($\pm 12\%$). The value plotted for pyrex glass is an average of eight different sample measurements. The larger error for pyrex rods may reflect problems due to humidity. The error bars shown for pyrex are one standard deviation about the mean. Polystyrene and PMMA rods both had relatively large diameters (.97 cm and 1.91 cm, respectively). Since Al_2O_3 has an anisotropic ε_r, the theoretical value chosen for use in Fig. 3 was the average of the perpendicular and parallel values of ε_r. It may be remarked that the graph shown is rather insensitive to the choice of dielectric constant values in this region. The experimental results for all six materials agree quantitatively with the predictions of Eq. 15 (or Eq. 34), and show irreconsilability with the predictions of Eq. 21 (or Eq. 35).

We conclude that from both the theoretical and experimental aspects that the preferred description of the $\vec{F}$-E^2 relation is that of Eq. 15.

Appendix A

Theoretical Calculations of the Dielectrophoretic Force For Various Model Systems

In this section we shall present and compare the results for the dielectrophoretic forces on various bodies as calculated by the different available approaches. We shall assume that the bodies are homogenous and isotropic. The situations considered are: a sphere in a slightly nonuniform field in a vacuum, a sphere in a slightly nonuniform field established in a dielectric medium, an ellipsoid and a cylinder in such a field in a vacuum and in a dielectric medium, and spherical shell in the field of a point charge located at its center.

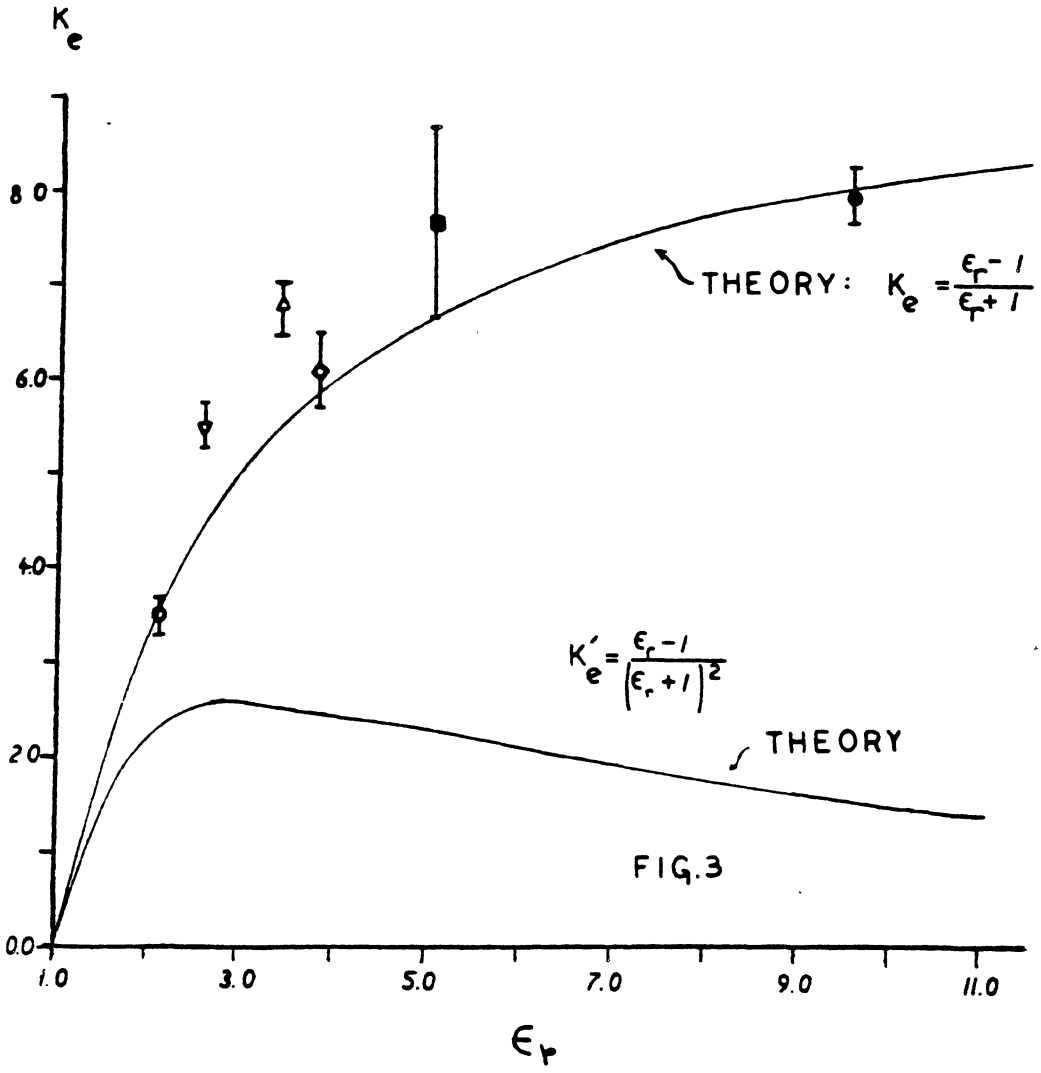

Fig. 3. Predicted and observed values for K_e, the "excess" effective dielectric constant. Note that the observed values follow rather closely the prediction of upper theoretical curve, for K_e, and deviate rather strongly from those predicted by the lower relation, for K'_e. (See Eqs. 34 and 35).

A. Small Sphere in a Vacuum

Consider a uniform field $\vec{E}_0$ of infinite extent to be established in a vacuum and that a small homogenous sphere of permittivity ϵ_2 is placed in the field. A standard calculation[3,4,12,20] shows that the field inside the sphere is given by

$$\vec{E}_{in} = \frac{3\epsilon_0}{\epsilon_2 + 2\epsilon_0} \vec{E}_0 \tag{A-1}$$

Since dielectrophoresis requires a nonuniform field, let us assume that the external field is slightly nonuniform, but that the value of the field is still given by Eq. (1) to the first approximation. The force on the particle can then be computed by various methods.

1. Maxwell-Stratton approach. The net force on the sphere is given by[4]

$$\vec{F} = \int_s \left[\epsilon_0 \vec{E}(\vec{E}\cdot\hat{n}) - \frac{\epsilon_0}{2} E^2 \hat{n} \right] da \tag{A-2}$$

where the integral is evaluated over any surface enclosing the sphere. If the uniform field equations are used, the force integral gives zero. This is, of course, as it should be since a particle will not experience a translational force in a uniform field.

2. Dipole approach. The force is given by

$$\vec{F} = \int_{\text{body}} (\vec{P}\cdot\nabla)\vec{E}_{\text{ext}}\, dv \tag{A-3}$$

where for this case $\vec{E}_{\text{ext}} = \vec{E}_0$ and

$$\vec{P} = (\epsilon_2 - \epsilon_0)\vec{E}_{in} = \frac{3\epsilon_0(\epsilon_2 - \epsilon_0)\vec{E}_0}{\epsilon_2 + 2\epsilon_0}. \tag{A-4}$$

Assuming that the field does not vary appreciably over the extent of the sphere and using the fact that $(\vec{E}_0\cdot\nabla)\vec{E}_0 = \frac{1}{2}\nabla(E_0^2)$ gives the force as

$$\vec{F} = \frac{3}{2}\epsilon_0 \frac{(\epsilon_2 - \epsilon_0)}{(\epsilon_2 + 2\epsilon_0)} \nabla E_0^2 \int dv = 2\pi a^3 \epsilon_0 \frac{(\epsilon_2 - \epsilon_0)}{(\epsilon_2 + 2\epsilon_0)} \nabla E_0^2. \tag{A-5}$$

where the volume of the sphere ($\frac{4}{3}\pi a^3$) has been introduced.

3. Energy approach. The energy of the body in the field is given by

$$U = \tfrac{1}{2} \int_{\text{body}} (\epsilon_0 - \epsilon_2)\vec{E}\cdot\vec{E}_0\, dv. \tag{A-6}$$

Substituting Eq. (A-1) for E gives

$$U=\tfrac{1}{2}\int_{\text{body}}(\varepsilon_0-\varepsilon_2)\left(\frac{3\varepsilon_0}{\varepsilon_2+2\varepsilon_0}\right)E_0^2\,dv. \qquad \text{(A-7)}$$

Performing this integration and introducing the volume of the sphere gives

$$U=2a^3\frac{\varepsilon_0(\varepsilon_0-\varepsilon_2)}{(\varepsilon_2+2\varepsilon_0)}E_0^2. \qquad \text{(A-8)}$$

The force is the negative gradient of the energy as the body moves through the field. The result is

$$\vec{F}=-\nabla U=2\pi a^3\varepsilon_0\frac{(\varepsilon_2-\varepsilon_0)}{(\varepsilon_2+2\varepsilon_0)}\nabla E_0^2, \qquad \text{(A-9)}$$

which is identical to that given by the dipole approach.

B. Small Sphere in a Dielectric Medium

Consider a sphere of permittivity ε_2 placed in an approximately uniform field $\vec{E}_1$ rather than in a vacuum. The field inside the sphere is now given by

$$\vec{E}_{in}=\frac{3\varepsilon_1}{(\varepsilon_2+2\varepsilon_1)}\vec{E}_1. \qquad \text{(B-1)}$$

1. Maxwell-Stratton approach. Again, this procedure gives no net force for a perfectly uniform field.

2. Dipole approach. The question here is what to use for the polarization inside the sphere. Should the "strict" definition of polarization

$$\vec{P}=(\varepsilon_2-\varepsilon_0)\vec{E}$$

be used? Or, is an "effective" polarization, $\vec{P}=(\varepsilon_2-\varepsilon_1)\vec{E}$ more appropriate? If the latter choice is made, the calculation of the force is identical to that for a sphere in a vacuum, except that ε_1 and $\vec{E}_1$ are substituted for ε_0 and E_0. The result is

$$\vec{F}=2\pi a^3\varepsilon_1\frac{(\varepsilon_2-\varepsilon_1)}{(\varepsilon_2+2\varepsilon_1)}\nabla E_1^2. \qquad \text{(effective polarization)} \qquad \text{(B-2)}$$

If the strict definition of the polarization is used, then the result is

$$\vec{F}=2\pi a^3\varepsilon_1\frac{(\varepsilon_2-\varepsilon_0)}{(\varepsilon_2+2\varepsilon_1)}\nabla E_1^2. \qquad \text{(total polarization)} \qquad \text{(B-3)}$$

Another approach that has been suggested (19) uses the "total" polarization, but instead of using the external field $\vec{E}_1$, it uses the local field, E_{in}, and then subtracts off a "buoyancy" term. That is:

$$\vec{F}=\int(\vec{P}_{\text{body}}\cdot\nabla)\vec{E}_{in}\,dv-\int(\vec{P}_{\text{fluid}}\cdot\nabla)\vec{E}_1\,dv \tag{B-4}$$

or

$$F=\int[(\varepsilon_2-\varepsilon_0)\vec{E}_{in}\cdot\nabla]\vec{E}_{in}\,dv-\int[(\varepsilon_1-\varepsilon_0)\vec{E}_1\cdot\nabla]\vec{E}_1\,dv.$$

This approach gives the force, after algebraic manipulation, as

$$\vec{F}=\frac{2\pi a^3}{3}(\varepsilon_2-\varepsilon_1)\left[\frac{\varepsilon_1(4\varepsilon_1+5\varepsilon_0)-\varepsilon_2(\varepsilon_1-\varepsilon_0)}{(\varepsilon_2+2\varepsilon_1)^2}\right]\nabla E_1^2. \tag{B-5}$$

3. **Energy approach.** The energy of the body is given by

$$U=\tfrac{1}{2}\int_{\text{body}}(\varepsilon_1-\varepsilon_2)\vec{E}\cdot\vec{E}_1\,dv \tag{B-6}$$

which is identical to the vacuum case except that ε_0 and $\vec{E}_0$ are replaced by ε_1 and $\vec{E}_1$. Hence, the result is

$$\vec{F}=2\pi a^3\varepsilon_1\frac{(\varepsilon_2-\varepsilon_1)}{(\varepsilon_2+2\varepsilon_1)}\nabla E_1^2 \tag{B-7}$$

Note that this result agrees with that of the effective polarization approach and disagrees with the results of the two attempts to introduce the total polarization. From these calculations we can infer that in order to obtain the force equation for an object in an insulating medium, one needs only to compute the force for the object in a vacuum and then substitute ε_1 for ε_0.

C. Ellipsoids, Cylinder, and Plate in a Slightly Nonuniform Field

For certain simple geometrical shapes it is possible to express the field inside the body in terms of the original applied field $\vec{E}_1$ as[30]

$$\vec{E}_{in}=\frac{\varepsilon_1\vec{E}_1}{\varepsilon_1+A(\varepsilon_2-\varepsilon_1)} \tag{C-1}$$

where A is called the depolarization factor and ε_1 and ε_2 are the permittivities of the medium and object respectively. The force is then given by effective polarization

and energy approaches as

$$\vec{F} = \frac{\varepsilon_1(\varepsilon_2 - \varepsilon_1)}{2[\varepsilon_1 + A(\varepsilon_2 - \varepsilon_1)]} v \nabla E_1^2. \tag{C-2}$$

where v is the volume of the body.

For ellipsoids of axes a, b, and c, the value of A depends on the relative lengths of the axes. For the special case of a sphere. $a = b = c$, and $A = \frac{1}{3}$. Eq. (C-2) then reduces to Eq. (B-2).

For a cylinder with $\vec{E}_1$ perpendicular to its length, the depolarization factor A is 1/2. Hence, the force is

$$\vec{F} = \frac{\varepsilon_1(\varepsilon_2 - \varepsilon_1)}{(\varepsilon_1 + \varepsilon_2)} v \nabla E_1^2. \qquad \text{(cylinder)} \tag{C-3}$$

For a thin plate with the applied field perpendicular to its face, $A = 1$ and

$$\vec{F} = \frac{\varepsilon_1(\varepsilon_2 - \varepsilon_1)}{2\varepsilon_2} v \nabla E_1^2. \qquad \text{(plate)} \tag{C-4}$$

D. Force on Half of a Spherical Shell in the Field of a Point Charge in a Vacuum

As a further theoretical check on the correctness of the approaches that can be used for computing dielectrophoretic forces, it is useful to compare the results of a Maxwell stress calculation with the other methods. Generally it is difficult to find a sample system for which all the calculations can be made because of the nature of the information required for the different approaches. As noted earlier, the energy approach and the effective polarization approach require knowledge of the field throughout the body both before and after the introduction of the body. The Maxwell approach and the total polarization suggested by Lorrain and Corson only require knowledge of the field after the object is in place. The Maxwell approach requires the field outside the body; the Lorrain-Corson approach uses the field inside the body. In the following example we shall compare the results of the Maxwell approach to that of the Lorrain-Corson approach and show that they differ. We shall also use energy methods to obtain agreement with the Maxwell result.

1. Maxwell-Stratton approach. The sample system consists of a spherical shell of inner radius R_1 and outer radius R_2 made of insulting material whose permittivity is ε_2. All other space is assumed to be *vacuum* and a charge Q is placed at the center of the shell as shown in Fig. D-1. We want to compute the force on the right half of the shell as shown in Fig. D-2. The Maxwell approach as detailed by

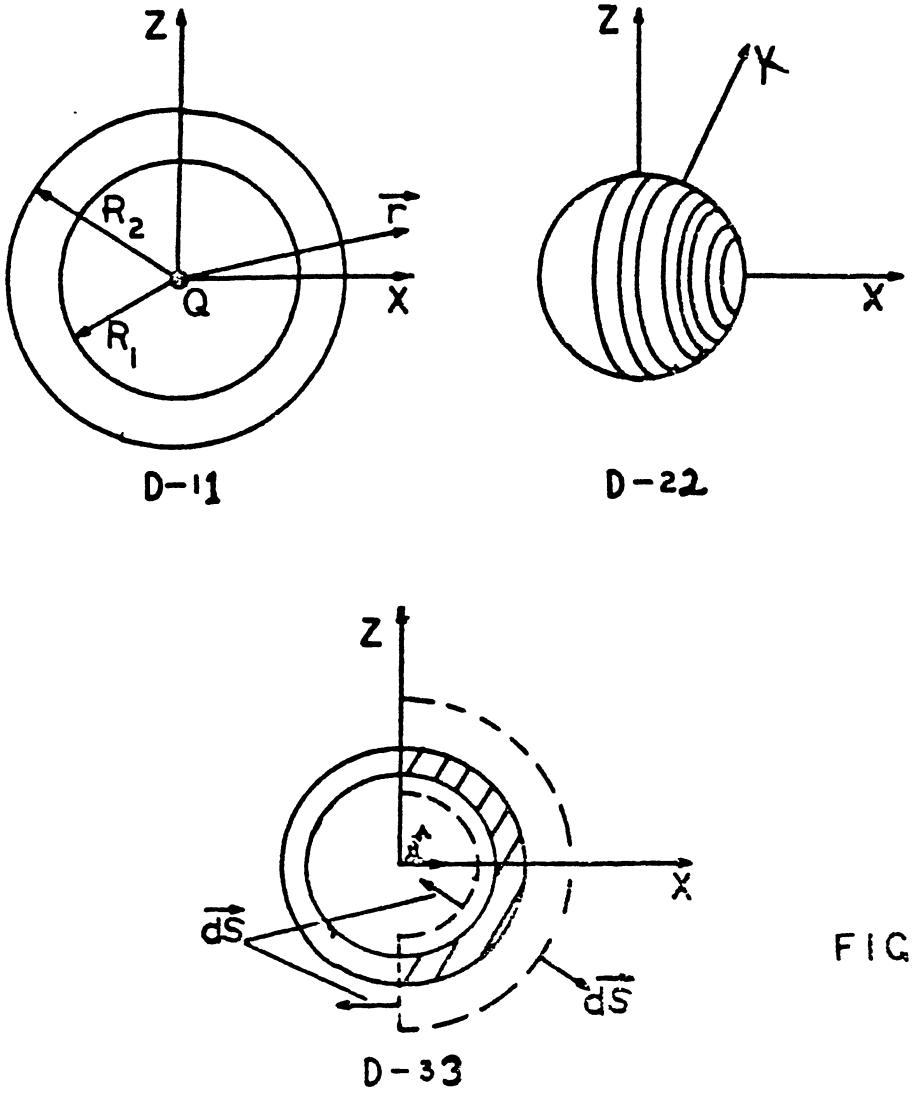

FIG. D

Fig. D-1. Charge Q at center of a spherical shell of thickness $R_2 - R_1$.

Fig. D-2. Half-shell as from FIG. D-1

Fig. D-3. Diagram of section through the half-shell.

Stratton gives the force as

$$\vec{F} = \int_s \varepsilon \vec{E}(\vec{E}\cdot d\vec{S}) - \int_s \frac{\varepsilon}{2} E^2 d\vec{S}. \tag{D-1}$$

This is a difference of two *vector* integrals evaluated over any surface enclosing the body where $d\vec{S}$ is a differential vector perpendicular to the chosen surface. The surface chosen here is shown in Fig. D-3 and consists of another hemispherical shell just enclosing the right hemisphere and passing through the sphere in the y-Z plane.

The evaluation of Eq. (D-1) requires knowledge of $\vec{E}$ at every point on the surface of integration, which means we must known E both outside and inside the shell as well as in the material. By Gauss's law, the field inside and outside is

$$\vec{E}_0 = E_0\hat{r} = \frac{Q\hat{r}}{4\pi\varepsilon_0 r^2}, \qquad (r<R_1, r>R_2) \tag{D-2}$$

where $\hat{r}$ is the unit outward radial vector. Also by Gauss's law the field in the spherical shell is

$$\vec{E}_2 = E_2\hat{r} = \frac{Q\hat{r}}{4\pi\varepsilon_2 r^2}. \qquad (R_1<r<R_2) \tag{D-3}$$

Let us designate the first integral in Eq. (D-1) as $\int I$ and evaluate it first. For the part of the surface passing through the shell $\vec{E}$ is perpendicular to $d\vec{S}$, so that $\vec{E}\cdot d\vec{S}$ is zero there. Hence, the only contribution to this integral is due to the outside and inside surfaces. Outside, $d\vec{S}$ is given in spherical coordinates by

$$d\vec{S} = \hat{r}r^2 \sin\Theta\, d\Theta\, d\phi \tag{D-4}$$

so that

$$\vec{E}_0\cdot d\vec{S} = E_0 r^2 \sin\Theta\, d\Theta\, d\phi. \tag{D-5}$$

Then the integral over the outside becomes

$$\int_{I(\text{OUTSIDE})} = \int_{\text{OUTSIDE}} \varepsilon_0 \vec{E}_0(\vec{E}_0\cdot d\vec{S}) = \int_{\text{OUTSIDE}} \varepsilon_0 E_0^2 r^2 \sin\Theta\, d\Theta\, d\phi\hat{r}. \tag{D-6}$$

Since this is a vector integral and the direction of the integrand changes with Θ and ϕ, the vector $\hat{r}$ can be written in terms of the Cartesian coordinate unit vectors $\hat{i}, \hat{j}$, and $\hat{k}$. That is

$$\hat{r} = \hat{i}\sin\Theta\cos\phi + \hat{j}\sin\Theta\sin\phi + \hat{k}\cos\Theta. \tag{D-7}$$

Thus, Eq. (D-6) will have $\hat{i}$, $\hat{j}$, and $\hat{k}$ components. Since the test body is a

hemisphere, then by symmetry, the $\hat{j}$ and $\hat{k}$ components must add to zero. Eq. (D-6) then reduces to

$$\int_{I(\text{OUTSIDE})} = \hat{i}\int_{\text{OUTSIDE}} \varepsilon_0 E_0^2 r^2 \sin^2\Theta \cos\phi \, d\Theta \, d\phi. \tag{D-8}$$

For this surface r is equal to R_2, Θ goes from 0 to π, and ϕ takes on values from $-\pi/2$ to $\pi/2$. Performing the integration and substituting for E_0 gives

$$\int_{I(\text{OUTSIDE})} = \hat{i}\frac{Q^2}{16\pi\varepsilon_0 R_2^2}. \tag{D-9}$$

For the inside hemisphere,

$$d\vec{S} = -\hat{r}r^2 \sin\Theta \, d\Theta \, d\phi \tag{D-10}$$

and

$$\int_{I(\text{INSIDE})} = \frac{-\hat{i}Q^2}{16\pi\varepsilon_0 R_1^2}. \tag{D-11}$$

The total value of the first integral of Eq. (D-1) is then

$$\int_I = \frac{\hat{i}Q}{16\pi\varepsilon_0}\left(\frac{1}{R_2^2} - \frac{1}{R_1^2}\right). \tag{D-12}$$

Let us now proceed to evaluate the second integral of Eq. (D-1) which will be designated $\int II$. Along the outside hemisphere, $d\vec{S}$ is given by Eq. (D-4) so that

$$\int_{II(\text{OUTSIDE})} = \int_{\text{OUTSIDE}} \frac{\varepsilon_0 E_0^2}{2} r^2 \sin\Theta \, d\Theta \, d\phi \hat{r}. \tag{D-13}$$

Comparison of this result with Eq. (D-6) shows

$$\int_{II(\text{OUTSIDE})} = 1/2 \int_{I(\text{OUTSIDE})}.$$

Similarly,

$$\int_{II(\text{INSIDE})} = 1/2 \int_{I(\text{INSIDE})}.$$

We must now consider the contribution to $\int II$ made by the surface passing through the shell. This contribution is not zero. Here $d\vec{S}$ points in the negative X direction (see Fig. D-3) so that

$$d\vec{S} = -\hat{i}dS = -\hat{i}2\pi r \, dr \tag{D-14}$$

and

$$\int_{II(\text{EDGE})} = -i\int_{R_1}^{R_2}\left(\frac{\varepsilon_2}{2}E_2^2\right)(2\pi r\,dr)$$

$$= \frac{iQ^2}{32\pi\varepsilon_2}\left(\frac{1}{R_2^2}-\frac{1}{R_1^2}\right). \tag{D-15}$$

The total value of the second integral of Eq. (D-1) is

$$\int_{II} = \frac{iQ^2}{32\pi}\left(\frac{1}{R_2^2}-\frac{1}{R_1^2}\right)\left(\frac{1}{\varepsilon_0}+\frac{1}{\varepsilon_2}\right). \tag{D-16}$$

The total force is obtained by substituting Eqs. (D-12) and (D-16) into (D-1) which gives

$$\vec{F}_{(M-S)} = -\hat{i}\frac{Q^2}{32\pi}\left(\frac{1}{R_1^2}-\frac{1}{R_2^2}\right)\left(\frac{1}{\varepsilon_0}-\frac{1}{\varepsilon_2}\right). \tag{D-17}$$

This result shows that the force on the right hemispherical shell due to the point charge is to the left as would be expected since it moves to the region of stronger field, closer to the charge. Also notice the direction of the force is independent of the sign of the charge which is another characteristic of dielectrophoresis.

2. Lorrain-Corson (total polarization) approach. The suggested force expression is given by Eq. (B-4). Since the present problem considers a spherical shell in a vacuum, there is no "buoyancy" term due to a surrounding fluid and the equation reduces to

$$\vec{F} = \int_{\text{body}} (\vec{P}_2\cdot\nabla)\vec{E}_2\,dv. \tag{D-18}$$

Here $\vec{P}_2$ is the total polarization inside the body and $\vec{E}_2$ is the electric field inside the body. From Eq. (D-3)

$$\vec{E}_2 = \frac{Q\hat{r}}{4\pi\varepsilon_2 r^2}. \tag{D-19}$$

By definition

$$\vec{P}_2 = (\varepsilon_2-\varepsilon_0)\vec{E}_2. \tag{D-20}$$

Eq. (D-18) then becomes

$$\vec{F} = \int\left[(\varepsilon_2-\varepsilon_0)\vec{E}_2\cdot\nabla\right]\vec{E}_2\,dv = \int\frac{\varepsilon_2-\varepsilon_0}{2}\nabla\left(E_2^2\right)dv, \tag{D-21}$$

where the same vector identity has been used here as was used in deriving Eq. (A-5). From Eq. (D-19)

$$E_2^2 = \vec{E}_2 \cdot \vec{E}_2 = \frac{Q^2}{16\pi^2\epsilon_2^2 r^4} \tag{D-22}$$

and so

$$\nabla(E_2^2) = -\frac{Q^2\hat{r}}{4\pi^2\epsilon_2^2 r^5}.$$

Substitution of this expression into Eq. (D-21) gives

$$\vec{F} = -\frac{Q^2(\epsilon_2 - \epsilon_0)}{8\pi^2\epsilon_2^2}\int\frac{\hat{r}\,dv}{r^5}. \tag{D-24}$$

This is also a vector integral which must be evaluated over the volume of the hemispherical shell. As in the previous section, the radial unit vector must be expressed in terms of its Cartesian components (Eq. (D- 7)), and again due to symmetry the $\hat{j}$ and $\hat{k}$ components are zero. Hence, the force equation becomes

$$\vec{F} = \frac{-\hat{i}Q^2(\epsilon_2 - \epsilon_0)}{8\pi^2\epsilon_2^2}\int_{R_1}^{R_2}\int_0^{\pi}\int_{-\pi/2}^{\pi/2}\frac{\sin^2\Theta\cos\phi\,d\phi\,d\Theta\,dr}{r^3} \tag{D-25}$$

or

$$\vec{F}_{L-C} = \frac{-\hat{i}Q^2(\epsilon_2 - \epsilon_0)}{16\pi\epsilon_2^2}\left(\frac{1}{R_1^2} - \frac{1}{R_2^2}\right). \tag{D-26}$$

Comparison of Eqs. (D-17) and (D-26) shows that the two approaches disagree by the factor $2\epsilon_0/\epsilon_2$. This can be attributed to the use of the internal field rather than that which existed before the insertion of the hemisphere.

3. **Energy approach.** In order to make a straightforward calculation of the force from energy considerations, one must know the electric field in the test body and the original field in the region before the body is inserted. For the present case of the force on half of a spherical shell in the field of a point charge, the field inside the body is simple, but the original field is very difficult to determine. It is the field due to the point charge and the polarized other half of the shell. Hence, a straightforward energy calculation cannot readily be made.

It is possible, however, to use energy considerations and a slightly circuitous procedure to obtain an expression for the force. The procedure is to first compute the energy of the entire spherical shell. This can easily be done, since the original field is now just that due to a point charge. Next, allow the radius of the shell to change slightly and determine the corresponding energy change. Attribute this change in energy to work done by a radial force and compute the force. Finally,

integrate this force vectorially over the hemisphere. The details of this procedure follow.

For the entire spherical shell as the body, the energy integral, Eq. (A-6), is

$$\mathcal{U} = \frac{1}{2}\int_{\text{body}} (\varepsilon_0 - \varepsilon_2)\vec{E}_2 \cdot \vec{E}_0 \, dv \tag{D-27}$$

where $\vec{E}_0$ and $\vec{E}_2$ are given by Eqs. (D-2) and (D-3), and dv is the differential volume element. In spherical coordinates

$$dv = r^2 \sin\Theta \, dr \, d\Theta \, d\phi. \tag{D-28}$$

Substitution of these expressions gives

$$\mathcal{U} = \frac{(\varepsilon_0 - \varepsilon_2)Q^2}{32\pi^2\varepsilon_0\varepsilon_2}\int_{R_1}^{R_2}\int_0^{\pi}\int_0^{2\pi}\frac{\sin\Theta \, d\phi \, d\Theta \, dr}{r^2}$$

$$= \frac{(\varepsilon_0 - \varepsilon_2)Q^2}{8\pi\varepsilon_0\varepsilon_2}\left(\frac{1}{R_1} - \frac{1}{R_2}\right). \tag{D-29}$$

Suppose we allow R_1 and R_2 to change slightly while the thickness $\Delta R = R_2 - R_1$ remains constant. The energy will change by an amount

$$\Delta\mathcal{U} = \frac{\partial\mathcal{U}}{\partial R_1} dR_1 = \frac{-(\varepsilon_0 - \varepsilon_2)Q^2}{8\pi\varepsilon_0\varepsilon_2}\left(\frac{1}{R_1^2} - \frac{1}{R_2^2}\right)dR_1. \tag{D-30}$$

The change in energy per unit of surface area is $\Delta\mathcal{U}/A$ where

$$A = 4\pi R_1^2 \tag{D-31}$$

is the surface area of the sphere. Work must be done to change the energy and so a force must be acting on each surface element. Due to the spherical symmetry, this force must be radial. The electrical force per unit area $\left(\frac{\vec{F}}{A} \equiv \vec{f}\right)$ is related to the change in energy by

$$\vec{f} \cdot d\vec{R}_1 = f dR_1 = \frac{-\Delta\mathcal{U}}{A} \tag{D-32}$$

which, when combined with Eqs. (D-30) and (D-31) gives

$$\vec{f} = \frac{(\varepsilon_0 - \varepsilon_2)Q^2}{32\pi^2\varepsilon_0\varepsilon_2 R_1^2}\left(\frac{1}{R_1^2} - \frac{1}{R_2^2}\right)\hat{r}. \tag{D-33}$$

This expression is the force per unit area acting at each little surface element of the spherical shell. If we want to obtain the force on a section of the shell, we merely integrate the force vectorially over that section. For our hemisphere centered on the

x-axis, we again replace $\hat{r}$ by its Cartesian components and integrate over the hemisphere to obtain

$$\vec{F}_e = \int \vec{f}\, dS = \frac{-iQ^2}{32\pi}\left(\frac{1}{R_1^2} - \frac{1}{R_2^2}\right)\left(\frac{1}{\varepsilon_v} - \frac{1}{\varepsilon_2}\right). \tag{D-34}$$

Note that this result is identical with Eq. (D-17) obtained using the Maxwell-Stratton approach, but differs from the "total" polarization, internal field approach of Lorrain and Corson, Eq. (D-26).

E. Force on Half of a Spherical Shell in the Field of a Point Charge in a Dielectric Medium

We now change the problem by assuming that the regions inside and outside the spherical shell are filled with a dielectric medium of permittivity ε_1. The charge Q is still assumed to be at the center of the shell.

1. Maxwell-Stratton approach. The only change which must be made here is that the field inside and outside the shell is given by

$$\vec{E}_1 = \frac{Q\hat{r}}{4\pi\varepsilon_1 r^2}. \qquad (r<R_1, r>R_2) \tag{E-1}$$

That is, wherever there appears an ε_0, it must be replaced by ε_1. This ultimately gives the force on the hemisphere as

$$\vec{F}_{M\cdot S} = \frac{-iQ^2}{32\pi}\left(\frac{1}{R_1^2} - \frac{1}{R_2^2}\right)\left(\frac{1}{\varepsilon_1} - \frac{1}{\varepsilon_2}\right). \tag{E-2}$$

2. Lorrain-Corson approach. The force equation is given by Eq. (B-4). The first part, the integral over the body, is unaffected by the outside medium, so that its contribution is still given by Eq. (D-26). The second integral is

$$-\int (\vec{P}_{\text{fluid}}\cdot\nabla)\vec{E}_1\, dv = -\int \left[(\varepsilon_1 - \varepsilon_0)\vec{E}_1\cdot\nabla\right]\vec{E}_1\, dv$$

$$= \frac{iQ^2(\varepsilon_1 - \varepsilon_0)}{16\pi\varepsilon_1^2}\left(\frac{1}{R_1^2} - \frac{1}{R_2^2}\right). \tag{E-3}$$

Adding Eqs. (D-26) and (E-3) gives the force as

$$\vec{F}_{L\cdot C} = \frac{-iQ^2}{16\pi}\left(\frac{1}{R_1^2} - \frac{1}{R_2^2}\right)\left(\frac{\varepsilon_2 - \varepsilon_0}{\varepsilon_2^2} - \frac{\varepsilon_1 - \varepsilon_0}{\varepsilon_1^2}\right). \tag{E-4}$$

3. **Energy approach.** Again the only change here is the replacement of the original field $\vec{E}_0$ by the field $\vec{E}_1$ which is done by replacing ε_0 by ε_1. The force expression then becomes

$$\vec{F}_\varepsilon = \frac{-\hat{i}Q^2}{32\pi}\left(\frac{1}{R_1^2}-\frac{1}{R_2^2}\right)\left(\frac{1}{\varepsilon_1}-\frac{1}{\varepsilon_1}\right). \tag{E-5}$$

Notice again that the energy approach and the Maxwell-Stratton approach give the same result while the total polarization, internal field approach produces an expression barely resembling the others.

For the sake of completeness, it would be useful to compute the force predicted by the method using the effective polarization and the original field. But since the original field is that due to the point charge plus the other half of the shell, the calculation appears to be quite formidable and therefore has not been performed. However, in the cases where the fields can be evaluated, such as in the examples of spheres and cylinders, the predicted results do agree with the apparently correct energy approach. Hence, on theoretical grounds, we can conclude that there are three equivalent methods for computing dielectrophoretic forces. These are the Maxwell-Stratton stress approach, the energy approach, and the effective polarization approach.

F. Effects of A.C. Fields

The previous considerations have been restricted to pure dielectric materials and electrostatic fields. In practice this is usually not possible because most of the materials of interest have significant conductivities and if the fields are static, electrophoretic effects mask the dielectrophoresis. The question then arises as to what changes must be made in the methods of computation to take into account such things as conductivity, frequency, and phase lags. As a general rule these effects can be incorporated into the theory for sinusoidal time-varying fields by introducing complex quantities. Thus, the conductivity and the permittivity of a material would each have a real part and an imaginary part. The imaginary parts result from the particular conduction or polarization mechanisms not being able to keep up with the applied fields and producing phase lags. Since an out-of-phase polarization behaves like a conduction and an out-of-phase conduction has the properties of a polarization, it is possible to combine both polarization effects and conduction effects into a single complex parameter called the complex dielectric factor. It is defined as[36]

$$\xi = \varepsilon - \frac{i\sigma}{\omega} = \varepsilon_e - \frac{i\sigma_e}{\omega}, \tag{F-1}$$

where ε is the complex permittivity, σ is the complex conductivity, ε_e and σ_e are real quantities called the effective permittivity and effective conductivity, i is $\sqrt{-1}$, and ω is the angular frequency of the applied field.

Using an energy approach, it is possible to obtain a generalized expression for the instantaneous force on an object placed in a fluid and subjected to an alternating field. It is given by[15, 36]

$$\vec{F}(t) = -\frac{\nabla}{4}\left\{ R_e\left[\int_{\text{body}} \xi_1^* \left(1 - \frac{\xi}{\xi_1}\right) \vec{E}_1^* \cdot \vec{E}\, dv \right] \right\}, \tag{F-2}$$

where ξ_1 and ξ are the complex dielectric factors of the fluid and the object respectively, $\vec{E}_1^*$ is the complex conjugate of the instantaneous field before the body is inserted, $\vec{E}$ is the field inside the body, and R_e means to take the real part of the expression.

For the case of a sphere in a slightly nonuniform field, the time-averaged force is[15, 36]

$$\vec{F} = 2\pi a^3 \nabla E_1^2 \,\mathrm{Re}\left[\xi_1^* \frac{(\xi_2 - \xi_1)}{(\xi_2 + 2\xi_1)} \right]. \tag{F-3}$$

where E_1 is the R.M.S. value of the field. Comparison of this result with Eq. (B-7) shows that the A.C. case can be obtained from the static result by replacing ε's with ξ's and taking the complex conjugate of the first ξ. Similar substitutions hold for other simple shapes.

Appendix B

To obtain stable electrical localization or confinement of a polarizable particle of dielectric permittivity ε_2 situated in a fluid medium of permittivity ε_1, there are two requirements. First, the sum of the forces, dielectrophoretic and gravitational, $\vec{F}_d(r_0)$ and $\vec{F}_g$ at the equilibrium site must be zero. Second, the rate of change of the electrical force with height, x, must be negative, i.e., the net force must be such as to stabilize the position of the particle.

For small particles the dielectrophoretic force is known to vary as

$$\vec{F}_d = (3/2)\,(\text{volume})\frac{\varepsilon_1^*(\varepsilon_2 - \varepsilon_1)\vec{\nabla}(E)^2}{(\varepsilon_2 + p\varepsilon_1)} \tag{B-1}$$

where p is a constant, for example, equal to 2, 1 or 0 for the special cases of spheres, cylinders, and plates, respectively. The important feature for us at this juncture is that

$$\vec{F}_d \propto (\varepsilon_2 - \varepsilon_1)\vec{\nabla}(E)^2 \tag{B-2}$$

To obtain conformance with the first requirement in the non-trivial cases of $\varepsilon_2 \neq \varepsilon_1$, it is necessary that

$$\vec{\nabla}(E)^2 = \hat{i}\partial E^2/\partial x + \hat{j}\partial E^2/\partial y + \hat{k}\partial E^2/\partial z = 0 \tag{B-3}$$

Conformance with the second requirement, that the rate of spatial change of $\bar{F}_d$ be negative, implies for the case of a "dielectrically bouyant" particle, i.e. for $\varepsilon_2 < \varepsilon_1$, that in the neighborhood of r_0,

$$\partial^2 E^2/\partial x^2 > 0; \quad \partial^2 E^2/\partial y^2 > 0; \quad \text{and} \quad \partial^2 E^2/\partial z^2 > 0. \tag{B-4}$$

Similarly for the case of "dielectrically anti-bouyant" particles, i.e., for $\varepsilon_2 > \varepsilon_1$, that in the neighborhood of r_0 the similar terms of the second derivative will all be less than zero, i.e.:

$$\partial^2 E^2/\partial x^2 < 0; \quad \partial^2 E^2/\partial y^2 < 0; \quad \partial^2 E^2/\partial z^2 < 0. \tag{B-5}$$

Equation (B-4), which describes the conditions for dielectrically bouyant ($\varepsilon_2 < \varepsilon_1$) particles (e.g. bubbles in a liquid, etc.) implies that a minimum in $|E|$ exists locally in the region about r_0, whereas those of Equation (B-5) giving the conditions for a "dielectrically heavy" particle describe a local maximum in $|E|$. As demonstrated by Maxwell,[34] isolated maxima do not exist in regions detached from electrode surfaces in space-charge free electrostatic fields. On the other hand, although we do not present here a rigorous proof of the existence of three-dimensional minima in electrical fields, it is appreciated that there are many practical examples of such minima (zeros). Pin-point to plane electrode geometries, etc. are common examples. Granting this, then the theorem for the possible existence of a stable confinement of dielectrically bouyant particles in a medium can be considered to be proven. The corollary to the Earnshaw theorem extended to dielectrics may be stated:

"Stable electrical localization or confinement of dielectric bodies is possible only if their permittivity is less than that of the surrounding medium, and if in (strong) nonuniform electrical fields." It is not intended that this corollary apply directly to the operation of dynamically stabilized procedures.

Acknowledgements:

The support of a portion of this work by the National Science Foundation on Grant No. PCM 76-21467 is sincerely appreciated. Numerous helpful discussions with Professor Paul Lorrain over the considerable time it took to make this study are gratefully acknowledged.

References

[1]D. J. Korteweg, Wied. Ann. der Physik und Chemie **9**, 48–61 (1880).

[2]H. von Helmholtz, ibid **13**, 385 (1881).

[3]M. Abraham and R. Becker, 1932. *Classical Electricity and Magnetism*, Blackie Ltd., London.

[4]J. A. Stratton, 1941, *Electromagnetic Theory*, McGraw-Hill Book Co., N.Y.

[5]E. Durand, 1953, *Electrostatique et Magnetostatique*, Masson, Paris.

[6]J. Larmor, Phil. Trans. Roy. Soc. A **190**, 280 (1897).

[7]G. H. Livens, Phil. Mag. **32**, 162 (1916).

[8]R. Cade, Proc. Phys. Soc. A, **64**, 665 (1951).

[9]S. S. Hakim, Inst. Elec. Engrs., Monograph 475M, (1961).

[10]S. S. Hakim and J. B. Higham, Proc. Phys. Soc. **80**, 190 (1962).

[11]H. A. Pohl, J. Appl. Phys. **22**, 869 (1951).

[12]A. R. von Hippel, Dielectrics and Waves, John Wiley & Sons, N.Y., 1954, p. 39.

[13]H. A. Pohl, J. Appl. Phys. **29**, 1182 (1958).

[14]L. D. Sher, Nature **220**, 695 (1968).

[15]H. A. Pohl and J. S. Crane, J. Theor. Biol. **37**, 1 (1972).

[16]J. S. Crane and H. A. Pohl, ibid. **37**, 15 (1972).

[17]M. Javid and P. M. Brown, *Field Analysis and Electromagnetics*, McGraw-Hill, N.Y., 1963.

[18]J. Neufeld, Phys. Rev. **152**, 708 (1966).

[19]P. Lorrain and D. Corson, *Electromagnetic Fields and Waves*, W. H. Freeman and Co., San Francisco, 1970, p. 135.

[20]O. Jefimenko, *Electricity and Magnetism*, Appleton-Century-Crofts, N.Y., 1966.

[21]L. D. Landau and E. M. Lifschitz, *Electrodynamics of Continuous Media*, Pergamon Press, New York, 1960.

[22]J. Neufeld, Il Nuovo Cimento, LXVB, **33** (1970); LXVIB, **51** (1970).

[23]J. Neufeld, Int. J. Electronics **27**, 301 (1969).

[24]G. Schwartz, J. Chem. Phys. **39**, 2387 (1963).

[25]J. S. Crane and H. A. Pohl, J. Electrostatics **5**, 11 (1978).

[26]T. B. Jones and G. W. Bliss, J. Appl. Phys. **48**, 1419 (1977).

[27]W. F. Brown, Jr., Amer. J. Phys. **19**, 333 (1951).

[28]H. Greinacher, Helv. Phys. Acta. **21**, 261 (1948).

[29]R. M. Fano, L. J. Chu, and R. B. Adler, *Electromagnetic Fields, Energy, and Forces*, p. 356, John Wiley & Sons, New York, 1960.

[30]J. A. Reynolds and J. M. Hough, Proc. Phys. Soc. **B70**, 769 (1957).

[31]H. A. Pohl and R. Pethig, J. Phys., E, **10**, 190 (1977).

[32]D. S. Parmar and A. K. Jalaluddin, Jap. J. Appl. Phys. **13**, 793 (1974).

[33]J. H. Winckler, *Essai sur la Nature, Effets et les Causes de l'Electricite'*, Vol. 1., Sebastian Jorry, Paris, 1748.

[34]J. C. Maxwell, *A Treatise on Electricity and Magnetism*, (Dover, New York, 1954) Article 116.

[35]L. Epstein, Amer. J. Phys. **33**, 406 (1975).

[36]H. A. Pohl, *Dielectrophoresis*, Cambridge University Press, 1978.

APPENDIX C

ELECTRODE GEOMETRIES FOR VARIOUS DIELECTROPHORETIC FORCE LAWS

Journal of Electrostatics, 5 (1978) 337—342

© Elsevier Scientific Publishing Company, Amsterdam — Printed in The Netherlands

Paper No. 5-A

ELECTRODE GEOMETRIES FOR VARIOUS DIELECTROPHORETIC FORCE LAWS

Herbert A. Pohl and Kent Pollock
Dept. of Physics, Oklahoma State University, Stillwater, OK 74074

ABSTRACT

Electrode shapes needed to produce dielectrophoretic force upon neutral bodies in nonuniform electric fields are discussed. The shape can be arranged readily to produce a force which varies as r^n, where n = -3 to +3, and r is the radial coordinate.

INTRODUCTION

In order to take advantage of the force exerted upon neutral objects by nonuniform electric fields it is desirable to have available electrode shapes which can produce forces that vary in preselected manners with distance. Our objective here is to describe some of the more useful electrode shapes and their applications.

The motion induced by the action of a nonuniform electric field on a neutral body is called dielectrophoresis (ref. 1). It is distinct from electrophoresis, the motion induced by the action of an electric field (uniform or nonuniform) upon a charged object. The dielectrophoretic force, $\vec{F}$, exerted, for example, by a nonuniform electric field, $\vec{E}_o$, upon a small sphere of radius $\underline{a}$, and of (complex) permittivity ε_2 in a medium of (complex) permittivity ε_1 is given by (refs. 2-4)

$$\vec{F} = 2\pi\, \underline{a}^3\, \frac{\varepsilon_1^*(\varepsilon_2 - \varepsilon_1)\vec{\nabla}}{(\varepsilon_2 + 2\varepsilon_1)} |\underline{E}_o|^2 = \frac{\alpha}{2}\, \underline{v}\, \vec{\nabla} |\underline{E}_o|^2; \qquad (1)$$

where ε_1^* is the complex conjugate of ε_1, α is the effective polarizability, and $\underline{v}$ is the volume. For bodies of shape other than spherical, the term involving the particle dimensions and permittivity will vary, but the relation $\vec{F} \propto \vec{\nabla} |\underline{E}_o|^2$ persists.

In the present discussion we shall focus upon this and how it may be used to obtain desired geometrically desirable force relations. In particular, we shall require that cylindrical coordinates ($\underline{z}$,$\underline{r}$,θ) are implied, that no variation is

permitted in the z-direction, and that the force varies along the radial coordinate, r, as

$$F_r = kr^n \tag{2}$$

From the assumption of zero free charge throughout the volume of interest,

$$\vec{\nabla}^2 V = 0 \tag{3}$$

for which a solution in cylindrical coordinates is

$$V = Ar^m \sin m\theta \tag{4}$$

as

$$\vec{E} = -\vec{\nabla}V = -\hat{a}_r \frac{\partial V}{\partial r} - \hat{a}_\theta \frac{1}{r}\frac{\partial V}{\partial \theta}\ ; \tag{5}$$

$$\vec{E} = -mAr^{m-1}\left[\hat{a}_r \sin m\theta + \hat{a}_\theta \cos m\theta\right]; \tag{6}$$

and

$$|E|^2 = m^2 A^2 r^{2m-2} \tag{7}$$

independent of θ. Then from (2) and (7)

$$\vec{\nabla}|E|^2 = \hat{a}_r\, m^2(2m-2)\, A^2 r^{2m-3} = \hat{a}_r \frac{2k}{\alpha v} r^n \tag{8}$$

which implies

$$n = 2m-3 \tag{9}$$

The surface of constant potential, V producing such field conditions can then be written, for

$$m\theta^o = \pi/2 \tag{10}$$

$$V = Ar^m \sin m\theta = V_{\theta o}\left(\frac{r}{r_{\theta o}}\right)^m \sin m\theta; \tag{11}$$

The surface of constant potential, $V = V_{\theta o}$, is described by

$$r^m = r_{\theta o}^m \left[\sin m\theta\right]^{-1} \tag{12}$$

or

$$\underline{r} = \underline{r}_{\theta o} \left[\sin \underline{m}\theta\right]^{-1/\underline{m}} \tag{13}$$

$$\underline{r} = \underline{r}_{\theta o} \left[\sin \left(\frac{\underline{n}+3}{2}\right)\theta\right]^{-\frac{2}{\underline{n}+3}} \tag{14}$$

Here, $\underline{r}_{\theta o}$ is a characteristic radial distance for each system, and is the minimum distance from the coordinate center to the electrodes. The electrode shapes which produce a dielectrophoretic force varying as $\underline{r}^{\underline{n}}$, where $\underline{n}$ is -3, -2, -3/2, (-1), -1/2, 0, 1, 2, and 3 are shown sketched in Fig. 1. Note that for $3 \geq \underline{n} > -1$, the system has three electrodes, one neuter, and that for $-1 > \underline{n} \geq -3$, the system has but two electrodes. The case for $\underline{n} = -1$ is special in that a solution of the form of Eqn. (4) is not applicable. Here, $\underline{V} = \underline{A}\underline{r} \sin \theta$ from Eqn. 4, requiring $\nabla(\underline{E})^2 = 0$, and a trivial solution with $\underline{F} = 0$ everywhere. (The equation $\underline{V} = \underline{A}\ \underline{r} \sin \theta$ calls for parallel plate electrodes.) Parenthetically, the case for $\underline{n} = -5$ is gotten by spherically symmetric electrodes. The case for $\underline{n} = 0$ is of especial interest. It describes the useful "isomotive" field configuration (ref. 5) in which the dielectrophoretic force on the small body is independent of its position within the electrode volume (Fig. 1d). This has applications in particle separations (refs. 5-9), in the determination of the dielectric constant of solids (ref. 10), in the characterization of biological particles such as living cells (refs. 8, 9, 11) and in levitation (ref. 12).

The unique usefulness of the isomotive configuration can be readily appreciated by comparing the dielectrophoretic force for several electrode configurations. Let us assume that the medium is, in effect, a simple isotropic and homogeneous one. This implies that the suspension is a dilute one. A frequently used electrode configuration is that of a rounded wire tip extending into a hollow formed by an outer electrode. It can be described as approximating a spherical capacitor with a central radius $\underline{r}_1$ and an outer radius $\underline{r}_2$. For such a system

$$\vec{F} \propto \vec{\nabla}|\underline{E}_o|^2 = (\text{constant})\ \underline{r}^{-5}$$

Another frequently approximated electrode condiguration is that having cylindrical symmetry (Fig. 1i) in which

$$\vec{F} \propto \underline{r}^{-3}$$

Practical electrode arrangements which do this are: a central wire held coaxially within an outer cylindrical electrode; a wire-plate combination with two components

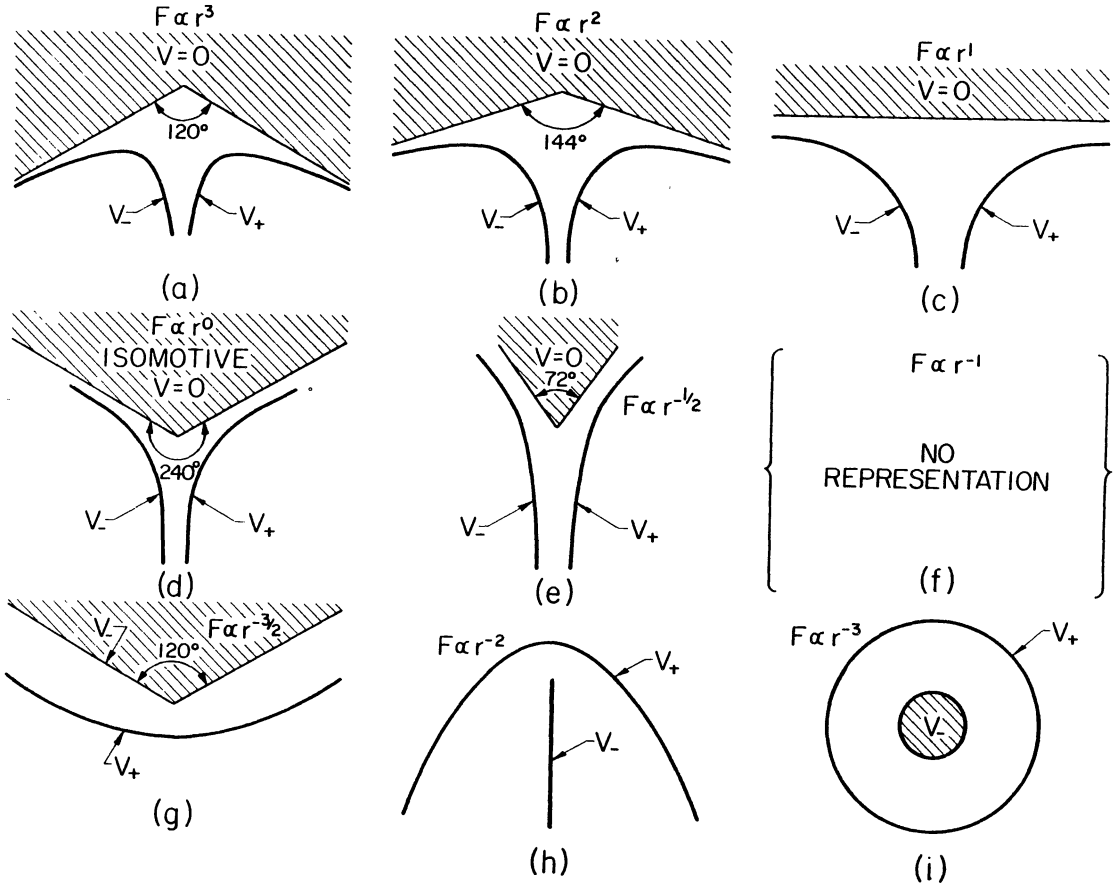

Fig. 1. Electrode shapes for producing dielectrophoretic force, F proportional to r^n, where r is the radial coordinate of a cylindrical coordinate system. The origin lies at the opices of the various angles shown.

parallel; and lastly, a wire-wire electrode pair made of parallel wires.

The major problem with the approximately spherical or cylindrical field geometries is that the fields are too inhomogeneous. They produce dielectrophoretic forces which vary rather drastically with the position of the test object in the locale of the electrodes. I.e.,

$$\vec{F}(\text{sphere}) \propto \underline{r}^{-5}$$

$$\vec{F}(\text{cylinder}) \propto \underline{r}^{-3}$$

but

$$\vec{F}(\text{isomotive}) \propto \underline{r}^{0}$$

In the first two cases it proves to be quite difficult to arrange for uniform treatment of a suspension of materials passing by the electrodes. Consider, for example, that two like particles of the same size and dielectric properties are being carried by fluid past electrodes of spherical symmetry. Let the two particles lie at radial distances $\underline{r}'$ and $\underline{r}''$ from the electrode center. If $\underline{r}'/\underline{r}'' = 3$, for example, the dielectrophoretic force on the otherwise identical particles would differ by a factor of $(\underline{r}'/\underline{r}'')_{sph} = 243$. Similar and only slightly less severe remarks would apply to the use of cylindrically symmetric electrode systems. Here, $(\underline{r}'/\underline{r}'')^{3}_{cyl} = 27$.

With such large differences in the dielectrophoretic force arising merely because of the geometric placement of the particles, it would seem nearly impossible to expect that sharp analytical separations would be obtainable between particles that differed only slightly in dielectric properties. It is here that the isomotive field configuration proves helpful. A practical realization of the ideal isomotive electrode system is shown sketched in Fig. 2. Electrodes of the isomotive design have proven capable of providing very satisfactory differential separations of particle mixtures (ref. 6). In practice, the bunching effect, the mutual dielectrophoresis of particles in an external field, operates in non-dilute suspensions of mixtures to mask and thus reduce the separability (ref. 11). Ways to minimize this but not involving electrode configurations are discussed elsewhere (ref. 11).

ACKNOWLEDGEMENTS

The authors express their appreciation to the National Science Foundation for support of this work.

REFERENCES

1 H.A. Pohl, J. Appl. Phys. 22(1951)869.

2 L.D. Sher, Nature 220(1968)695.
3 H.A. Pohl and J.S. Crane, J. Theoret. Biol. 37(1972)1.
4 J.S. Crane and H. A. Pohl, ibid., 37(1972)15.
5 H.A. Pohl, J. Electrochem. Soc. 115(1968)1c.
6 H.A. Pohl and C.E. Plymale, ibid., 107(1960)390.
7 H.A. Pohl, U.S. Patent 3,162,592 (Dec. 22, 1964).
8 H.A. Pohl and J.S. Crane, Chap. 15, in Electrostatics and its Applications, edited by A.D. Moore. John Wiley and Sons, New York, N.Y., 1974.
9 H.A. Pohl, J. Biol. Phys. 1(1973)1.
10 H.A. Pohl and R. Pethig, J. Physics E. 10(1977)190.
11 H.A. Pohl, Dielectrophoresis, Cambridge University Press (in press).
12 T.B. Jones and G.W. Bliss, J. Appl. Phys. 48(1977)1412.

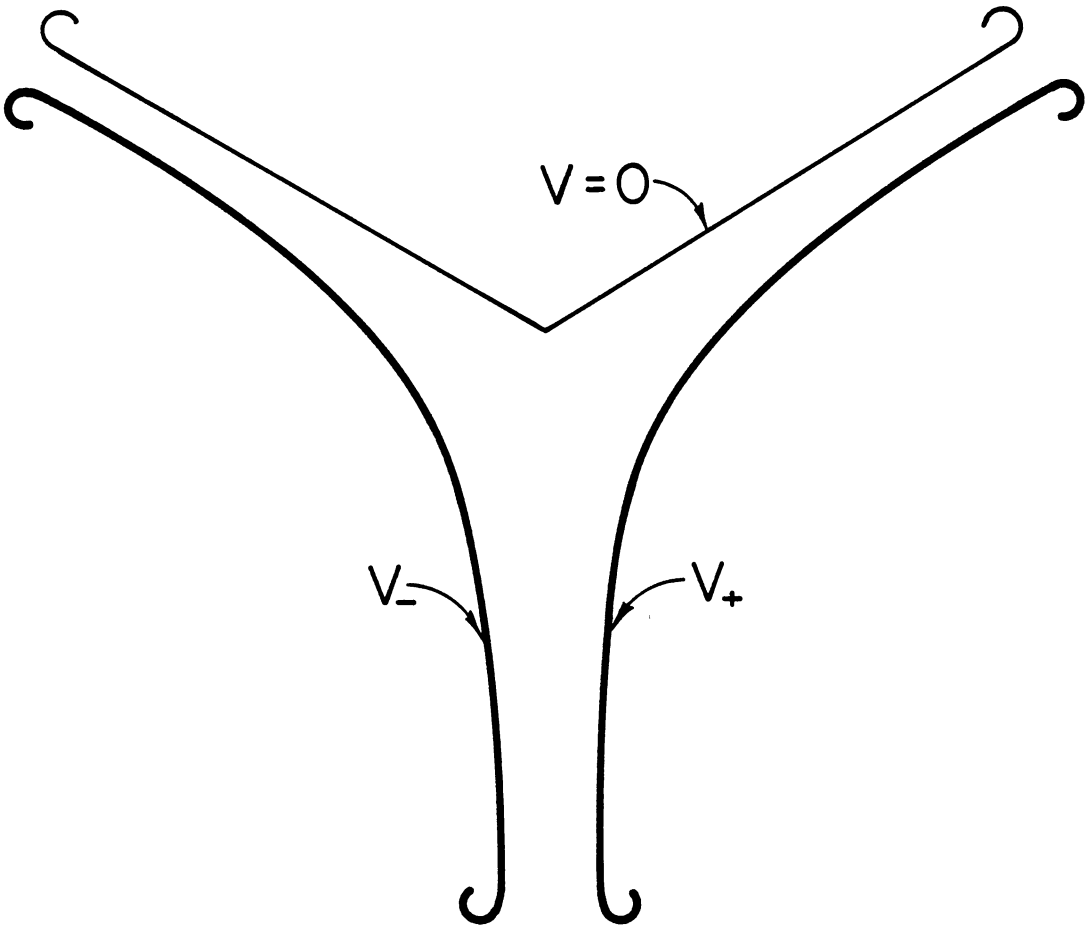

Fig. 2. Sketch of a practical design for electrodes producing an isomotive dielectrophoretic force field. The electrodes are drawn with care to permit guidance in crafting copies. In use with ac voltage supplies, the neuter electrode would connect with the center-tap of the transformer.

VITA

Jay Kent Pollock

Candidate for the Degree of

Doctor of Philosophy

Thesis: ELECTRICAL PROPERTIES OF CELLS USING NONUNIFORM FIELD EFFECTS

Major Field: Physics

Biographical:

Personal Data: Born in Bartlesville, Oklahoma, August 21, 1950, the son of Lyle W. and Jean Pollock.

Education: Graduated from Sooner High School, Bartlesville, Oklahoma, in May, 1968; received Bachelor of Science Degree in Physics from Oklahoma State University in May, 1972; completed requirements for the Doctor of Philosophy degree at Oklahoma State University in December, 1986.

Professional Experience: Teaching Assistant, Department of Physics, Oklahoma State University, August, 1972 to July 1974; Head Teaching Assistant, Department of Physics, Oklahoma State University, August, 1974 to July, 1976; Research Associate, Department of Physics, Oklahoma State University, August, 1976 to July, 1981; Research Associate, Pohl Cancer Research Laboratory, July, 1982, to present.